# TESTING AND MODELING TENSILE STRESS-STRAIN CURVE FOR PRESTRESSING WIRES IN RAILROAD TIES

by

YU-SZU CHEN

B.S., University of Tamkang, 2010

A THESIS

submitted in partial fulfillment of the requirements for the degree

MASTER OF SCIENCE

Department of Civil Engineering
College of Engineering

KANSAS STATE UNIVERSITY
Manhattan, Kansas

2016

Approved by:

Major Professor
Dr. Robert J. Peterman

# Copyright

# Abstract

Prestressed concrete is commonly used for bridges, pavement and railroad ties because of economic advantages in cost, sustainability service life, and environmental friendliness. In general concrete design standard, the ultimate moment strength in flexure design is computed by finding the equilibrium of the internal force in the section (the compressive force in concrete and tension force in the steel and reinforcement). To predict tension force in steel one generally applies the 7-wire low-relaxation prestressing strand equation from the PCI manual even though the design employed prestressing wires instead of strand. The other method is to use equations from the ACI Code which is over conservative.

Considering both approaches are lack accuracy, this research will provide an accurate estimation of the stress in prestressing wires through an experimental program and analytical modeling. The real stress-strain curves are collected through experimental testing in 13 types of prestressing wire. Experimental results are then used for modeling existing equations. As a result a more precise estimation is achieved. Additionally, this research simplifies the procedure for utilizing the equations which offers convenience in practical application.

# Table of Contents

List of Figures ..... vi
List of Tables ..... viii
Chapter 1 Introduction ..... 1
Overview ..... 1
Objectives ..... 2
Scope ..... 2
Chapter 2 Literature Review ..... 4
2.1 Experimental Testing of Prestressing Wire ..... 4
2.1.1. Stress-Strain Curve ..... 5
2.1.2. Modulus of Elasticity ..... 6
2.1.3. Yield Point ..... 7
2.1.4. Yield Strength ..... 7
2.1.5. Ultimate Tensile Strength ..... 8
2.2 Analytical Models for Wires and Strands ..... 9
2.2.1. Ramberg-Osgood (1943) ..... 11
2.2.2. Warwaruk Sozen and Siess (1962) ..... 12
2.2.3. Goldberg and Richard (1963) ..... 13
2.2.4. Giuffrè and Pinto (1970) ..... 14
2.2.5. Menegotto and Ponto (1973) ..... 15
2.2.6. Naaman (1977) ..... 16
2.2.7. Mattock (1979) ..... 17
Chapter 3 Experimental Program ..... 19
3.1 Wire Specimens ..... 19
3.2 Testing Machine ..... 26
3.3 Test Setup/ Procedure ..... 28
3.4 Performance of Test ..... 30

Chapter 4 Modeling Stress-Strain Curve — *Power Formula* ..... 35
4.1 Analytical Modeling Using the Power Formula ..... 35
4.2 Results and Discussions ..... 38
4.3 Recommended Design Curves for Wire Grades Using the Power Formula ..... 42
4.4 Conclusion ..... 47
Chapter 5 Modeling Stress-Strain Curve — *PCI Equation* ..... 48
5.1 Analytical Modeling Using PCI Equation for Prestressing Wire ..... 48
5.2 Development of Regression Equations ..... 51
5.3 Design and Recommendation for a Wire Using PCI Equation ..... 56
5.4 Conclusion ..... 62
Chapter 6 Recommendations Using Equations ..... 63
References ..... 66
Appendix A. Wire Measurement ..... 69
Appendix B. Schematic of Tensile Testing Machine ..... 76
Appendix C. Tensile Testing Results ..... 77
Appendix D. Analytical and Modeling Curves by Power Formula ..... 87
Appendix E. Analytical and Modeling Curves by PCI Equation ..... 97

# List of Figures

Figure 2.1 Stress-strain curve ..... 5
Figure 2.2 Offset method for determination of yield strength on σ-ε curve ..... 8
Figure 2.3 Rectangular stress distribution in ultimate strength analysis ..... 9
Figure 2.4 Stress-strain graphical representation of the Warwaruk Sozen and Siess formulation 12
Figure 2.5 Stress-strain curve corresponding to Mattock's formulation..... 18
Figure 3.1 Wire used in the study with specific labels ..... 19
Figure 3.2 Wires' indentations ..... 20
Figure 3.3 Specimen weight measurement ..... 21
Figure 3.4 Prestressing reinforcement surface geometrical feature ..... 22
Figure 3.5 Universal tensile testing machine ..... 26
Figure 3.6 Displacement measurement installation ..... 26
Figure 3.7 Gripping heads..... 27
Figure 3.8 Gripping section ..... 27
Figure 3.9 Specimen alignment examples ..... 28
Figure 3.10 Wire performance ..... 30
Figure 3.11 Experimental stress-strain curves ..... 34
Figure 4.1 Analysis and modeling procedure ..... 35
Figure 4.2 Stress-strain curve corresponding to the power formula. ..... 37
Figure 4.3 Regression relationship for constant $Kf_{py}$..... 40
Figure 4.4 Regression relationship for constant R..... 41
Figure 4.5 Regression relationship for constant $K^{*}f^{*}_{py}$ ..... 43
Figure 4.6 Regression relationship for constant $f^{*}_{py}$ ..... 44
Figure 4.7 Stress-Strain curve plot by redesigned power formula..... 46
Figure 5.1 Experimental stress-strain curves compared with current PCI strand 270 ksi and 250 ksi represented curves ..... 48
Figure 5.2 Offset method for determining yield point on experimental stress-strain curve ..... 50
Figure 5.3 Regression relationship for constant $f^{*}_{pu}$ ..... 54
Figure 5.4 Regression relationship for constant "a" ..... 55
Figure 5.5 Regression relationship for yield stress, $f^{\wedge}_{py}$..... 57
Figure 5.6 Stress-strain curves plotted by redesigned PCI equation ..... 61

Figure 6.1 Comparisons of WG wire experimental results and re-developed equations..... 65

# List of Tables

Table 3.1 Measured-wire properties ..... 24
Table 3.2 Comparison to manufacturer properties ..... 25
Table 3.3 Experimental reliable results ..... 31
Table 3.4 Experimental wire performance results ..... 33
Table 4.1 Parameters from modeling experimental stress-stain curve and percentage error ..... 38
Table 4.2 Parameters from regression analysis and the percentage error ..... 42
Table 4.3. Parameters and wire grade for the design-oriented power formula ..... 45
Table 5.1 Parameters evaluated from fitting experimental curves for the PCI equation ..... 52
Table 5.2 Parameters from regression analysis and percentage of variance ..... 56
Table 5.3 Proportional limit point ($\varepsilon^{\wedge}_{ps}$) with corresponding wire strength ($f^{\wedge}_{pu}$) ..... 59
Table 5.4 Parameters for designed PCI equation ..... 60
Table 6.1 Newly developed power formula design parameter for specific prestressing wire type and grade ..... 64
Table 6.2 Parameters or re-designed equations ..... 64

# Chapter 1 Introduction

Prestressed concrete is commonly used for bridges, buildings, pavement, and railroad ties because of economic advantages in cost, sustainability, service life, and environmental friendliness. In concrete standards, the ultimate-moment strength in flexural design is computed by finding the equilibrium of the internal force in the section, i.e. the compressive force in concrete and tension force in the steel strand reinforcement. The compressive force in concrete is typically computed using the equivalent rectangular behavior proposed by Whitney (1937). Whitney's stress block converts compressive stresses from parabolic stress distribution to rectangular stress block. To predict tension force in steel, one would generally apply the seven-wire, low-relaxation, prestressing strand equation from the PCI manual (2010), even in cases where prestressing wires are used instead of prestressing strands. The other way to deal with this issue is to use equations from the ACI 318-14 Code (2014), which are over conservative.

Considering both approaches lack sufficient accuracy, this research will provide an accurate estimation of the stress in prestressing wires through an experimental program and analytical modeling process. The actual stress-strain curves were collected through experimental testing of 13 different types of prestressing wires. Experimental results were then used for modeling the stress-strain curves using existing equations. As a result, a more precise prediction was achieved. Additionally, this research simplified the procedure for utilizing the equations, which offers convenience in practical application.

## Overview

This thesis is organized into six chapters. Chapter 1 gives a background about the research. Chapter 2 discusses previous literature studies in two parts: experimental testing and analytical models. Experimental testing focuses on the review of tensile testing. The analysis models review the "power formula" presented by Mattock (1979) and the general PCI seven-wire strand's equation (Precast / Prestressed Concrete Institute, 2010), which were modified from the Ramberg-Osgood equation. Furthermore, Chapter 3 covers details of testing specimens and experimental methodology, including wire specimens, testing machine, measuring extensometer, tensile testing setup, and test performance and procedure. Each test is presented in graphical and tabular form for further analysis. Chapter 4 focuses on discussing the modeling procedure and results using the power formula. Chapter 5 focuses on discussing the PCI equation, including the

modeling process and performance. Lastly, Chapter 6 concludes design recommendations using the two equation types that will be offered for use in future design.

## Objectives

In the computation of tension force in flexural design, it is common to calculate the average stress in prestressing steel at ultimate load capacity, $f_{ps}$, using the PCI (2010) seven-wire, low-relaxation, prestressing strand equation or the ACI318 (2014) equations, instead of pursuing the real behavior of prestressing wires. The existing equations either overestimate the stress in prestressing wires or provide highly conservative predictions. This results in applying extra/less tension force, which in turn results in reducing/increasing the compression force while maintaining equilibrium. Therefore, the primary objective of this research was to investigate individual and average prestressing wires' stress from actual stress-strain curves, using experimental data to modify the existing PCI strand equation and power formula. The modified equations could determine more accurate $f_{ps}$ for prestreesing wire in ultimate strength design.

## Scope

To achieve the research objectives, the scope of work includes both experimental and analytical programs. Literature related to tensile testing and existing equations of average prestressing stress was reviewed. The equation review included a summary of the evolution of the power formula and the PCI seven-wire strand equation. Both formulas were modified from the Ramberg and Osgood equation published in 1943 (Ramberg & Osgood, 1943).

The experimental tensile test requirements follow the ASTM A881 standard specification for mechanical properties of prestressing steel wire. A universal testing machine was used with two extensometers for the tension test. Trapezium material-testing software (Shimadzu, 2009) was applied to record and collect data every 0.5 second. Furthermore, a tensile test was applied to 13 different types of prestressing wires, and this research program intends to keep three reliable data curves for each prestressing wire broken within the extensometer measure range for each type of wire. If the wire broke outside the extensometer measure gage length, such as at the chuck jaw, the stress-strain curve data was discarded.

The analytical program was applied after the experimental data was collected. The experimental load versus displacement data was interpolated based on wire elongation at 0.1% strain interval until failure was achieved. Then, by converting the results into stress and strain,

the stress-strain curves were plotted. Also the modulus of elasticity ($E_p$), yield stress and strain ($f_{py}$ and $\varepsilon_{py}$), and ultimate stress and strain ($f_{pu}$ and $\varepsilon_{pu}$) were redefined according to the experimental data. Afterwards, the various equation parameters were correlated through regression analysis, and the regression expressions of excellent correlations were used to solve for the constants of the equations. These newly developed equations can be used when the wire type and grade is known priori. They may also be used for quality control purposes. In addition, the same equations were re-developed for design-oriented computations when the level of ultimate prestressing stress was specified or assumed.

# Chapter 2 Literature Review

Chapter two serves as a background search for the analytical and experimental program. This chapter discusses the mechanical properties and performance of wires and strands, in addition to equations computing average stress in prestressed steel up to ultimate capacity.

## 2.1 Experimental Testing of Prestressing Wire

It is important to understand mechanical properties of various materials due to the large number of materials with completely unlike characteristics used for construction. If the individual physical characteristics are understood and quantified, structural members and components could be designed more accurately for the purpose of preventing unacceptable levels of deformation and failure. Thus, it is necessary to know not only design theories and processes, but also features of materials the design is using.

Tension testing is a designed laboratory experiment that duplicates service conditions, and the experimental results present the mechanical behavior on a graph (Callister, 2007). Test results are displayed as nominal stress versus nominal strain, as "the mechanical behavior of a material reflects the relationship between its response or deformation to an applied load or force" (Callister, 2007). Tensile testing slowly applies incremental axial (quasi-static) load to specimen materials that primarily respond in uniaxial tension. The experimental process is continued with increased uniaxial load until reaching a desired level of deformation or the test specimen is fractured. In addition, the material’s deformation involves several stages before breakage, including un-deformed state, elastic point, yield point, strain hardening, maximum stress point, and failure, shown in Figure 2.1 (Byars, Snyder, & Plants, 1925). During the tensile test, the applied load is measured by a load cell, and the resulting material ductility is recorded by attached extensometer or strain gage.

Tensile testing results are primarily used for engineering design and quality control by the producer, user, and designer. In the engineering design process, the failure theory is based on ultimate strength (concrete-compressive and steel-tensile strength), or serviceability that relates to deflection, cracking, or vibration. In addition, material use and selection is important to ensure material properties are strong and rigid enough to withstand actual loads under a variety of conditions. Material characteristics may be sensitive to size and shape of specimen, time, temperature, and condition of the testing machine. In order to avoid factors that will influence

the testing result, experiments follow common standards and procedures which have been published by the American Standard of Testing Materials (ASTM) International (ASTM E8/E8M, 2015).

### 2.1.1. Stress-Strain Curve

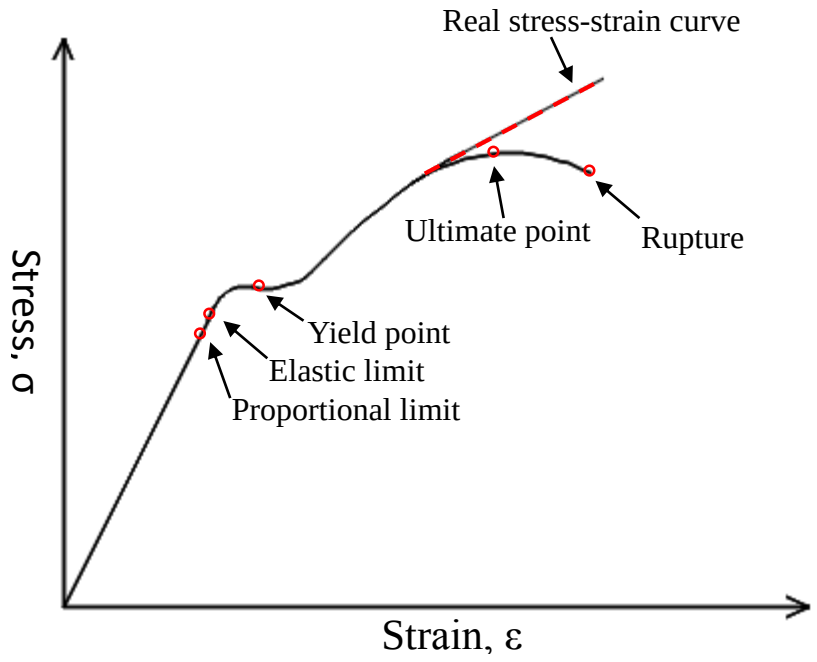


Figure 2.1 Stress-strain curve

"It is desirable to plot the data, results of tensile testing, of the stress-strain curve if the results are to be used to predict how a metal will behave under other forms of loading" (ASTM International, 2004). Stress-strain curve is the output of tensile testing and it describes two important concepts: mechanics of materials and mechanics of deformable bodies. The stress-strain is usually plotted as load/force corresponding to elongation, with the stress along the y-axis and the strain along the x-axis.

The nominal stress, σ, is defined as

$$\sigma = \frac{\text{Load}}{\text{Original area}} = \frac{P}{A_o} \qquad \text{Equation (2-1)}$$

The nominal (engineering) strain, ε, is defined as

$$\varepsilon = \frac{\text{Deformed length} - \text{Initial length}}{\text{Initial length}} = \frac{l_i - l_o}{l_o} = \frac{\Delta l}{l_o} \qquad \text{Equation (2-2)}$$

The basic curve can be divided into two regions: elastic and plastic. In basic engineering design, the material starts in linear elastic region. In the elastic region, the tensile stress is proportional to the strain with the constant of proportionality, and the stress-strain curve is linear. This linear relationship was found by Sir Robert Hooke in 1678, which is also called Hook's law, and most materials comply to Hook's law with reasonable approximation in the early portion of the stress-strain curve (Beer, Johnston, DeWolf, & Mazurek, 2015).

$$\sigma = E\varepsilon \qquad \text{Equation (2-3)}$$

### 2.1.2. Modulus of Elasticity

The constant of proportionality is the modulus of elasticity, or Young's modulus "E," and the elastic modulus can also be described as the slope of the linear portion of the stress-strain curve. The elastic modulus represents the material's stiffness. For example, the greater the modulus, the more stiff the material. The elastic modulus decreases while its load crosses over the elastic limit into the plastic range. Furthermore, the elastic modulus is a significant design parameter for determining elastic displacement, since the material will return to its original shape after the stress is released. However, for some materials (e.g. rubber and many polymers), the elastic deformation is nonlinear so the elastic modulus could not be defined to follow the above theory (Callister, 2007). In current ASTM standards, the modulus of elasticity for the seven-wire, low-relaxation, prestressing strand is 28500 ksi (196.5E3 MPa), 29000 ksi (199.9E3 MPa) for prestressing wire, and 30,000 ksi (206.8E3 MPa) for prestressing bar (ASTM A881/A881M, 2015).

The elastic modulus, E, is defined as

$$E = \frac{\Delta\sigma}{\Delta\varepsilon} \qquad \text{Equation (2-4)}$$

When estimating the elastic modulus, stress and strain are relatively small or less than the elastic limit, or the proportional limit. In the transition of elastic-plastic deformation, the first deviation from linearity of the stress-strain curve is called the proportional limit or yield point (Byars, Snyder, & Plants, 1925).

### 2.1.3. Yield Point

As stated in the ASTM A370 standard, "Yield point is the first stress in a material, less than the maximum obtainable stress, at which an increase in strain occurs without an increase in stress" (ASTM A370, 2014). Beyond the yield point, or plastic region, the material deformation is plastic or permanent, and the stress is no longer proportional to the strain (Callister, 2007). The yield point is an important tensile property, since it is desirable to know whether or not the structure has the capability to function where and when yielding occurs. "If the stress-strain diagram is characterized by a sharp knee or discontinuity," the yield point can be determined by one of the following methods according to ASTM A370 (2014):

a) Drop-of-the-beam or halt-of-pointer method
b) Autographic-diagram method
c) Total extension-under-load method (EUL)

When the tested material does not exhibit a clear yield point, the EUL method with a recorded machine may be the proper approach. When applying this approach, the yield point is not more than 80 ksi (551.58 MPa) and total extension is limited to approximately 0.005 in (0.127 mm) (ASTM A370, 2014). For the exception, if the force is beyond 80 ksi (551.58 MPa), the limiting total extension should be increased as mentioned in ASTM A370 (2014).

### 2.1.4. Yield Strength

It is hard to define the yield point, because some materials lack the existence of a sharp knee or discontinuity. Hence the deviation from the proportionality of stress to strain could be indicated by the offset method, or stress at around 1% strain.

The offset method is accomplished by constructing the straight line of slope E (line AC in Figure 2.2) and drawing the line BD parallel to line AC, spaced by the proper amount of permanent strain (AB) — 0.2% being commonly applied for most metallic materials (ASTM A370, 2014). Then, yield strength, $\sigma_y$, is located by finding point E, which is on the intersection of the line BD and stress-strain curve as it bends through the inelastic range. This construction is shown in Figure 2.2, with point F representing the value of yield strength.

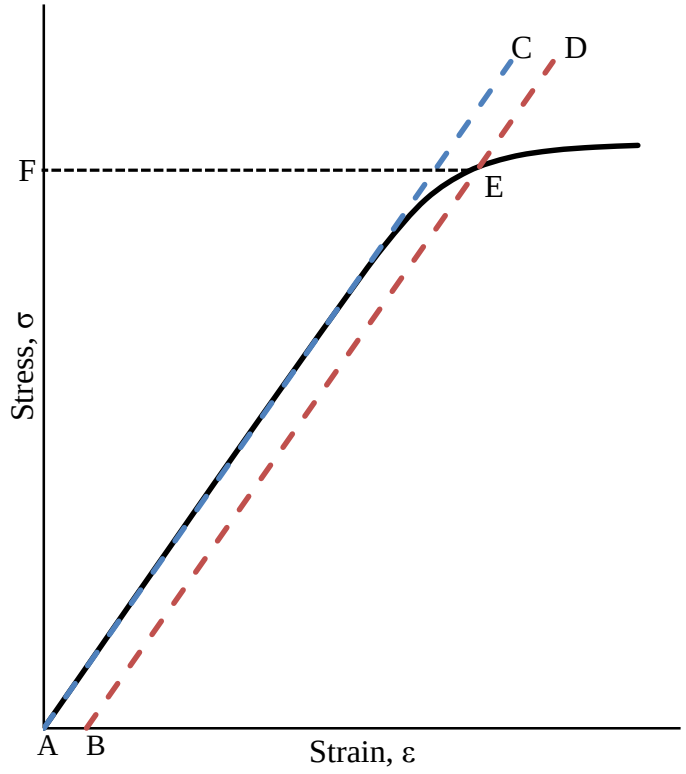


Figure 2.2 Offset method for determination of yield strength on σ-ε curve

Additionally, in ASTM A881 — the “standard specification for steel wire, indented, low-relaxation for prestressed concrete railroad ties”, specifically identifies yield strength for this type of prestressing wire to fall at the load corresponding to 1% extension (ASTM A881/A881M, 2015).

### 2.1.5. Ultimate Tensile Strength

The stress-strain curve continues to develop after yielding and plastic deformation of the material, until reaching maximum stress before decreasing to eventual fracture. Ultimate strength, $\sigma_u$, is the highest point on the stress-strain curve and is the strength the structure can sustain in tension (Whitney, 1937). After the material reaches the uppermost point on the stress-strain curve, necking phenomenon initiates. Necking occurs shortly before final rupture. The material's cross-sectional area reduces, and the specimen becomes weakened during the necking process (Byars, Snyder, & Plants, 1925). Therefore, the applied load drops promptly until fracture. Rupture stress/strength is not always the same as ultimate stress/strength, depending on some material factors. Rupture stress is the stress at the time of rupture, but this stress “is not

usually an important quantity for design standpoint" according to Byars, Snyder and Plants (1925).

## 2.2 Analytical Models for Wires and Strands

Many analytical expressions have been developed for modeling the stress-strain curve of concrete or reinforcing steel. However, the number of expressions developed for prestressing steel, especially prestressing wire, is limited. Current ACI (2014) and PCI (2010) estimations provide very conservative predictions for prestressing wire, resulting in an "erroneous estimate of deformations and deflections" (Naaman, 1985). Additionally, PCI estimations were originally intended for use with seven-wire, low-relaxation, prestressing strand. Various investigations have shown a more accurate estimation of average stress in prestressing steel ($f_{ps}$) between various formulations and experimental results (Naaman, 1985).

The most common assumption of ultimate flexural strength analysis is related to the stress-strain distribution in the concrete, or the stress in steel for reinforced or prestressed concrete shown in Figure 2.3.

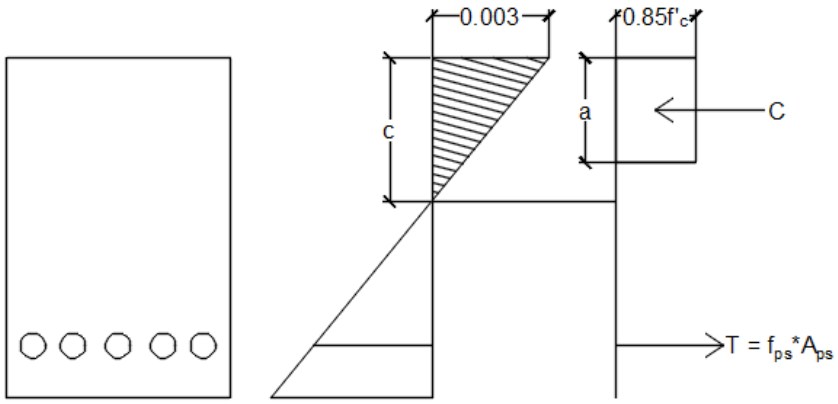


Figure 2.3 Rectangular stress distribution in ultimate strength analysis

In the ACI code, average stress in prestressing steel at ultimate flexural capacity, $f_{ps}$, is usually found by applying the approximate equation in ACI 318 (2014) with specific limitations, which are defined as

$$f_{ps} = f_{pu}\left\{1 - \frac{\gamma_p}{\beta_1}\left[\rho_p \frac{f_{pu}}{f_c'} + \frac{d}{d_p}(\omega - \omega')\right]\right\} \qquad \text{Equation (2-5)}$$

$d_p$ = distance from extreme compression fiber to centroid of prestressing steel, in.
$f_{pu}$ = tensile strength of prestressing steel, psi.

$\gamma_p$ = factor for type of prestressing steel (0.55 for $f_{py}/f_{pu} \geq 0.8$; 0.4 for $f_{py}/f_{pu} \geq 0.85$; and 0.28 for $f_{py}/f_{pu} \geq 0.9$)

$\beta_1$ = factor relating depth of equivalent rectangular compressive stress block to neutral axis depth

$\omega$ = tension reinforcement, $\rho f_y / f_c'$

$\omega'$ =compression reinforcement, $\rho f_y' / f_c'$

Equation (2-5) is the estimated stress in bonded tendons and the stress in prestressing steel after allowance losses ($f_{se}$), which should not be less than half of ultimate strength ($f_{pu}$) (American Concrete Institute, 2014). Furthermore, the PCI seven-wire, low-relaxation prestressing strands equation is another option for estimating stress in prestressing steel. It is defined as follows (Precast / Prestressed Concrete Institute, 2010):

for the 270 ksi strand,

$$\varepsilon_{ps} \leq 0.0086 \qquad f_{ps} = E\varepsilon_{ps} \qquad \text{Equation (2-6) and}$$

$$\varepsilon_{ps} > 0.0086 \qquad f_{ps} = 270 - \frac{0.04}{\varepsilon_{ps} - 0.007} \qquad \text{Equation (2-7);}$$

and for the 250 ksi strand,

$$\varepsilon_{ps} \leq 0.0076 \qquad f_{ps} = E\varepsilon_{ps} \qquad \text{Equation (2-8) and}$$

$$\varepsilon_{ps} > 0.0076 \qquad f_{ps} = 250 - \frac{0.04}{\varepsilon_{ps} - 0.064} \qquad \text{Equation (2-9);}$$

where E is 28,500 ksi (196.5E3 MPa), and the minimum yield strength is at 1% elongation. Yield strength is estimated as 90% of ultimate strength of strand. The elastic limit is located at a strain of 0.0086 for 270 ksi strand (1,862 MPa) and 0.0076 for 250 ksi strand (1,724 MPa) (Precast / Prestressed Concrete Institute, 2010).

For improving the perdition of curvature and corresponding stress/strain response, a

nonlinear analysis may be followed (Naaman, 1985). Nonlinear analysis requires the experimental stress-strain curves or "an accurate analytical representation of the curves" in order to have a more precise estimation of the stress-strain curve and various key parameters defining it (Naaman, 1985). Typical characteristics of prestressing steel do not have an obvious yield point, but rather a curve gradually transitioning from elastic to inelastic response. Most stress-strain curves in prestressing steel are represented by two straight lines with two or more parameters describing its bilinear response. Other curves are divided into three parts: a linear part, "a sharply curved part in the vicinity of the nominal yield point, and an almost linear but slightly strain-hardening part reaching to failure" as described by Mattock (1979).

### 2.2.1. Ramberg-Osgood (1943)

The stress-strain curve has generally been reproduced through several empirical equations. The most common and earliest version used to conduct a cyclic stress-strain curve is the Ramberg-Osdoog relationship. The Ramberg-Osgood equation was proposed by Walter Ramberg and William Osgood in 1943. This relationship could be used for describing the behavior of various materials and systems exhibiting elastic-plastic response. Accordingly, this expression has been widely used in many engineering applications, such as the development of moment-curvature relationship, the perdition of cyclic deformation, and determination of structural deflection and numerical modeling of the stress-strain relationship (Abdella, 2012). The formulation gives a smooth continuous curve with a spine curve in the transition region, which is the best expression for the stress-strain behavior of metals without a clear yield point.

The expression is defined as (Ramberg & Osgood, 1943):

$$\varepsilon = \frac{f}{E} + K\left(\frac{f}{f_y}\right)^n \qquad \text{Equation (2-10),}$$

where K and n are constants for a particular metal type. The equation involves modulus of elasticity (E) and yield strength ($f_y$). It was originally developed for examining the stress-strain curve of aluminum alloy, but it has proven appropriate for developing the stress-strain curve of other nonlinear metals (Rasmussen, 2006).

### 2.2.2. Warwaruk Sozen and Siess (1962)

Miscellaneous enhanced versions of the Ramberg-Osgood relationship have improved its accuracy of stress-strain relationship. In 1962, Warwaruk Sozen and Siess proposed the progressively improved version of analytical relations for prestressing steel (Naaman, 1985):

$$\boldsymbol{f \le f_p} \qquad \boldsymbol{f = E\varepsilon} \qquad \text{Equation (2-11),}$$

$$\boldsymbol{f_p < f \le f_l} \qquad \varepsilon = \frac{f}{E} + K\left(f - f_p\right)^n \qquad \text{Equation (2-12), and}$$

$f_l$ : stress defining the start of the second linear portion.

Warwaruk Sozen and Siess redefined the nonlinear section of the stress-strain curve, which changes from $f_p$ to $f_l$ instead of the yielding point. They divided the curve into three parts shown in Figure 2.4. The first region is below the proportional limit strength ($f_p$), which is a linear relationship. The second region is from the proportional limit strength ($f_p$) to the starting point of the second linear section ($f_l$). There are two constants, K and n, and n determines the sharpness of the curve of the stress-strain diagram. The last region is from the starting point of the second linear section ($f_l$) to ultimate strength ($f_u$), assuming a linear relationship (Naaman, 1985).

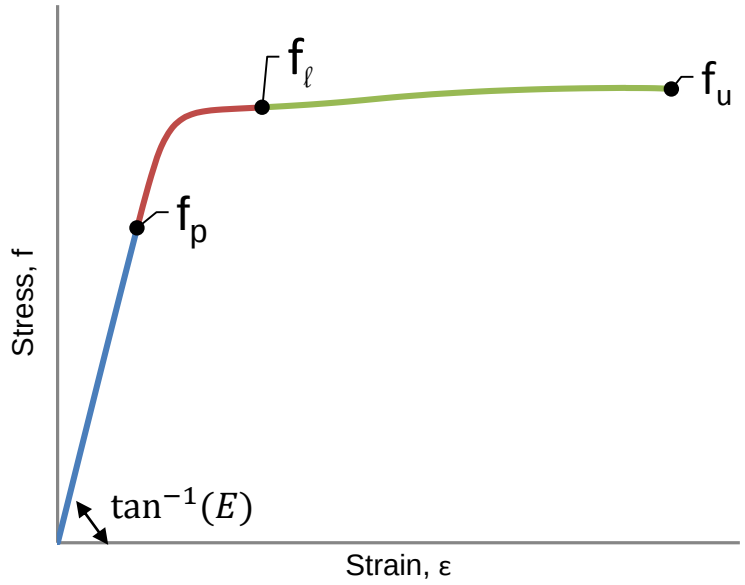


Figure 2.4 Stress-strain graphical representation of the Warwaruk Sozen and Siess formulation

### 2.2.3. Goldberg and Richard (1963)

In considering safety of structures, Goldberg and Richard's approach is based on limiting stress and more accurate estimations of ductile materials, resulting in preventing failing and raising the level of safety. In 1963, Goldberg and Richard provided an equation form to represent the stress-strain behavior of prestressing steel. This equation intends to simplify the mathematical expression, while providing accuracy of the stress-strain relationship (Goldberg & Richard, 1963). The Goldberg and Richard relationship "corresponds essentially to the inverse of Ramberg-Osgood polynomial representation of the stress-strain relationship," related to the Ramberg-Osgood polynomial shown in Equation (2-13) (Goldberg & Richard, 1963). Moreover, the inverse relationship is suitable for expressing the monotonic stress-strain relationship taking place in materials without a distinct yield point (Goldberg & Richard, 1963). The Goldberg and Richard relationship is shown in Equation (2-14):

$$\varepsilon = \frac{f}{E} + \frac{3}{7}\frac{\varepsilon_o}{E}\left(\frac{\varepsilon}{\varepsilon_o}\right)^n \qquad \text{Equation (2-13)}$$

E is initial modulus of elasticity.
$\sigma_o$is stress at 0.7E.
n is the coefficient determining the shape of the stress-strain curve.

$$f = \frac{E\varepsilon}{\left[1 + \left(\frac{E\varepsilon}{f_u}\right)^R\right]^{1/R}} \qquad \text{Equation (2-14),}$$

where E is the initial modulus of elasticity.

In Equation (2-14), R is the parameter defining the general nonlinear relationship between the stress (f) and strain (ε) (Goldberg & Richard, 1963). Parameter R, when chosen appropriately, has the ability to represent "a wide range of stress-strain curves with an acceptable degree of accuracy," and a higher degree of nonlinearity may be possible when including strain-hardening effects (Goldberg & Richard, 1963).

### 2.2.4. Giuffrè and Pinto (1970)

The improved approach was suggested by Giuffrè and Pinto (Equation (2-15)), and the relationship is similar to Ramberg and Osgood's equation by discovering stress from nominalized stress ($f^*$) (Bosco, Ferrara, Ghersi, Marino, & Rossi, 2014).

$$f^* = \frac{\varepsilon^*}{(1 + |\varepsilon^*|^R)^{1/R}} \qquad \text{Equation (2-15)}$$

The relationship includes normalized stress ($f^*$) and strain ($\varepsilon^*$), and it replaces the uniaxial stress (f) and strain epsilon. The normalized stress and strain are

$$\boldsymbol{f^* = \frac{f}{f_y}}; \qquad \text{Equation (2-16) and}$$

$$\boldsymbol{\varepsilon^* = \frac{\varepsilon}{\varepsilon_y}} \qquad \text{Equation (2-17),}$$

which are for the curve of first loading or the virgin envelope curve (Bosco, Ferrara, Ghersi, Marino, & Rossi, 2014). The normalized stress and strain after the first unloading could be presented as

$$f^* = \frac{f - f_r}{2f_y} \qquad \text{Equation (2-18) and}$$

$$\varepsilon^* = \frac{\varepsilon - \varepsilon_r}{2\varepsilon_y} \qquad \text{Equation (2-19),}$$

where $\varepsilon_r, f_r$ are the last reversal point.

After applying the normalized stress and strain from the first loading into Equation (2-15), the equation may be alternatively expressed as follows:

$$f = \frac{E\varepsilon}{\left[1 + \left|\frac{E\varepsilon}{f_y}\right|^R\right]^{1/R}} \qquad \text{Equation (2-20)}$$

This enhanced approach is "suggested to describe the behavior of elasto-perfectly plastic steel," which is a material that does not harden (Albanesi & Nuti, 2007).

### 2.2.5. Menegotto and Ponto (1973)

In 1973, Menegotto and Ponto proposed the model which is used to simulate the cyclic response of reinforcing bar (Bosco, Ferrara, Ghersi, Marino, & Rossi, 2014). Menegotto and Ponto enhanced the previous version of the model that Giuffrè and Pinto published in 1970, "taking into account the kinematic hardening feature of the response" (Bosco, Ferrara, Ghersi, Marino, & Rossi, 2014).

$$f = (E_o - E_\infty)\frac{\varepsilon_s}{\left(1 + \left(\frac{\varepsilon_s}{\varepsilon_o}\right)^R\right)^{1/R}} + E_\infty \varepsilon_s \qquad \text{Equation (2-21)}$$

The general Menegotto and Ponto approach is written as Equation (2-21), and represents the stress-strain curve transition from one straight-line asymptote with initial slope ($E_o$) to another line asymptote with slope ($E_\infty$), which equals zero (Bosco, Ferrara, Ghersi, Marino, & Rossi, 2014). In addition, if the strain ($\varepsilon_s$) is infinite, the relationships between initial tangent modulus to secondary tangent modulus are presented as

$$f = E_\infty \varepsilon_s + (E_o - E_\infty) \qquad \text{Equation (2-22)}$$

Equation (2-21) could be written in dimensionless form, which is used to illustrate the cyclic response.

$$f^* = (1 - b)\frac{\varepsilon^*}{\left(1 + \varepsilon^{*R}\right)^{1/R}} + b\varepsilon^* \qquad \text{Equation (2-23)}$$

The normalized stress and strain are

$$f^* = \frac{f}{f_o} \qquad \text{Equation (2-24) and}$$

$$\varepsilon^* = \frac{\varepsilon}{\varepsilon_o} \qquad \text{Equation (2-25),}$$

where $f_o$ is the yield stress and $\varepsilon_o$ is the yield strain (Menegotto & Pinto, 1973). Menegotto and Ponto defined the stress and strain as normalized by yield point instead of ultimate point. Then Equation (2-23) can be expressed as

$$f = E\varepsilon\left[b + \frac{1-b}{\left(1+\left(\frac{\varepsilon E}{f_y}\right)^R\right)^{1/R}}\right] \quad \text{Equation (2-26)}$$

The formulation could predict the behavior of prestressing steel with an improved approximation. The included constant b is the strain-hardening ratio, which determines the slope of the hard-working line. Furthermore, the constant R decides the shape of the transition curve and reflects the Bauschinger effect (Menegotto & Pinto, 1973).

$$b = \frac{E_\infty}{E_o} \quad \text{Equation (2-27)}$$

$$R(\xi) = R_o - \frac{a_1\xi}{a_2+\xi} \quad \text{Equation (2-28)}$$

In Equation (2-27), $E_\infty$ is the second modulus of elasticity happening beyond the transition curve, and $E_o$ is the initial Young's modulus. In Equation (2-28), $R_o$ is the value of parameter R during first loading, and $a_1$ and $a_2$ are determined through experimental results (Bosco, Ferrara, Ghersi, Marino, & Rossi, 2014). R is influenced by the plastic excursion $\xi$, which is the difference of strain between the current loading path intersected on the previous loading and unloading paths (Bosco, Ferrara, Ghersi, Marino, & Rossi, 2014).

### 2.2.6. Naaman (1977)

Two ways to obtain the value $f_{ps}$ are to use a single equation or multiple polynomial equations. Naaman discussed a more precise approach in 1977, where he estimated the stress-strain curve of prestressing steel through three numerical equations — two linear equations representing initial and finial region of the curve, and one non-linear equation representing the transition region (Naaman, 1977). Naaman's approach was to lower the maximum error down to 0.4% compared with the actual experimental curve (Naaman, 1977). However, Naaman's approach is designed by "using a computer to solve the equations of equilibrium and compatibility" when "the stress-strain curve for prestressing steel was expressed algebraically" (Mattock, 1979).

## 2.2.7. Mattock (1979)

Naaman's approach was closer to the experimental results, but it was more complicated to use in design or in checking the material response quality by engineers or manufactures. Thus the other approach, a single equation as suggested by Mattock, may be more suitable for applying in design or quality control analysis. Mattock's equation is a modified version of Menegotto and Ponto's model. This formulation is also called the "power formula" because it can closely represent the stress-strain relationship for any type of prestressing steel with only 1 percent error or lower compared to the actual number of stress-strain curves used (Mattock, 1979). Equation (2-23) has been adopted to predict the stress-strain curve of prestressing wire by introducing the following equations:

$$f_o = Kf_{py} \qquad \text{Equation (2-29), and}$$

$$\varepsilon_o = \frac{Kf_{py}}{E} \qquad \text{Equation (2-30)}$$

where K is a coefficient, and $f_{py}$ is the yield strength of prestressing steel. Then the equation becomes

$$f_{ps} = E\varepsilon\left[Q + \frac{1-Q}{\left(1+\left(\frac{\varepsilon E}{Kf_y}\right)^R\right)^{1/R}}\right] \qquad \text{Equation (2-31),}$$

where R is the constant determined by solving Equation (2-31) when the ε is at the yielding point (ε=0.01) and $f_{ps} = f_{py}$ (Mattock, 1979). Q is the slope in the third part of the curve, expressed as

$$Q = \frac{f_{pu} - Kf_{py}}{\varepsilon_{pu}E - Kf_{py}} \qquad \text{Equation (2-32),}$$

where $f_{pu}$ and $\varepsilon_{pu}$ are the ultimate tensile strength and strain of prestressing steel.
Equation (2-31) "can be made to correspond very closely to actual stress-strain curves" if the value of coefficient K, Q, and R is properly evaluated (Mattock, 1979). It is important to realize the constants Q and K should be solved prior to finding the constant R. To determine K, the

intersection of the two linear parts of the stress-strain curve is sought as shown in Figure 2.5 (Mattock, 1979).

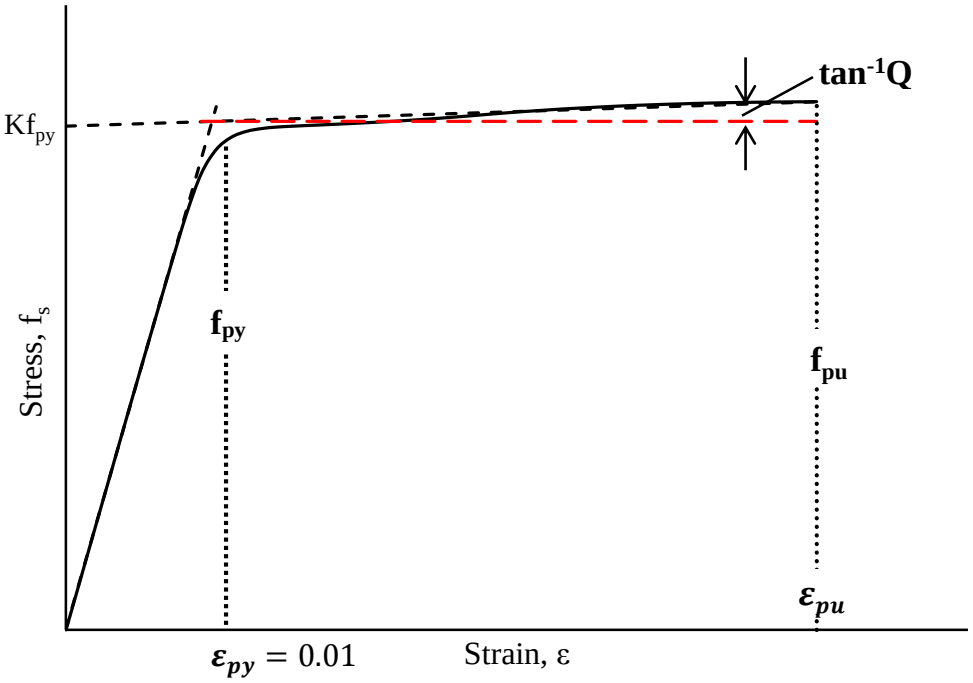


Figure 2.5 Stress-strain curve corresponding to Mattock's formulation

When a complete stress-strain curve is missing from experiments, K could be assumed as 1.04 for a seven-wire strand (Mattock, 1979). Then, the Q and R constants can be determined for a particular prestressing steel, once the yield point and ultimate point are fully estimated.

On the other hand, Naaman (1985) gives slightly unlikely parameters by applying Equation (2-20) and Equation (2-31) under the ASTM standard and actual behavior. Naaman confirmed these parameters through various trials of numerical values for different prestressing steels (Naaman, 1985). Several authors, such as Mattock (1979), Naaman (1977), and Menegotto and Ponto (1973) claim the power formula is the closest fit formulation to simulate the stress-strain relationship for prestressing steel. Parameters E, K, Q, and R are important factors to directly and accurately determine preciseness of the curves. The detail coefficient under different constraints is referred to in "Partially Prestressed Concrete: Review and Recommendations" by Naaman (1985).

# Chapter 3 Experimental Program

The purpose of this testing program was to develop tensile stress-strain curves for low-relaxation prestressing wires to be a quality control guideline and design aid. Also, it will be used to check whether the steel wire used for prestressed concrete railroad ties attains and satisfies the mechanical property requirements in the ASTM A881/A881M-15 standard (ASTM A881/A881M, 2015).

## 3.1 Wire Specimens

A total of 13 types of 5.32-mm-diameter reinforcement wires were considered. These were obtained from six prestressing wire manufacturers around the world. Each of the wires had various indentation patterns — smooth, chevron, spiral, diamond, two-dot, and four-dot. The wire reinforcements were generally labeled as [WA] through [WM], as shown in Figure 3.1: from left to right in alphabetical order. Figure 3.2 shows the indentation of each wire under microscope observation.

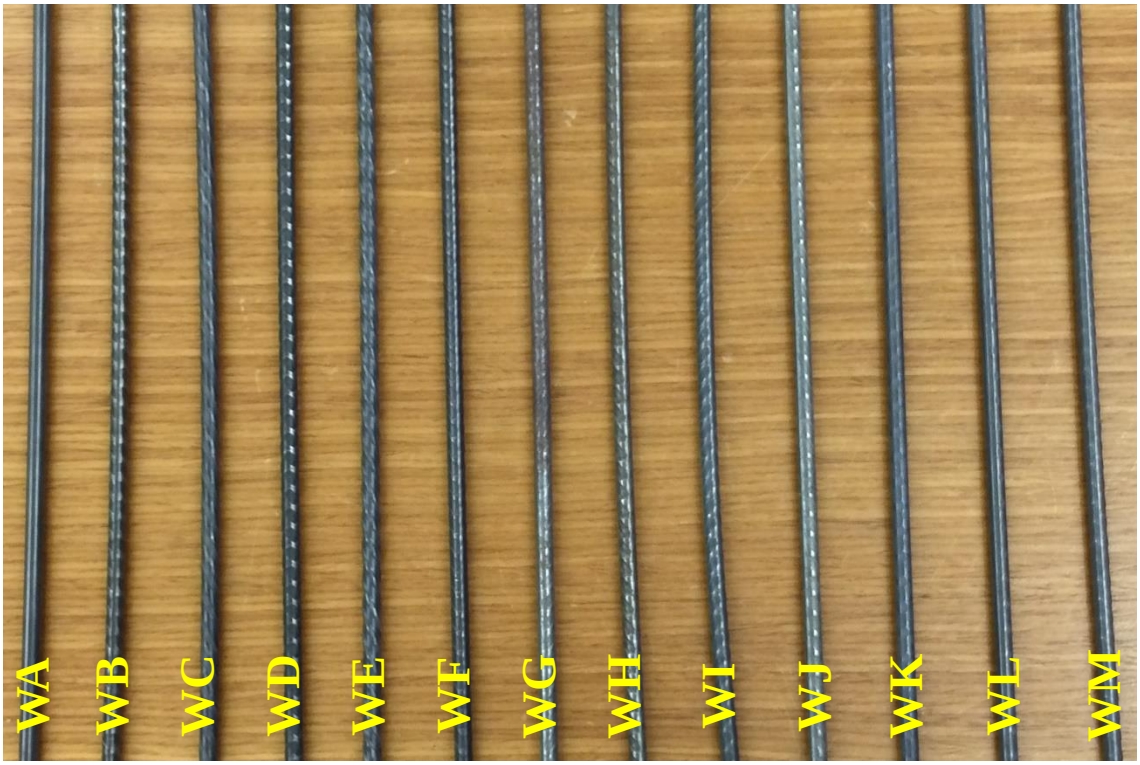


Figure 3.1 Wire used in the study with specific labels

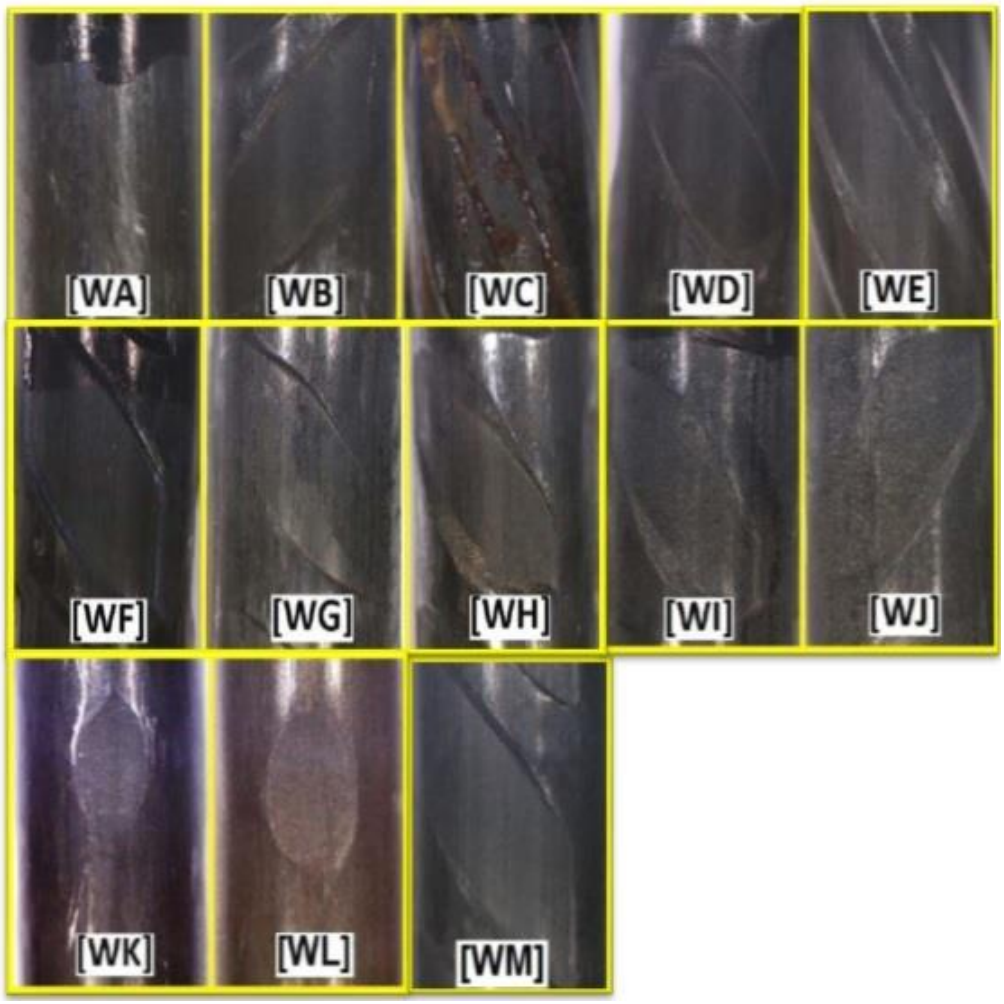


Figure 3.2 Wires' indentations
Adapted from "Improving Pre-Stressed Reinforcement for Concrete Railroad Ties via Geometrical Dimensioning and Tolerancing" by M. D. Hayness (2015).

The general prestressing wire geometric property was a 0.2094-inch nominal diameter and a 0.0344-in$^2$ nominal area, according to ASTM A881M (2015). However, the wire diameter and area varied depending on the shape and character of the indentations (ASTM A881/A881M, 2015). In order to sustain the accuracy of the testing result, the nominal area of prestressing wire was calculated as

$$A = \frac{W}{L \times \rho} \qquad \text{Equation (3-1)}$$

A = nominal area of prestressing wire (in$^2$)

W = weight of prestressing wire (lb)

L = length of prestressing wire (in)

$\rho$ = density of prestressing wire, 0.2836 lb/in$^3$ (weight of one-in$^3$ steel)

The length of prestressing wire was measured by a Vernier Caliper, using hands to push prestressing wire down for vertical alignment and a metal block for horizontal alignment. The direct reading of measurement was precise down to thousandths of a decimal point as shown in Appendix A. 10 Weight of prestressing wire was measured by a Scientech electronic balance with precision to ten thousandths of a point (Figure 3.3). The measurement results are presented in Table 3.1.

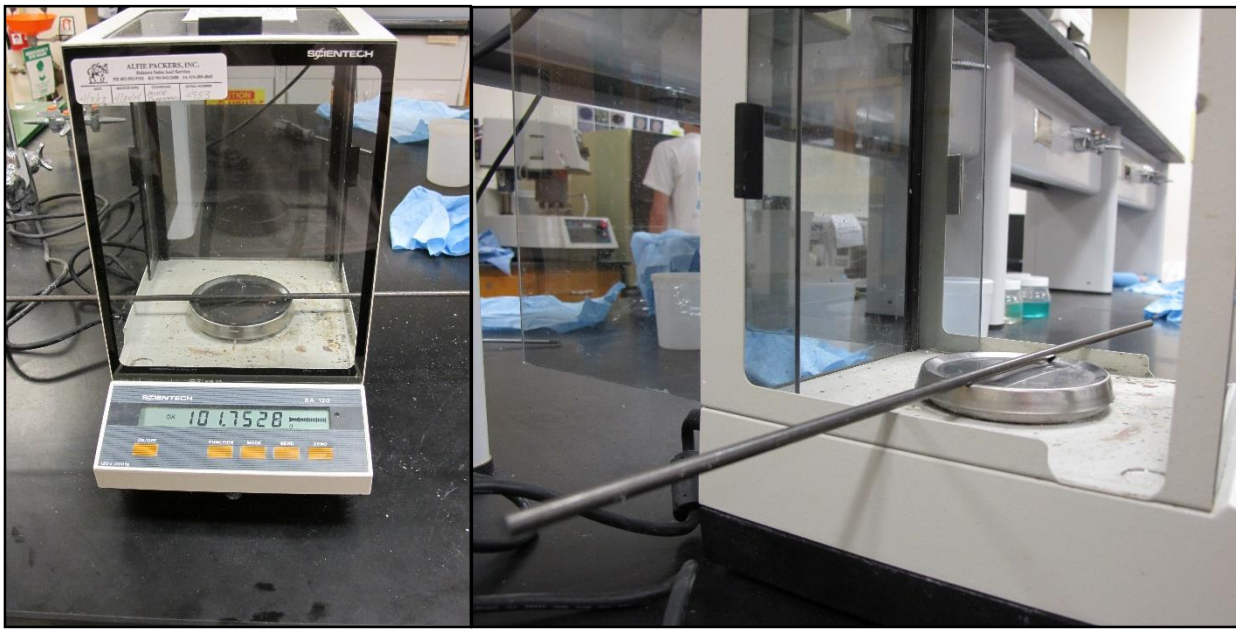


Figure 3.3 Specimen weight measurement

Furthermore, actual wire-indent geometries were measured by graduate student Mark Haynes, who was focusing on discovering the influence of a surface feature of prestressing wire to concrete bond in railroad ties at Kansas State University. The wire-indent measurement presented in Table 3.1 refers to “Improving Prestressed Reinforcement for Concrete Railroad Ties via Geometrical Dimensioning and Tolerancing” by Mark Haynes (Haynes M. D., 2015). Note the smooth wire (WA) did not have indentation. The spiral wires (WC and WE) did not have nominal length and pitch, because the wire did not have individual indentation. Dimensions of the prestressing wire are presented in Figure 3.4.

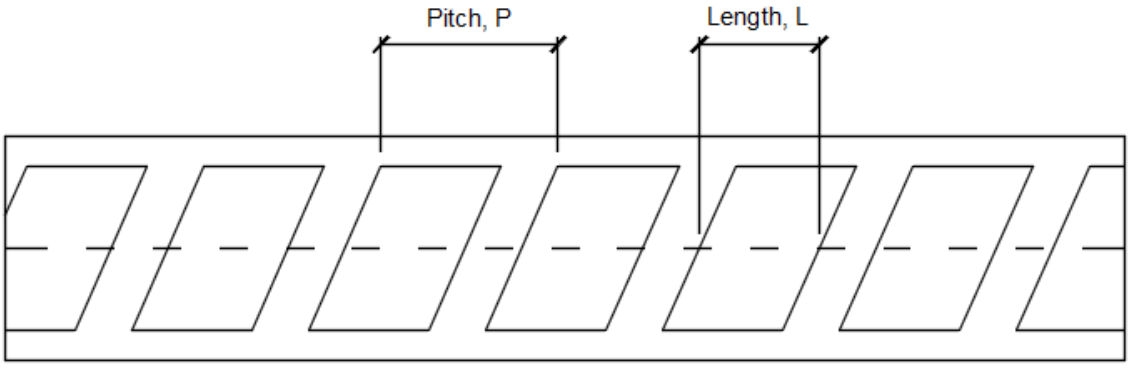


**Top view of wire**

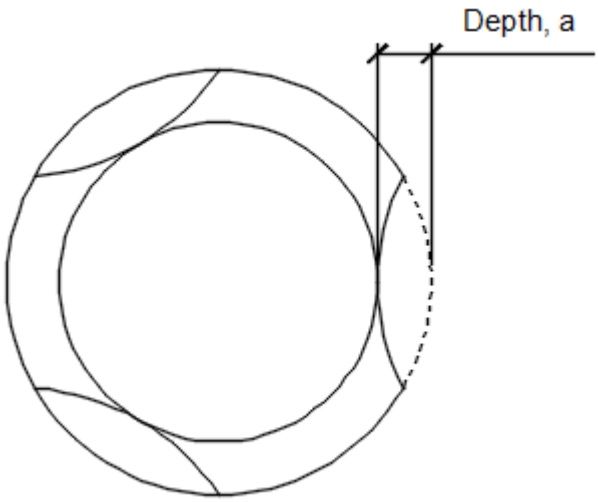


**Cross-section view of wire**

Figure 3.4 Prestressing reinforcement surface geometrical feature

The measured wire property data is shown in Table 3.1 and the comparisons of wire properties is presented in Table 3.2. The diameter, as determined by weight of the indented wire, did not vary out of the range ± 0.003-inch of nominal diameter (0.2094 in) as stated in ASTM A881M. In addition, Table 3.2 also shows the difference between the nominal area and diameter by comparing the calculated wire properties to the data from Mill Certs. The difference ranged from 0.32% to 6.67% for the nominal area, and 0.16% to 3.39% for the nominal diameter. Even though the wire properties had differences compared to the manufacturer-listed results, all testing wire properties were qualified ASTM A881M requirements.

In this testing protocol, gage length was eight inches long, and overall specimen length was approximately 18 inches, including the gripping section. A total of 13 types of prestressing wires

and eight specimens for each type of wire were needed in order to get at least three test results where the wire broke within the gage length. Thus a total of 104 specimens, with 18-inch-long prestressing wires, were prepared.

Table 3.1 Measured-wire properties

| **Wire label** | **Indentation types** | **Indent depth ,in. [mm]** | **Nominal length ,in. [mm]** | **Nominal pitch ,in. [mm]** | ***Measured-wire properties*** | | | | |
|---|---|---|---|---|---|---|---|---|---|
| | | | | | **Length ,in. [mm]** | **Average weight ,lb. [g]** | **Steel density ,lb/in$^3$. [kg/mm$^3$]** | **Nominal area ,in$^2$. [mm]** | **Nominal diameter ,in. [mm]** |
| **WA** | Smooth | N.A. | N.A. | N.A. | 17.833 [452.96] | 0.1748 [79.273] | 0.2836 [7.852e$^{-6}$] | 0.0346 [22.297] | 0.2098 [5.329] |
| **WB** | Chevron | 0.006 [0.15] | 0.226 [8.19] | 0.2283 [5.80] | 18.031 [457.99] | 0.1680 [76.225] | | 0.0329 [21.200] | 0.2046 [5.197] |
| **WC** | Spiral | 0.0076 [0.19] | N.A. | N.A. | 18.150 [461.01] | 0.1760 [79.815] | | 0.0342 [22.058] | 0.2086 [5.298] |
| **WD** | Chevron | 0.0063 [0.16] | 0.2577 [6.55] | 0.2150 [5.46] | 18.253 [463.63] | 0.1744 [79.115] | | 0.0337 [21.735] | 0.2071 [5.260] |
| **WE** | Spiral | 0.0117 [0.30] | N.A. | N.A. | 17.843 [453.21] | 0.1693 [76.801] | | 0.0335 [21.587] | 0.2064 [5.243] |
| **WF** | Diamond | 0.008 [0.20] | 0.3185 [8.09] | 0.2165 [5.50] | 17.363 [441.02] | 0.1626 [73.760] | | 0.0330 [21.303] | 0.2051 [5.210] |
| **WG** | Chevron | 0.0037 [0.09] | 0.2713 [6.89] | 0.2232 [5.67] | 23.396 [594.26] | 0.2285 [103.657] | | 0.0344 [22.219] | 0.2094 [5.319] |
| **WH** | Chevron | 0.0067 [0.17] | 0.3020 [7.67] | 0.2193 [5.57] | 17.792 [451.92] | 0.1639 [74.338] | | 0.0325 [20.955] | 0.2034 [5.166] |
| **WI** | Chevron | 0.0047 [0.12] | 0.2916 [7.41] | 0.2177 [5.53] | 17.835 [453.01] | 0.1693 [76.801] | | 0.0335 [21.600] | 0.2065 [5.245] |
| **WJ** | Chevron | 0.0057 [0.14] | 0.2925 [7.43] | 0.2213 [5.62] | 18.045 [458.34] | 0.1718 [77.947] | | 0.0336 [21.664] | 0.2068 [5.253] |
| **WK** | 4-Dot | 0.0036 [0.09] | 0.1213 [3.08] | 0.2717 [6.90] | 23.211 [589.56] | 0.2243 [101.753] | | 0.0341 [21.987] | 0.2083 [5.291] |
| **WL** | 2-Dot | 0.0043 [0.11] | 0.1413 [3.59] | 0.2787 [7.08] | 17.844 [453.24] | 0.1733 [78.591] | | 0.0342 [22.090] | 0.2088 [5.304] |
| **WM** | Chevron | 0.0051 [0.13] | 0.1500 [3.81] | N.A | 17.929 [455.40] | 0.1673 [75.884] | | 0.0329 [21.226] | 0.2049 [5.204] |

Table 3.2 Comparison to manufacturer properties

| **Wire label indentation types** | | ***Measured-wire properties*** | | ***Manufacturer data*** | | ***Difference*** | |
|---|---|---|---|---|---|---|---|
| | | **Nominal area, $in^2$. [mm]** | **Nominal diameter ,in. [$mm^2$]** | **Nominal area ,$in^2$. [$mm^2$]** | **Nominal diameter ,in. [mm]** | **Nominal area , %.** | **Nominal diameter ,%.** |
| **WA** | Smooth | 0.0346 [22.297] | 0.2098 [5.329] | 0.0347 [22.387] | 0.2102 [5.339] | 0.42% | 0.21% |
| **WB** | Chevron | 0.0329 [21.200] | 0.2046 [5.197] | 0.0345 [22.258] | 0.2095 [5.321] | 4.67% | 2.36% |
| **WC** | Spiral | 0.0342 [22.058] | 0.2086 [5.298] | 0.0341 [22.000] | 0.2083 [5.291] | 0.32% | 0.16% |
| **WD** | Chevron | 0.0337 [21.735] | 0.2071 [5.260] | 0.0352 [22.710] | 0.2117 [5.337] | 4.28% | 2.16% |
| **WE** | Spiral | 0.0335 [21.587] | 0.2064 [5.243] | 0.0345 [22.258] | 0.2095 [5.321] | 2.92% | 1.48% |
| **WF** | Diamond | 0.0330 [21.303] | 0.2051 [5.210] | 0.0345 [22.258] | 0.2095 [5.321] | 4.20% | 2.12% |
| **WG** | Chevron | 0.0344 [22.219] | 0.2094 [5.319] | 0.0346 [22.323] | 0.2099 [5.331] | 0.47% | 0.23% |
| **WH** | Chevron | 0.0325 [20.955] | 0.2034 [5.166] | 0.0348 [22.452] | 0.2105 [5.347] | 6.67% | 3.39% |
| **WI** | Chevron | 0.0335 [21.600] | 0.2065 [5.245] | 0.0336 [21.677] | 0.2068 [5.253] | 0.34% | 0.17% |
| **WJ** | Chevron | 0.0336 [21.664] | 0.2068 [5.253] | 0.0350 [22.581] | 0.2112 [5.364] | 4.15% | 2.10% |
| **WK** | 4-Dot | 0.0341 [21.987] | 0.2083 [5.291] | 0.0346 [22.323] | 0.2098 [5.329] | 1.42% | 0.71% |
| **WL** | 2-Dot | 0.0342 [22.090] | 0.2088 [5.304] | 0.0346 [22.323] | 0.2098 [5.329] | 0.96% | 0.48% |
| **WM** | Chevron | 0.0329 [21.226] | 0.2049 [5.204] | N.A. | N.A. | N.A. | N.A. |

## 3.2 Testing Machine

The goal for the testing was to obtain stress-strain curves all the way to failure. The tensile tests used the universal testing machine: SHIMADZU AG-IC 50KN (Figure 3.5), operating with TRAPEZIUM X software (Shimadzu, 2009). The test-force precision was within ± 0.5% to 1% of indicated test force. The stress was continually measured and recorded by the TRAPEZIUM X (2009) software. The strain was measured and recorded by two single-point extensometers utilizing linear variable differential transformers (LVDTs). The extensometers were placed next to both sides of the specimen and fixed by the block on the wire (Figure 3.6). The extensometer's tip was depressed against the metal bar, which was tied to the top end of the wire. It moved, following with a specimen extension for collecting the complete strain elongation, while the specimen failed in between the gage length (Figure 3.6). The steel tube in between the extensometers was designed to protect experimenters from a failing wire.


Figure 3.5 Universal tensile testing machine

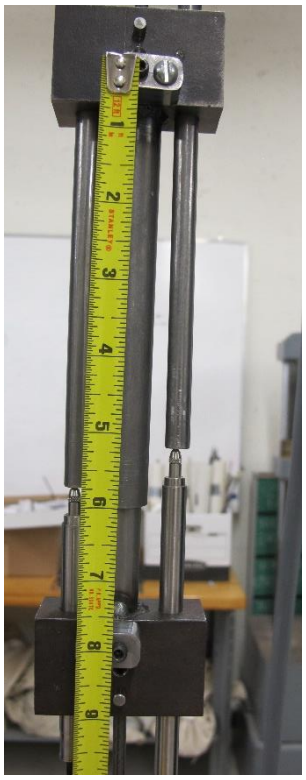

Figure 3.6 Displacement measurement installation

Two gripping heads were used, an upper fixed-wedge grip and a lower joint/movable grip (Figure 3.7 and Figure 3.8). The joint/movable grip was directly connected to a chuck jaw, which

allowed alignment of the specimen to the upper head, and the end of the wire was gripped by a threaded collar inside the chuck jaw. The two grips had to be properly aligned in order to avoid premature failure of the wire.


(a) Upper fixed gripping head

(b) Lower movable gripping head

Figure 3.7 Gripping heads

The upper end of the testing prestressing wire was clamped by the chuck jaw with a flat serrated-texture shoulder (Figure 3.8). The purpose of the flat shoulder was to ensure proper fit to the wedge-shaped jaws and provide sufficient force capacity. The detail schematic of the tensile testing machine is shown in Appendix B.

Figure 3.8 Gripping section

## 3.3 Test Setup/ Procedure

In this section, testing setup and procedures will be discussed. The most crucial part of the setup in tensile testing was wire alignment in the center of the grip. Proper placement of the specimen will result in good performance. Before attaching the wire to the testing machine, the extensometers must be set up. The extensometer was fixed on the testing wire with a gage length of eight inches, and each side of the specimen was exposed evenly for approximately four inches. When assembling the extensometers, it was necessary to align the wire on absolute axis.

Misalignment of the wire will cause premature failure outside of the gage length or inside the chuck jaw. This failure will not allow the LVDT to capture the completed testing result. Moreover, if the wire is not parallel or centered with the grips, bending force will be exerted onto it, resulting in load-measurement errors (ASTM International, 2004). Figure 3.9 gives examples of alignment specimens. Figure 3.9 (a) shows the appropriate lateral alignment. By contrast, Figure 3.9 (b) and (c) are examples of improper alignment.

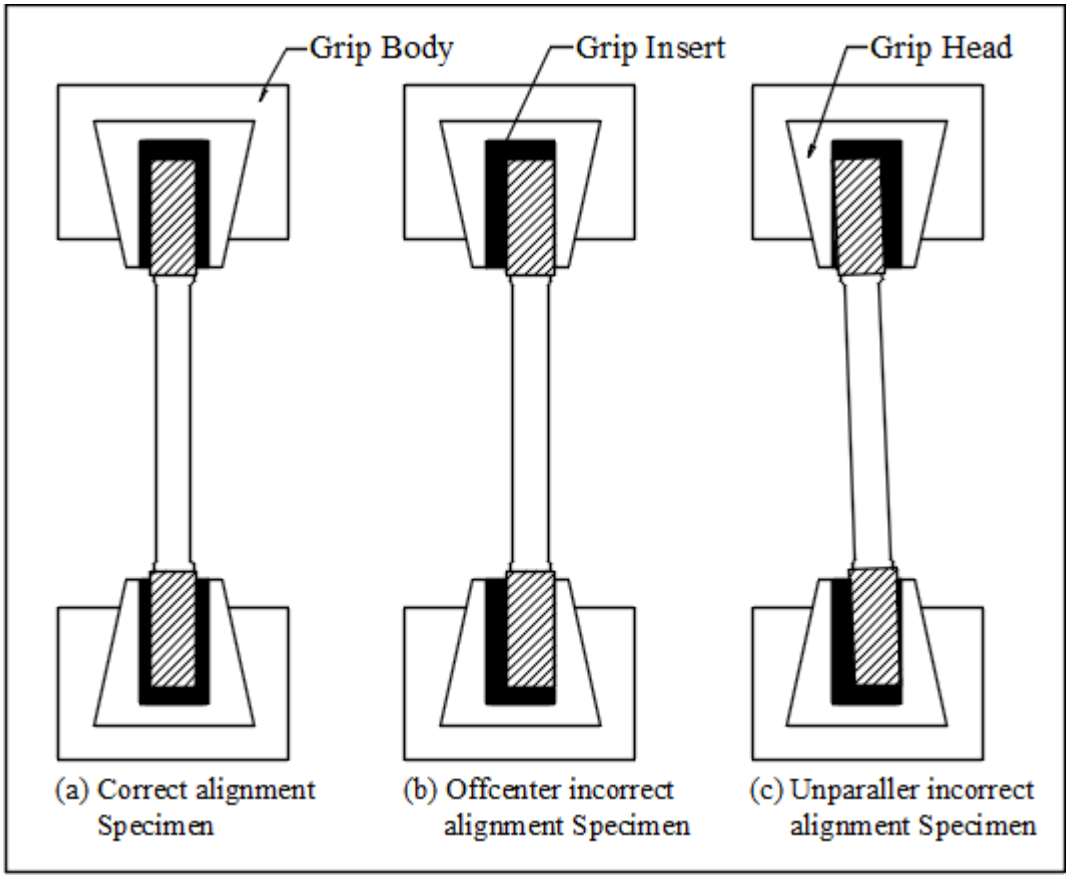


Figure 3.9 Specimen alignment examples

Next, the chuck jaw was installed on one end of the specimen and the specimen attached in a lower joint grip. The joint grip was rotated to adjust the position of the top grip on the chuck jaw to make sure the head was aligned. In order to ensure the specimen was placed in correct position, it was aligned with the grooved mark on the grip. The flat shoulder front should be parallel to the first groove mark and while tightening, not touch or lean on the grip insert. Also, the shoulder had to be adequately engaged in the wedge grip before tightening the upper grip. After the specimen and extensometers were placed, force and stroke were returned to zero through computer or controller.

Tests followed ASTM E8/E8M, which gives a specific method for tensile testing of metallic materials to help minimize errors from experimental works (ASTM E8/E8M, 2015). The universal testing machine can reach up to 10,000 pounds of force and will stop once the force achieves its maximum. Testing speed force was 1500 lb/min, recording at every 0.5-second interval using TRAPEZIUM X software. LVDT will record linear displacement, and the LVDT had to be properly aligned to the metal bar in order to collect complete displacements. Each testing took about eight to 12 minutes, varying based on the ductility of the wire. Testing for each wire type was repeated until three specimens were broken in between the gage length.

## 3.4 Performance of Test

Thirteen types of prestressing wire were considered in this study, and a total of 87 tests were performed. Many of the tests failed at the top or bottom of the grip, requiring further testing until three satisfactory results were obtained for each wire type. In the Figure 3.10, wire A shows a specimen before testing, and the measuring gage length is marked by blue tape. Wire B broke in between measured length, which was the anticipated result. Wire C was disqualified since the wire broke outside of gage length.

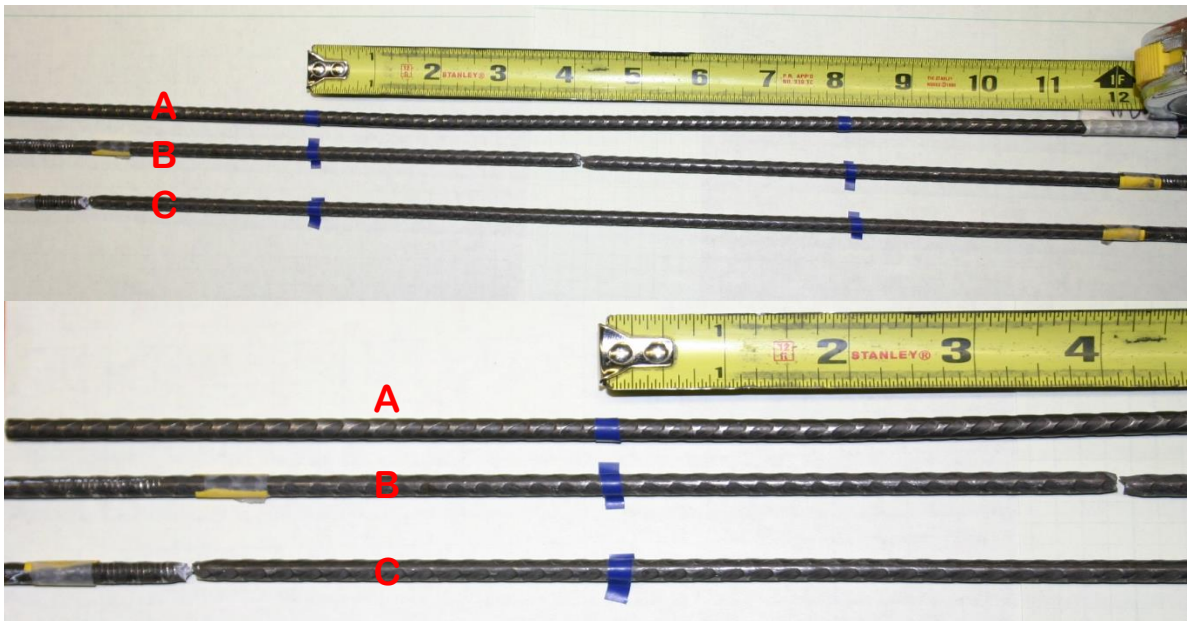


Figure 3.10 Wire performance

Due to testing performance, wires WA, WC and WK were excluded from further analysis because of the machine capability. Also, through cross-examination data from manufacturers, it was found that wire WA's breaking strength was too high for the testing machine. Wire data from WC and WK showed strength within the machine's capability. However, the mill cert data may not be the sole consideration, because manufacturers may stop wire testing once properties of the wire achieve ASTM A881 minimum requirements.

Wire WA reached the machine's ultimate capacity (10,000 lb) in the first testing, and wire mill cert data indicated the breaking load was 10,184 (lbs). This showed the testing machine did not have the ability to load the wire to failure. WC wires reached the maximum strength of the testing machine in the fourth test, while the wire mill cert data showed the breaking load was close to the machine's limit (9,892 lbs). Furthermore, nine attempts were made to collect data for the WK wire, but all failed either at the top fixed grip or bottom chuck jaw. Therefore, in the

following analytical and modeling section, 10 types of prestressing wire and a total of 28 test results are included. Each wire had three good results out of four to eight tests, except wire WI, which only had one acceptable result out of 12 experiments. Experimental reliable results are shown in Table 3.3.

Table 3.3 Experimental reliable results

| Type of wire | WB | WD | WE | WF | WG | WH | WI | WJ | WL | WM | Total |
|---|---|---|---|---|---|---|---|---|---|---|---|
| Reliable results | 3 | 3 | 3 | 3 | 3 | 3 | 1 | 3 | 3 | 3 | 28 |

The experimental results are displayed as load versus extension with more than 1,000 data observations. Data was collected at 0.001-inch displacement intervals and included two displacement transducers' corresponding force. Interpolation was used to find the average elongation at each interval. The interpolated force readings were converted to stress through dividing by corresponding nominal areas of prestressing wire. Also, displacement readings were converted to strain by dividing by gage length.

Each wire's area used for estimating stress is presented in Table 3.1 . Before plotting the stress-strain curves, the data selecting processes was repeated, and converted stress and strain for each wire was examined. Appendix C shows all individual wires' curves, including the average curve out of three successful results. Average curves of the respective wire patterns are shown in Figure 3.11. From Figure 3.11, all curves had a similar development shape after the proportional limit point, especially wires [WD], [WE], [WF], [WL], and [WM]. Each wire reached the ASTM minimum value of elongation, and some wires had the ability to withstand strain beyond 6%. Overall minimum elongation was 4%, and average maximum elongation was 5.57%.

To determine the elastic modulus, generally the proportional limit could be recognized at around 0.6% to 0.8% strain, or some higher point, depending on the specimen's characteristics. Thus, the data suggested the proportional limit to be at 0.7% strain through individual observation of curves, and calculating the elastic modulus by simply dividing stress by strain. The average elastic modulus out of 28 experimental results was approximately 29,400 ksi (202.7E3 MPa), higher than the ASTM standard value of 29,000 ksi (199.9E3 MPa). Specific wire results are displayed in Table 3.4.

The ASTM A881 (2015) minimum tensile strength requirement was 9,000 lbf with nominal diameter 0.2094 in (5.32 mm). Minimum tensile strength was corresponded to a

minimum tensile stress of 261.2 ksi (1,804 MPa) (ASTM A881/A881M, 2015). Yield strength at 1% strain was at least equal to 90% ASTM A881 minimum tensile strength (ASTM A881/A881M, 2015). However, from the experimental results, wire stiffness and elongation were larger. The majority of curves were a developing force in between 270 to 290 ksi (1,862 to 2,000 MPa) after elastic behavior. Average yield strength was $0.9033f_{pu,}$ which is close to the ASTM value, but the $f_{py}/f_{pu}$ was slightly changed, depending on types of wire indention. The majority experimental result indicated ultimate strength was 7% to 13% more than the assumption value of wire strength ($f_{pu}$=261.2 ksi) from ASTM A881 (2015), except for the [WG] wire, which was only 2.4% greater — the weakest wire tested. Average ultimate strain out of 28 experimental results was 5.09%, with a corresponding average ultimate stress of 283.53 ksi (1,955 MPa), satisfying the ASTM minimum tensile strength requirement of 261.2 ksi (1,803 MPa). Average yield stress was 256.13 ksi, which is noticeably higher than the ASTM value of 235 (ksi). Both yield and ultimate strengths were found to be significantly higher than ASTM minimum requirements. The detail testing result is presented in Table 3.4.

Table 3.4 Experimental wire performance results

| Wire type | Average E ,ksi [MPa] | Average fpy @ 1% ,ksi [MPa] | Average fpu ,ksi [MPa] | Average εpu, % | fpy/fpu | Average maximum elongation, % |
|---|---|---|---|---|---|---|
| [WB] | 29,420 [202,840] | 269.24 [1,856] | 296.01 [2,041] | 4.99 | 0.910 | 5.40 |
| [WD] | 29,760 [205,210] | 253.19 [1,746] | 281.54 [1,941] | 5.39 | 0.899 | 5.80 |
| [WE] | 29,060 [200,340] | 251.73 [1,736] | 281.73 [1,942] | 5.57 | 0.894 | 6.20 |
| [WF] | 28,780 [198,420] | 252.00 [1,737] | 279.42 [1,927] | 5.20 | 0.902 | 5.60 |
| [WG] | 28,890 [199,190] | 240.47 [1,658] | 267.47 [1,844] | 4.84 | 0.899 | 5.60 |
| [WH] | 30,880 [212,930] | 264.81 [1,826] | 290.39 [2,002] | 4.06 | 0.912 | 4.12 |
| [WI] | 29,260 [201,710] | 257.57 [1,776] | 282.35 [1,947] | 4.25 | 0.912 | 5.20 |
| [WJ] | 28,300 [195,110] | 258.62 [1,783] | 285.23 [1,967] | 4.55 | 0.907 | 5.40 |
| [WL] | 29,700 [204,750] | 258.76 [1,784] | 284.09 [1,959] | 5.98 | 0.911 | 6.30 |
| [WM] | 29,720 [204,920] | 254.95 [1,758] | 287.05 [1,979] | 6.10 | 0.888 | 6.60 |
| **Average** | **29,380 [202,540]** | **256.13 [1,766]** | **283.53 [1,955]** | **5.09** | **0.903** | **5.57** |

From Table 3.4 and Figure 3.11, [WM] was seen to have high stiffness and ductility; that is to say the entire elongation was more than 0.065 in (1.651 mm), and the initial elastic modulus was close to 29,800 ksi (205,460 MPa). On the contrary, [WH] was the stiffest wire in the elastic behavior because the initial modulus of elasticity was more than 30,000 ksi (206.80E3 MPa) but had low ductility since the strain only developed up to 0.04 in (1.016 mm). However, it had the second highest ultimate strength of approximately 290 ksi (2,000 MPa). In the case of the [WH] wire, it was extremely rigid, so the fracture occurred immediately after passing the ultimate point. Highest and lowest strength curves were wires [WB] (296 ksi, 2,041 MPa) and [WG] (267 ksi, 1,841 MPa), and the elongation of the two curves was slightly above 5%.

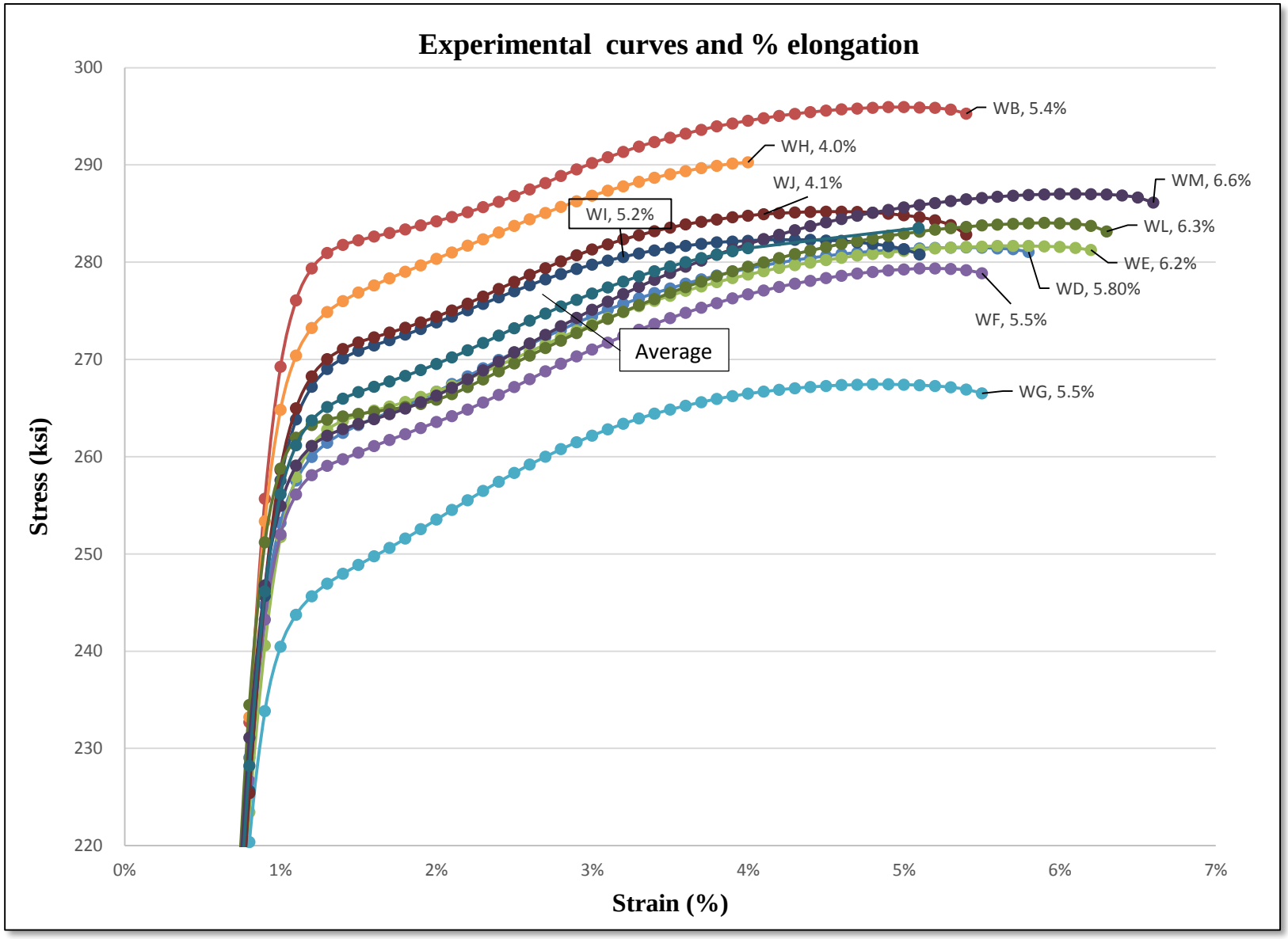


Figure 3.11 Experimental stress-strain curves

# Chapter 4 Modeling Stress-Strain Curve — *Power Formula*

## 4.1 Analytical Modeling Using the Power Formula

According to the observed experimental performance, respective types of wire display higher stress with longer extension than existing predictions and standard equations. Therefore, accuracy of the captured material response has to be improved. The analysis and modeling section considered the average curve out of three experimental outputs for each type of wire, totaling 10 stress-strain curves, including wire [WI]. The modeling procedure was performed by evaluating the parameters that best fit the experimental results first, then developing regression equations to generalize the constants based on the strongest correlation of variables, as shown in the flow chart in Figure 4.1.

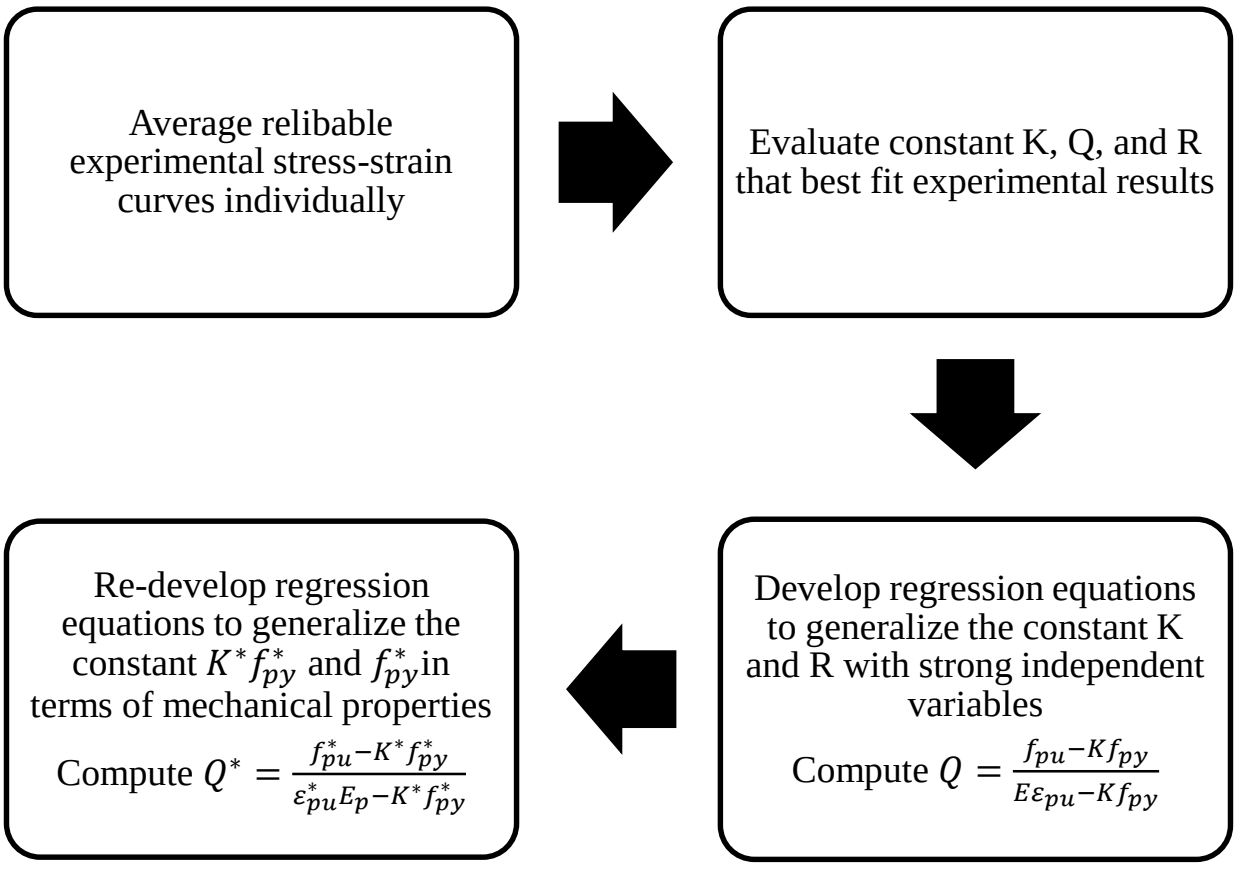


Figure 4.1 Analysis and modeling procedure

As stated by Mattock, the constant K could be defined either through the trials of assumption or using a complete stress-strain curve (Mattock, 1979). In order to represent a stress-strain curve with more accurate values, appropriate values of constants were evaluated based on experimental stress-strain curves. Once suitable parameters were determined from fitting experimental results, they were used as a basis for a more comprehensive analysis.

To determine constant K, two straight lines were produced in the experimental stress-strain curve. The first line had a slope of E, which is initial modulus of elasticity. The second linear portion was found by plotting a linear trend line from the experimental curve, at 0.3-inch elongation, to the ultimate point. Extending the two linear portions to intersect, the intersection corresponded to the stress $Kf_{py}$. K was obtained by dividing the resulting stress by the yield stress. The constant Q can be computed through the dimensionless slope of the second hardening line, Equation (2-32). The constant R could be acquired when assuming $f_{ps}= f_{py,}$ according to Mattock (Mattock, 1979) and as shown below:

$$f_{py} = \varepsilon_{py} E \left[ Q + \frac{1 - Q}{\left( 1 + \left( \frac{\varepsilon_{py} E}{K f_{py}} \right)^{R} \right)^{1/R}} \right] \qquad \text{Equation (4-1)}$$

$f_{py}$ and K $f_{py}$ are presrented in Table 4.1.

$\varepsilon_{py}$ is 0.01 strain.

Figure 4.2 demonstrates details for using a completed stress-strain curve to recover the constant "K".

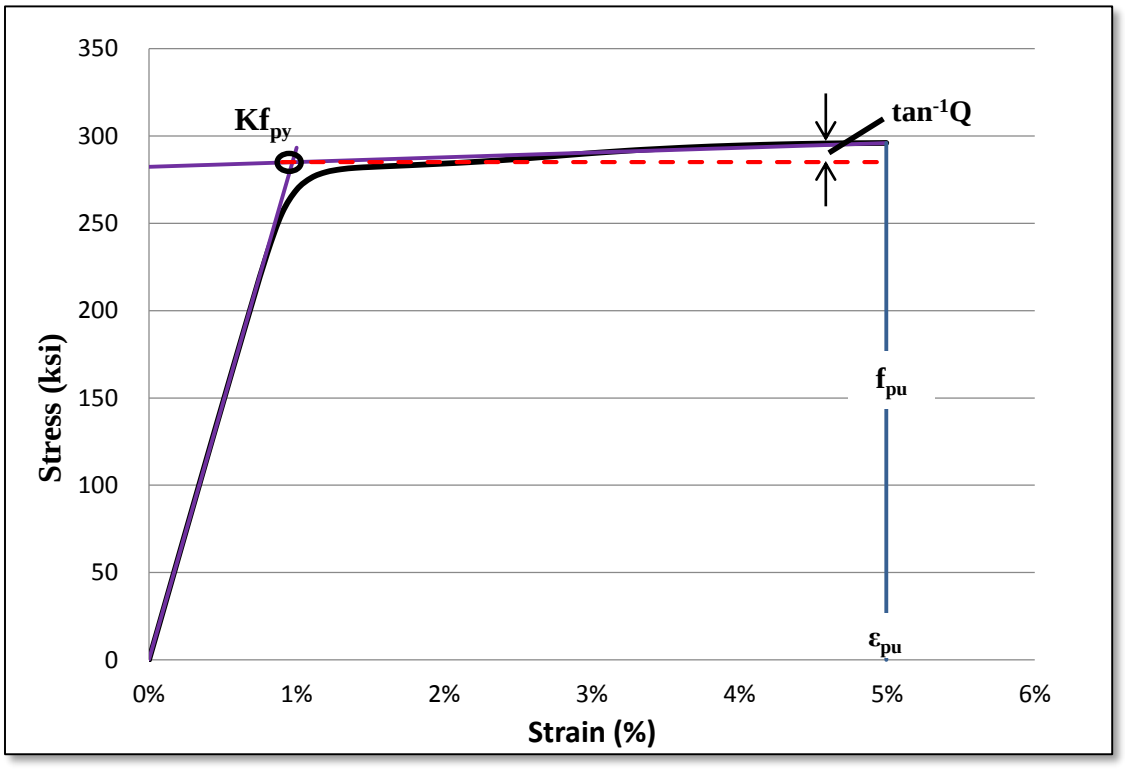


Figure 4.2 Stress-strain curve corresponding to the power formula.

Before developing the regression equations, it is advisable to plot the stress-strain curve generated compared with the actual experimental curve individually to ensure the desired accuracy. To accomplish the goal where the formula could be applied without providing the experimental stress-strain curve, regression equations were developed to correlate the most relevant parameters. Based on data from fitting actual experimental results, regression equations will generalize the constant K and R in terms of other mechanical properties. In the regression analysis, explanatory variables refer to E, $f_{py}$, $\varepsilon_{py}$, $f_{pu}$ and $\varepsilon_{pu}$ from experimental results (Table 3.4). Dependent variables are constant K and R. Trials of comparing with independent variable combinations were required to find strong correlations. Consequently, a strong negative /positive regression relationship will be proposed.

## 4.2 Results and Discussions

The representative stress-strain curves were closely fitted to the experimental curves, because proper values of the mechanical parameters were identified. During the modeling stage, parameter “R” determined the level of curvature on yielding evolution, and radius of curvature became sharp as the value of R increased. Constant “Q” decided the slope of the second linear part, and the linear portion became flatter when the value of Q was reduced. Moreover, the constant “K” decided not only the proportional limit point but also the ultimate strength for the developed curve. If the value of “K” decreased, the elastic behavior shortened, leading the plastic behavior to terminate at a lower force. On the other hand, overestimated value of "K" should be avoided because it will extend the elastic behavior with stiffer material characteristics. Hence, it was significant to define the correct values of the constants. Correlation of the fitted results to the experimental results is demonstrated in Table 4.1. From Table 4.1, it may be observed that constants "Q" and “K” have minor variations in terms of prestressing wire type, which implied insensitivity of the coefficients involved. On the other hand, the constant “R” varied randomly between seven and 11 for the different wires used.

Table 4.1 Parameters from modeling experimental stress-stain curve and percentage error

| Wire type | K | Q | R | Maximum error, % |
|---|---|---|---|---|
| **[WB]** | 1.049 | 0.012 | 10.347 | 0.68 |
| **[WD]** | 1.044 | 0.013 | 7.548 | 1.14 |
| **[WE]** | 1.052 | 0.012 | 7.607 | 0.96 |
| **[WF]** | 1.030 | 0.016 | 9.747 | 1.15 |
| **[WG]** | 1.035 | 0.016 | 7.494 | 1.38 |
| **[WH]** | 1.037 | 0.016 | 8.271 | 1.62 |
| **[WI]** | 1.062 | 0.009 | 7.656 | 1.19 |
| **[WJ]** | 1.047 | 0.014 | 10.401 | 0.93 |
| **[WL]** | 1.018 | 0.014 | 11.345 | 1.26 |
| **[WM]** | 1.037 | 0.015 | 8.259 | 1.43 |
| **Average** | 1.041 | 0.014 | 8.867 | 1.17 |

The representative fitted experimental stress-strain curves are shown in Appendix D. From Appendix D, [WB] wire graph, the actual experimental curve, and fitted-curve results matched very well in elastic and plastic regions with a maximum difference of 0.680%, which was the smallest overall error in all wire patterns. The highest error generated was from the [WH] wire at 1.62%. The average maximum error equated the maximum errors from 10 wires without considering the error before the proportional limit, and the average maximum error in fitting experimental results was 1.17%. The maximum error possible was either in the elastic region or the plastic region, and the errors were slightly larger in the elastic region for wires [WD], [WH], [WI] and [WJ]. Those four types of wire had maximum error at 0.1% strain, which was the first point in the elastic region, so maximum errors were the same after applying regression equations. However, elastic behavior was stable following Hooke's laws for all the wires. Additionally, the wires were bent due to transport requirements, and the experiment tests did no preloading to straight the specimen. Thus the testing machine was adjusting the specimen in the beginning, which indicated the initial experimental data contained more errors. Therefore, average maximum error excluded the difference in the elastic region. The closer result was discovered by equating the average maximum error out of 10 wires without including the elastic region, which was dropped from 2.6% to 1.2%. The precision of modeling the experimental curve was approximately 99%, which was taken as the 100% subtracted average maximum error out of 10 wires. After the observed fitted stress-strain curves (Appendix D) were compared to the experimental curves, it was concluded the modeling results were reliable and precise for carrying out further regression analysis.

The regression equations were identified through several cycles of trial and error without any assumptions, since the dependent variable's connection to the independent variable is unknown a priori. From regression analysis results, the independent variable $Kf_{py}$ had a strong positive relationship to yield stress $f_{py}$ with the coefficient of determination ($R^2$) equal to 0.8849. The linear regression graph associating $Kf_{py}$ to yield stress is shown in Figure 4.3, and the linear regression equation is presented below:

$$Kf_{py} = 1.1007 f_{py} - 15.2707 \quad (ksi) \qquad \text{Equation (4-2)}$$

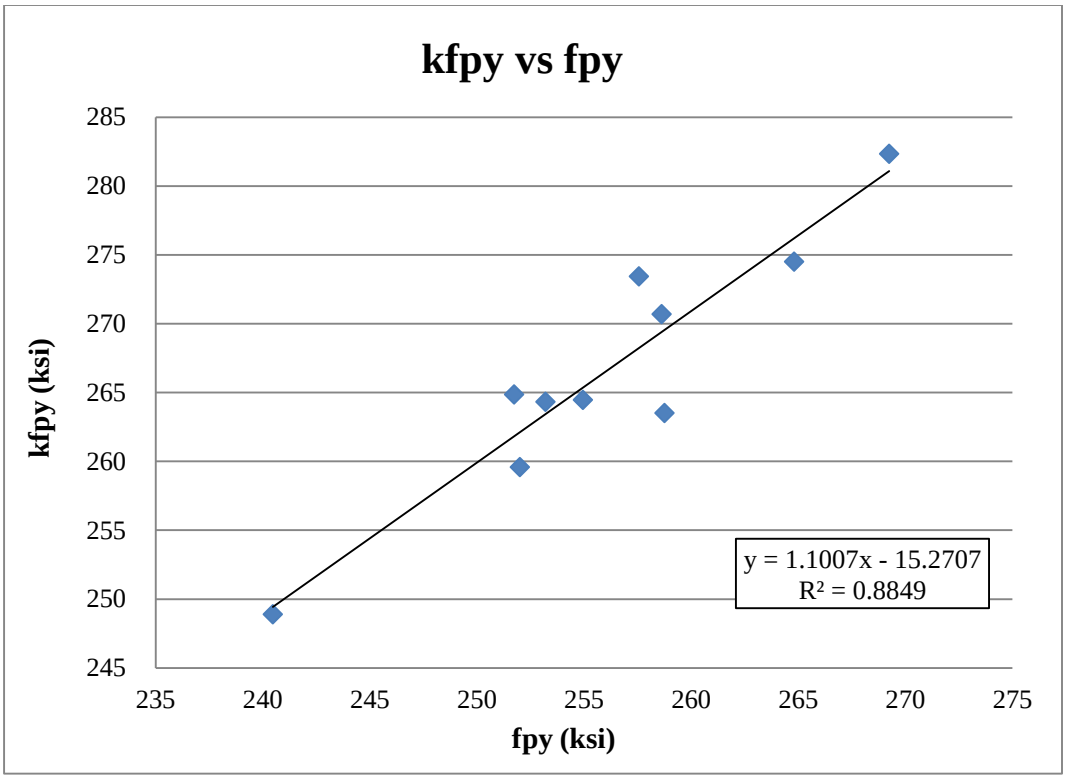


Figure 4.3 Regression relationship for constant $Kf_{py}$

Then, K was obtained by dividing Kfpy, calculated from Equation (4-2) by the yield stress from experimental results, corresponding to 1% strain (Table 3.4), and the value of Q could thus be computed according to Equation (2-32). On the other hand, a strong negative relationship was discovered between the constant "R" and the ratio of the elastic modulus times the yield strain over $Kf_{py}$. The regression analysis graph is shown in Figure 4.4.

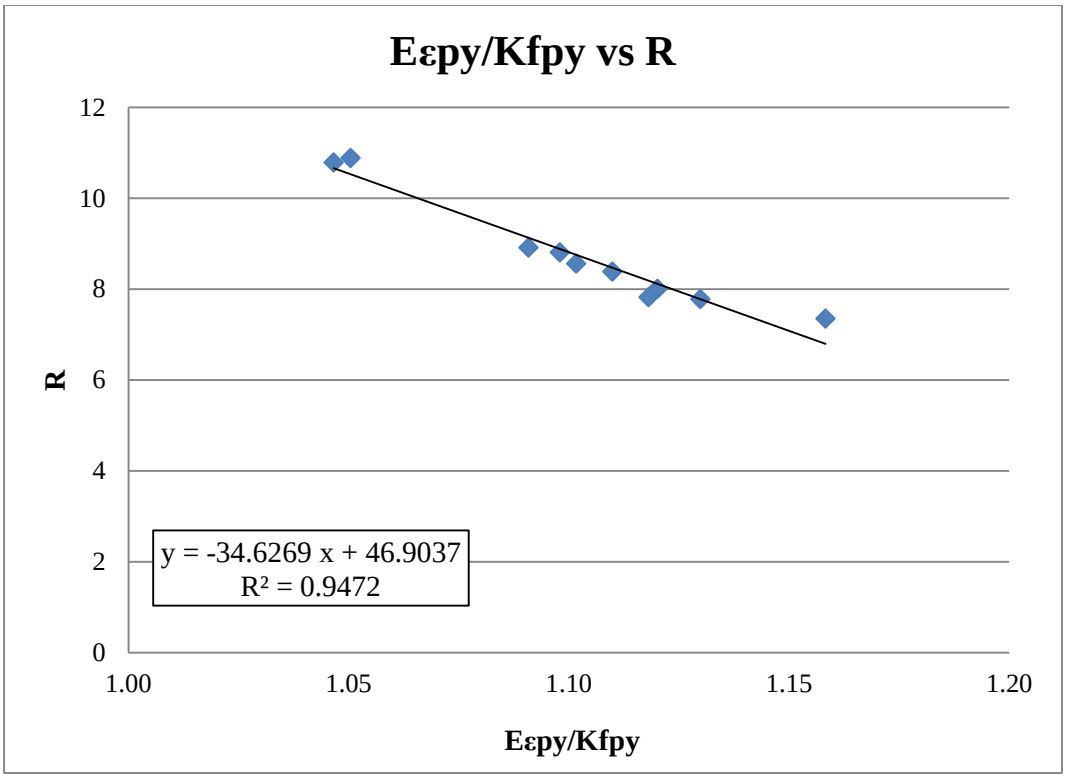


Figure 4.4 Regression relationship for constant R

$Kf_{py}$ was computed by Equation (4-2). The coefficient of determination ($R^2$) was 0.9472 in this case, and the regression equation became

$$R = -34.6269\frac{E\varepsilon_{py}}{Kf_{py}} + 46.9037 \qquad \text{Equation (4-3)}$$

Specific constants from the regression analysis are shown in Table 4.2. Individual re-generated wire stress-strain curves are presented in Appendix D. A majority of regression analysis results did not bring up accuracy and the overall average maximum error showed a minor increase from 1.17% to 1.48% because of errors contained in the linear regression analysis. According to regression analysis results, re-generated curves for [WD], [WI], and [WJ] wires were much closer to the experimental curves.

Table 4.2 Parameters from regression analysis and the percentage error

| Type of wire | K | Q | R | Maximum error, % |
|---|---|---|---|---|
| **[WB]** | 1.044 | 0.013 | 10.662 | 0.81 |
| **[WD]** | 1.040 | 0.014 | 7.779 | 1.26 |
| **[WE]** | 1.040 | 0.015 | 8.472 | 1.35 |
| **[WF]** | 1.040 | 0.014 | 8.884 | 1.47 |
| **[WG]** | 1.037 | 0.016 | 6.795 | 1.99 |
| **[WH]** | 1.043 | 0.015 | 8.188 | 1.72 |
| **[WI]** | 1.041 | 0.015 | 9.138 | 0.95 |
| **[WJ]** | 1.042 | 0.016 | 10.530 | 1.08 |
| **[WL]** | 1.042 | 0.010 | 8.755 | 2.61 |
| **[WM]** | 1.041 | 0.014 | 8.118 | 1.58 |
| Average | 1.041 | 0.014 | 8.732 | 1.48 |

## 4.3 Recommended Design Curves for Wire Grades Using the Power Formula

The purpose of this section was to develop the power formula that can be used in practical design applications as opposed to quality control. The design equation could estimate stress in terms of mechanical properties (ultimate strength), in addition to corresponding strain. The design-oriented power formula was properly designed for the wire's ultimate strength or grade ($f^*_{pu}$) at specific values from 250 ksi to 300 ksi (1,724 MPa to 2,068 MPa). The ultimate strength range was determined from the current equations and experimental results. From the experimental results, the prestressing wire's highest strength capacity was close to 300 ksi (20.68E2 MPa) such as the [WB] wire. The current PCI strand equation had an estimation for ultimate strength at 250 ksi (1,724 MPa) and 270 ksi (1,862 MPa).

Minimum elongation was adjusted from 3% to 4% strain ($\varepsilon^*_{pu}$), since all the wires extended to at least to 0.04 strain or more. The regression equations will be re-derived in accordance with the minimum elongation limit of 4% strain specified. The new design-oriented regression analysis was based on results determined from fitting the experimental curves (Table 4.1). Additionally, in order to maintain the precision of the response, the regression equations should

be limited in the design-oriented procedure to evaluating the constants. Two new regression equations were determined, the constant K and yield stress. According to previous analysis procedures, parameter $K^*$ had to be defined before other constants could be solved.

New regression analysis results indicated $K^* f_{py}^*$ was strongly and positively correlated with $f_{pu}^*$. The regression relationship graph is shown in Figure 4.5. The coefficient of determination is 0.9298, and the linear equation is

$$K^* f_{py}^* = 1.1607 f_{pu}^* - 60.0118 \qquad \text{Equation (4-4)}$$

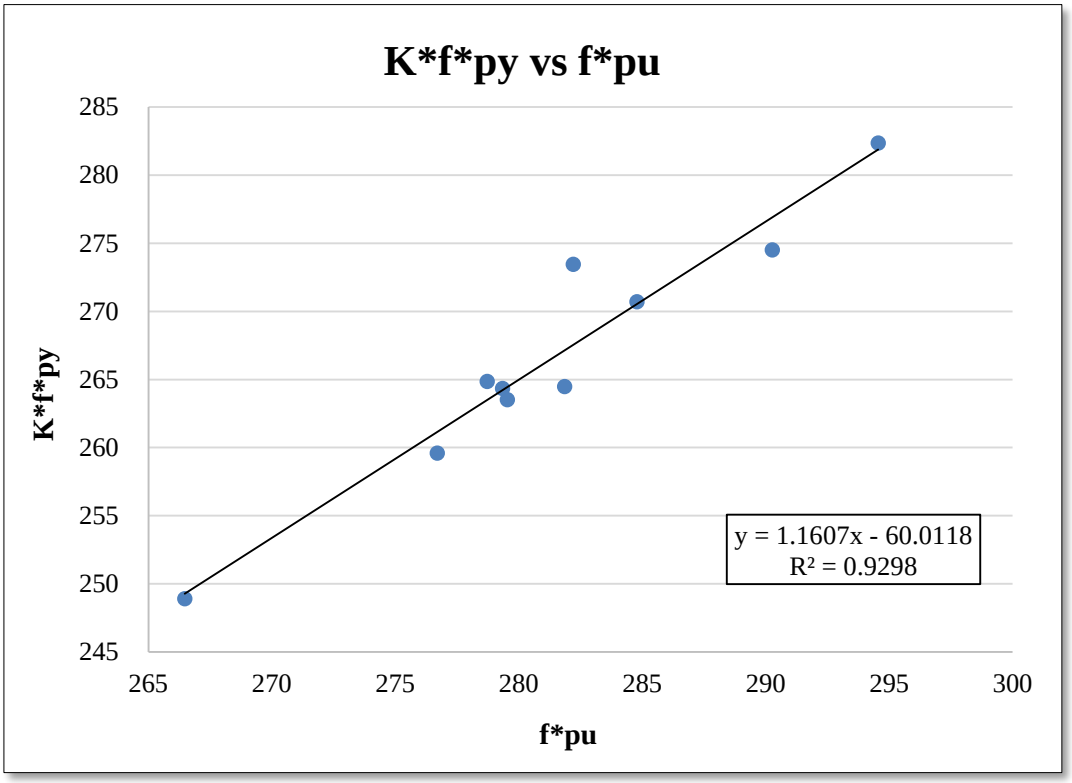


Figure 4.5 Regression relationship for constant $K^* f_{py}^*$

Considering the various levels of ultimate strength that will be applied, the associated yield strength ($f_{py}^*$) was required to make adjustments. Thus the regression relationship for $f_{py}^*$ is shown in Figure 4.6. The linear equation is

$$f_{py}^* = 1.0017 f_{pu}^* - 25.7794 \qquad \text{Equation (4-5)}$$

The coefficient of determination is 0.9481, and the yield strength has strong positive relationship to the ultimate strength. Hence, $K^*$ was obtained by dividing Equation (4-4) by Equation (4-5).

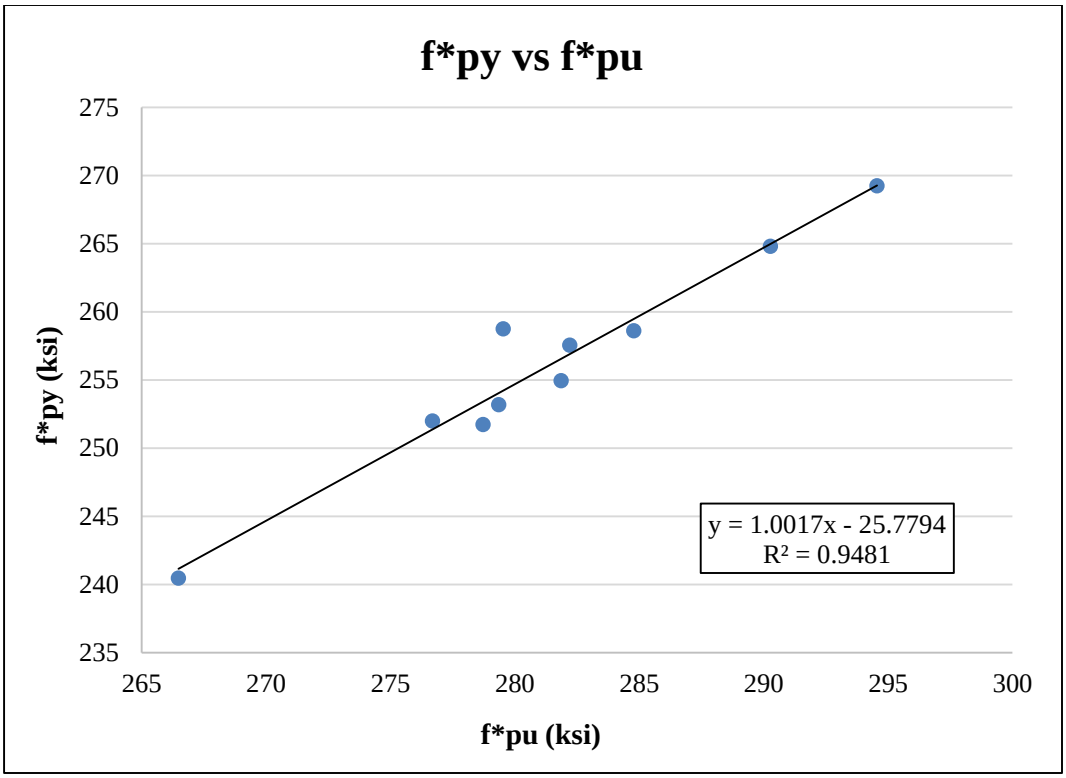


Figure 4.6 Regression relationship for constant $f^*_{py}$

Then the computed constant $Q^*$, by applying Equation (4-5), leads to Equation (4-7):

$$Q^* = \frac{f^*_{pu} - K^* f^*_{py}}{\varepsilon_{pu} E_p - K^* f^*_{py}} \qquad \text{Equation (4-6)}$$

$$Q^* = \frac{f^*_{pu} - (1.1607 f^*_{pu} - 60.01118)}{0.04 E_p - (1.1607 f^*_{pu} - 60.01118)} \qquad \text{Equation (4-7)}$$

The modulus of elasticity ($E_p$) is 29,376 ksi (20,2542 MPa), which is the average of 28 experimental results. The other constant R will be solved by iterations using the power formula when $f_{ps}=f^*_{py}$.

$$f^*_{py} = E_p \varepsilon_{py} \left[ Q^* + \frac{1 - Q^*}{\left(1 + \left(\frac{\varepsilon_{py} E_p}{K^* f^*_{py}}\right)^{R^*}\right)^{1/R^*}} \right] \qquad \text{Equation (4-8)}$$

$\varepsilon_{py}$ is the yield strain, 1%.

$f^*_{py}$ is from Equation (4-5).
$Q^*$ is from Equation (4-7).
$K^*f^*_{py}$ is from Equation (4-4).

Then Equation (4-8) becomes as below:

$$\left(1.0017f^*_{pu} - 25.7794\right) = 0.01E_p\left[\frac{f^*_{pu} - (1.1607f^*_{pu} - 60.01118)}{0.04E_p - (1.1607f^*_{pu} - 60.01118)} + \frac{1 - \frac{f^*_{pu} - (1.1607f^*_{pu} - 60.01118)}{0.04E_p - (1.1607f_{pu} - 60.01118)}}{\left(1 + \left(\frac{0.01Ep}{(1.1607f^*_{pu} - 60.01118)}\right)^{R^*}\right)^{1/R^*}}\right]$$

Parameter R* can be found through numerical trials. The results, for each wire grade are shown in Table 4.3.

Table 4.3. Parameters and wire grade for the design-oriented power formula

| $f^*_{pu}$ (ksi) | 250.00 | 260.00 | 270.00 | 280.00 | 290.00 | 300.00 |
|---|---|---|---|---|---|---|
| $f^*_{py}$ (ksi) | 224.65 | 234.66 | 244.68 | 254.70 | 264.71 | 274.73 |
| $f^*_{py}/f^*_{pu}$ | 0.899 | 0.903 | 0.906 | 0.910 | 0.913 | 0.916 |
| $K^*$ | 1.0246 | 1.0303 | 1.0355 | 1.0404 | 1.0449 | 1.0490 |
| $Q^*$ | 0.0210 | 0.0195 | 0.0180 | 0.0165 | 0.0149 | 0.0133 |
| $R^*$ | 6.2949 | 6.7733 | 7.4270 | 8.3401 | 9.6937 | 11.9475 |

The relationship between the yield and ultimate strength was increased following the increase in tensile strength as shown in Table 4.3. The yield stress was $0.899f^*_{pu,}$ which is less than the ASTM minimum (90% of the tensile strength) when the ultimate stress was 250 ksi (1,724 Mpa). Plotting the design-oriented stress-strain curves by applying the constants from Table 4.3, these curves are presented in Figure 4.7. From Figure 4.7, the stress at 4% strain did not exceed the actual ultimate strength. The proportional limit was slightly changed for different ultimate strength to provide smooth formula curves for each. The smaller ultimate strength had a lower proportional limit, assumed to be 0.06% strain for $f_{pu}$=250 ksi (1,724 MPa) and 260 ksi (1,730 MPa). On the other hand, the intermediate ultimate strength of 270 ksi (1,862 MPa) and 280 ksi (1,931 MPa) had a proportional limit of 0.07% strain, while the higher ultimate strength of 290 ksi (1,999 MPa) and 300 ksi (2,068 MPa) had a proportional limit of 0.08%. This was consistent with the 250 ksi vs. 270 ksi PCI strand equations that had different proportional limits.

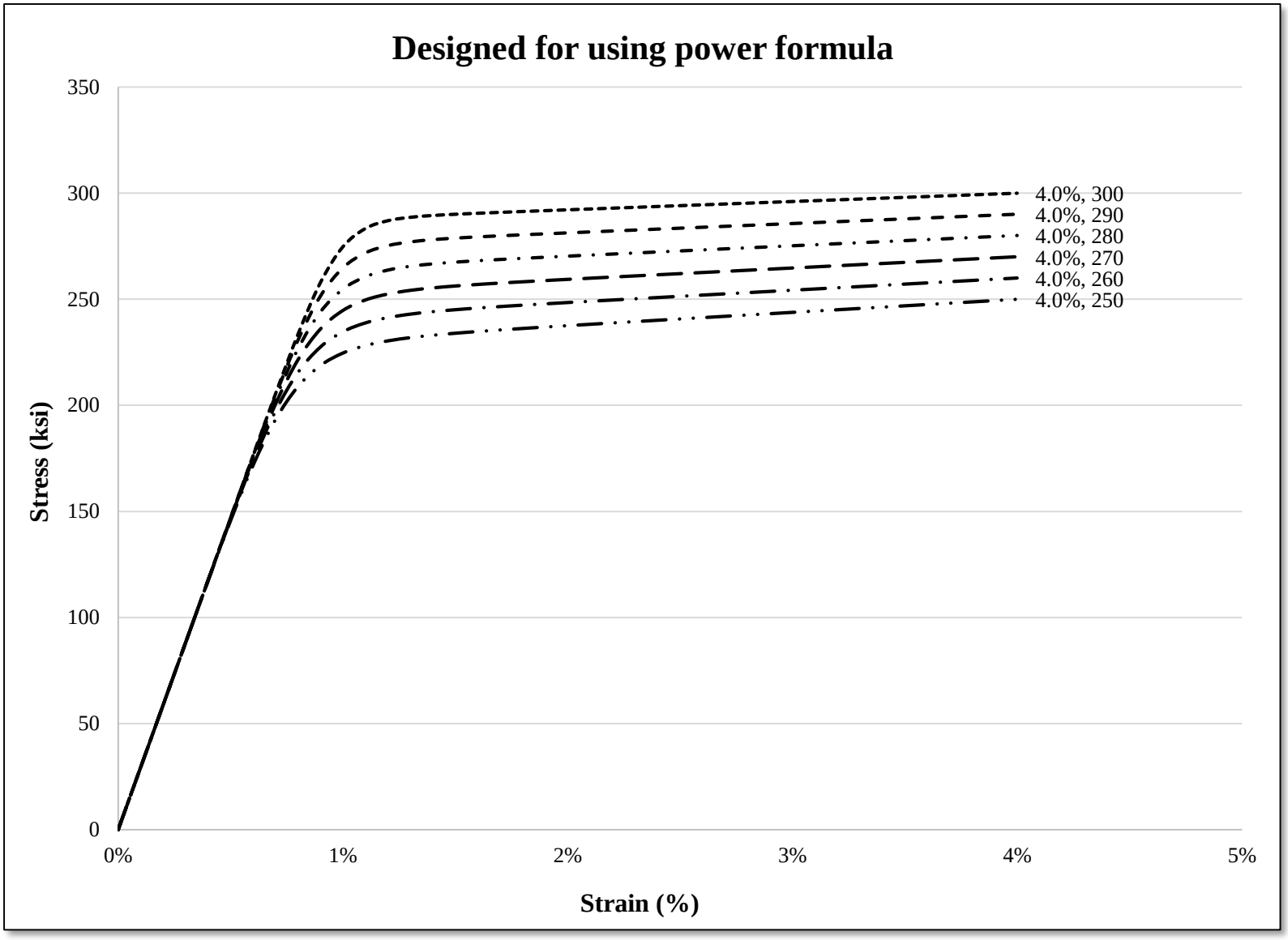


Figure 4.7 Stress-Strain curve plot by redesigned power formula

## 4.4 Conclusion

Prestressing wire is used in concrete railroad ties around the world. ASTM A881 (2015) is the standard for design and quality control of this type of wire. During specimen preparation, the difference in actual wire properties compared to those discovered by the ASTM standard. The majority of measured wire properties indicated some differences with the mill cert data. Additionally, the wire mechanical behavior satisfied ASTM A881 minimum requirements, but the overall wire experimental results indicated higher strengths with longer minimum elongation. Compared to the ASTM minimum requirements, even the lowest wire's tensile strength and percent elongation showed significant differences.

For predicting stress in prestressing wire, several existing equations can be adopted. However, resulting predictions were found to be inaccurate and typically underestimated the wires' true strength. This research captured the complete stress-strain development patterns experimentally. It further evaluated coefficients of the power formula through fitting experimental results individually. The modeled stress-strain curves improved the accuracy of the response when the proportional limit was taken at 0.7% strain. Consequently, the average error out of 28 curves was reduced to 3%.

Regression equations were developed for computing constants of the power formula using the basic known wire type and properties. The regression equations were devised to generalize the constants based on experimental fitting results, while the accuracy of the wire behavior was maintained.

For design purposes, limits of the power formula were modified to generate a series of curves based on prestressing wire strength at 4% ultimate strain. Yield strength ($f^*_{py}$) and the constant K* were generalized in terms of the wire's ultimate strength through a regression analysis. On the other hand, constant R was determined and tabulated for each strength level. According to the examined results, the design equation provided efficient utilization of the wire material behavior. Also the calibrated design equations were accurate, reliable, and slightly conservative.

# Chapter 5 Modeling Stress-Strain Curve — *PCI Equation*

## 5.1 Analytical Modeling Using PCI Equation for Prestressing Wire

From the observation of experimental performance, respective types of wire have developed higher stress values with longer strains than existing prediction and standard equations. Figure 5.1 compares the experimental curves with the current PCI strand equations' representative curves. From Figure 5.1, the PCI 250 ksi strand equation had a yield strength close to the [WG] wire but the [WG] wire had ultimate strength near 270 ksi (1,862 MPa), similar to the PCI 270 ksi strand equation. On the other hand, the 270 ksi strand representative curve miscalculated the force before the end of the yielding evolution. Thus, considering the PCI strand equation was not suitable for predicting the stress in prestressing wire, this study started by first adapting the PCI strand equation to better fit the prestressing wire curve through reevaluating the appropriate equation constants.

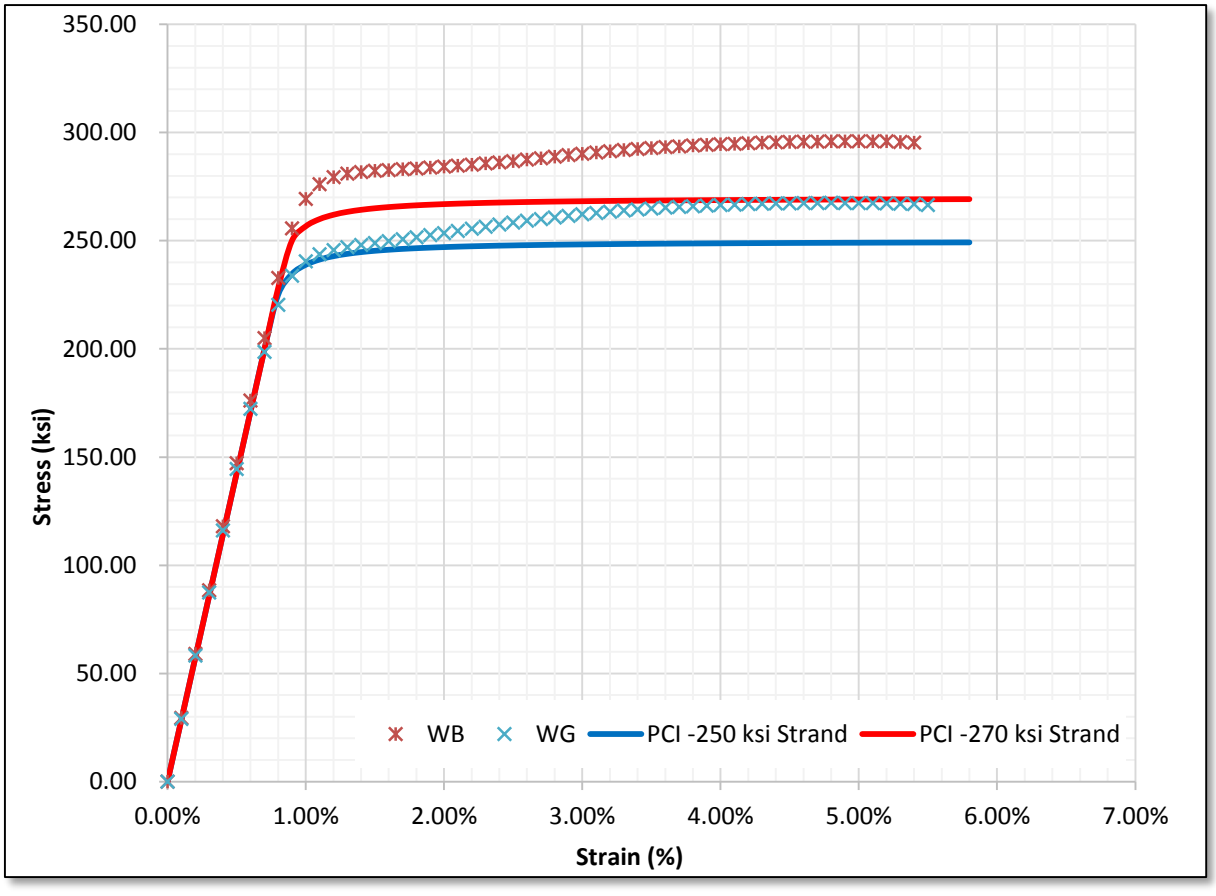


Figure 5.1 Experimental stress-strain curves compared with current PCI strand 270 ksi and 250 ksi represented curves

In the analysis and modeling part of this study, the experimental results utilized the average curve out of three reliable resulting curves, totaling 10 stress-strain diagrams used, including the [WI] wire. This study redefined the constants in the PCI strand equation as "a" and "b"; furthermore, it assumed the ultimate strength-related parameter as a third unknown, $f^*_{pu}$, because $f^*_{pu}$ will influence the curve's development after elastic behavior. The $f^*_{pu}$ should not be defined as the ultimate strength, and the new PCI equation can be written as follows:

$$f_{ps} = f_{pu}^* - \frac{a}{\varepsilon_{ps} - b} \qquad \text{Equation (5-1)}$$

For properly fitting the experimental curve, the three unknown parameters will be recovered through solving three simultaneous equations for $f_{ps}$ at yield, ultimate, and proportional limit points. The simultaneous equations are written as follows:

$$0.007E = f_{pu}^* - \frac{a}{0.007 - b} \qquad \text{Equation (5-2)}$$

$$f_{py} = f_{pu}^* - \frac{a}{0.15 - b} \qquad \text{Equation (5-3)}$$

$$f_{pu} = f_{pu}^* - \frac{a}{\varepsilon_{pu} - b} \qquad \text{Equation (5-4)}$$

The yielding point for modeling the PCI wire equation was not following the 0.2% offset method or stress at 1% extension in the ASTM A881 specification. The reason for this was that the proportional limit (0.7% strain) was too close to the stress at 1% strain. Also, the 0.2% offset method results showed the yield point was between 1.1% to 1.2% strain (Figure 5.2).

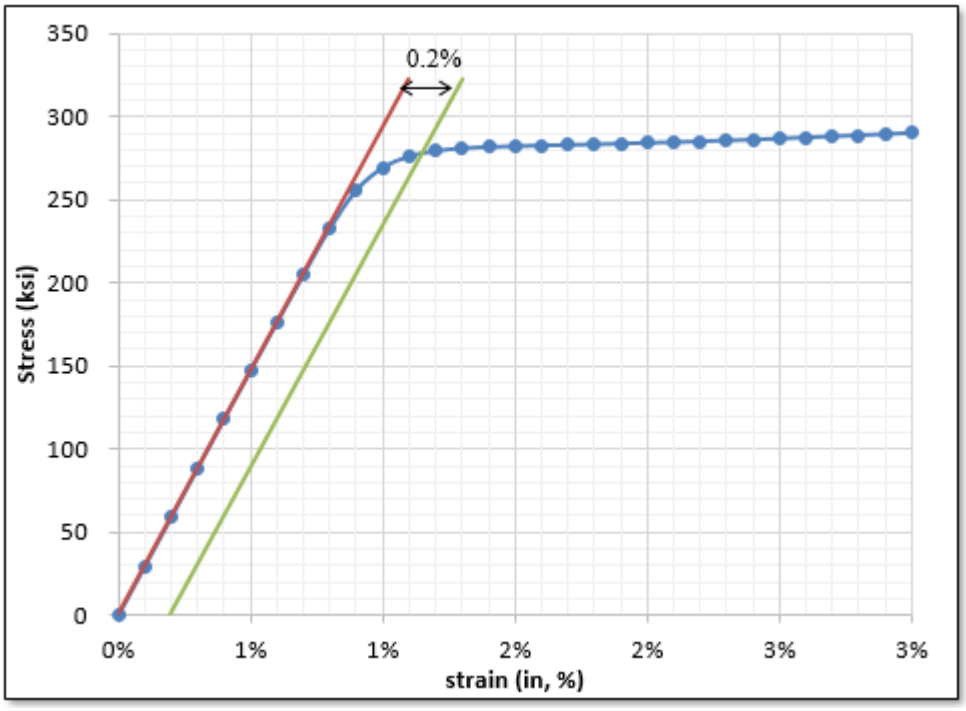


Figure 5.2 Offset method for determining yield point on experimental stress-strain curve

Neither the stress at 1% nor 1.2% elongation represented the actual yield point since Figure 5.2, showing the typical wire experimental stress-strain curve having the yield phenomenon, evolved between a stress shortly after 0.7% strain to 1.5% strain. Hence, the yield point was set at 1.5% strain through observed experimental results for the modeling of the PCI wire equation. Then, the proper three constants were extracted through solving the three simultaneous equations above [(Equation (5-2), Equation (5-3), and Equation (5-4)]. This will represent an analysis and quality control standard for further work. Also, plotting the predicted curves against the experimental curves affirmed the accuracy.

The three unknown parameters could be easy to recover when the completed stress-strain curves are available. In order to generalize these parameters for any curve, regression equations were developed for the purpose of reproducing absent experimental data. Based on the distinct mechanical properties of each curve, the relationship between the key variables (E, $f_{py}$, $\varepsilon_{py}$, $f_{pu}$ and $\varepsilon_{pu}$) and the dependent variables (a and $f^*_{pu}$) will be investigated. Trials of comparing various independent variable combinations with the two parameters (a and f*pu) were required until a tight correlation was identified. Consequently, the strong negative and/or positive regression relationship was detected for the constants "a" and "$f^*_{pu}$". After that determination, the constant b

could be analytically calculated when $f_{ps}$ equal to proportional limit point ($E\varepsilon_{ps}$) was expressed as follows:

$$b = \varepsilon_{ps} - \frac{a}{f^*_{pu} - E\varepsilon_{ps}} \qquad \text{Equation (5-5)}$$

where $\varepsilon_{ps}$ is 0.7% strain and the constants "a" and $f^*_{pu}$ are determined from their respective linear regression equations. To ensure the precision, drawing the stress-strain curve by utilizing the constant's regression equation was necessary.

## 5.2 Development of Regression Equations

The proper value of parameters were found, accordingly, to compare to the experimental curves that the represented stress-strain curve that was highly fitted. During the modeling, each constant was identified for influencing a part of the curve. Such as the parameter "a" determined the level of radius on yield evolution had been identified, and the radius became sharp with lower developing force while the value of a increased. Constant "b" decided the starting force on the first point after the proportional limit (0.7% strain). If the value of "b" was decreasing, the plastic part of the curve began in small stress, and eventually the 0.7% strain corresponding force dropped lower than the previous point. On the contrary, the stress at 0.7% strain increased while the constant "b" grew. Hence, it was significant to define the adequate value for constants, and discovered results from the simultaneous equations are demonstrated in Table 5.1. From Table 5.1, the constants had minor differences for fitting different types of wire, which implied the sensitivity of coefficients. Represented stress-strain curves are shown in Appendix E.

Proper values of the three constants needed to be found based on closely fitting the experimental curves. During the modeling process, each constant was identified to influence a certain part of the curve. For example, parameter "a" determined the level of radius on the yield evolution, and the radius became sharp with lower developing stress while the value of "a" was increased. Accordingly, this constant needed to be correlated to the yield strength value. The constant $f^*_{pu}$ determined ultimate strength level of the curve. Therefore, it needed to be correlated to the actual ultimate strength of each curve, $f_{pu}$. Constant "b" decided the starting stress on the first point after the proportional limit (0.7% strain). Accordingly, the proportional limit was used to compute this constant, as shown in Equation (5-5). Hence, it was significant to define the adequate values for the three constants, as recovered from the simultaneous equations

and listed in Table 5.1. From Table 5.1, the constants reflected minor differences for fitting different types of wire, which implied the sensitivity of these coefficients to variations in wire response. Represented stress-strain curves are shown in Appendix E.

Table 5.1 Parameters evaluated from fitting experimental curves for the PCI equation

| | **$f_{py}$ @ 1.5% strain ,ksi [MPa]** | **a** | **b** | **$f^*_{pu}$ ,ksi [MPa]** | **Maximum error, %** |
|---|---|---|---|---|---|
| **[WB]** | 282.23 [1,946] | 0.1740 | 0.0051 | 299.90 [2,068] | 2.66 |
| **[WD]** | 263.24 [1,815] | 0.2710 | 0.0036 | 286.91 [1,978] | 3.28 |
| **[WE]** | 264.27 [1,822] | 0.2415 | 0.0041 | 286.41 [1,975] | 2.51 |
| **[WF]** | 260.42 [1,796] | 0.2823 | 0.0036 | 285.25 [1,967] | 4.39 |
| **[WG]** | 248.87 [1,716] | 0.3157 | 0.0026 | 274.38 [1,892] | 3.84 |
| **[WH]** | 276.87 [1,909] | 0.2006 | 0.0045 | 295.94 [2,040] | 2.43 |
| **[WI]** | 270.88 [1,868] | 0.1543 | 0.0051 | 286.49 [1,975] | 3.30 |
| **[WJ]** | 271.76 [1,874] | 0.1775 | 0.0051 | 289.62 [1,997] | 1.98 |
| **[WL]** | 264.39 [1,823] | 0.2849 | 0.0035 | 289.15 [1,994] | 5.49 |
| **[WM]** | 263.35 [1,816] | 0.3711 | 0.0027 | 293.41 [2,023] | 4.78 |
| **Average** | 266.63 [1,838] | 0.2469 | 0.0040 | 288.74 [1,991] | 3.47 |

From Appendix E. 1, with the [WB] wire graph, the represented curve was a desired fit on elastic and plastic regions, but the transition part of the curve did not respond to the experimental curve well. There were two explanations. First the modeling curve had a larger radius, which indicated the constant "a" was larger. Secondly, the represented curve was yielded earlier than the experimental results, and the proportional limited point and constant "a" were affected. However, overall accuracy was above 96%, which was the average error of 28 observations minus 100%. The maximum error was the difference between the experimental curve and stress-strain curve, determined by solving simultaneous equations individually. Furthermore, maximum error did not include the error before the proportional limit. The uppermost difference of 5.49% was generated

from the [WL] wire. The smallest overall error was generated from the [WJ] wire, with the maximum difference of 1.98%. According to experimental results, the maximum error possible was either in the elastic or plastic region, but the errors were slightly larger in the elastic region such as the [WH] and [WJ] wires. Considering this, the elastic behavior followed the Hook laws for the wires and modeling theory. Also the testing machine was adjusted to straighten the specimen in the beginning of tensile testing to become calibrated. Therefore, the maximum error eliminated the errors performed before the 0.7% strain. The maximum error could be reduced about 1% without considering the elastic region curve. Then the precision of the represented curve could be raised to 96.5%. After examining the data in Table 5.1 and graphs in Appendix E, results from fitting experimental curves were reliable and proper for further regression analysis.

In the regression analysis, the regression equation was developed to generalize the constants, and the best relationship found in constants was associated with ultimate strength ($f_{pu}$). The linear regression graph (Figure 5.3) indicated a strong positive relationship with $R^2$ = 0.9872, and the linear regression equation is as below:

$$f_{pu}^{*} = 0.9214 f_{pu} + 27.5165 \qquad \text{Equation (5-6)}$$

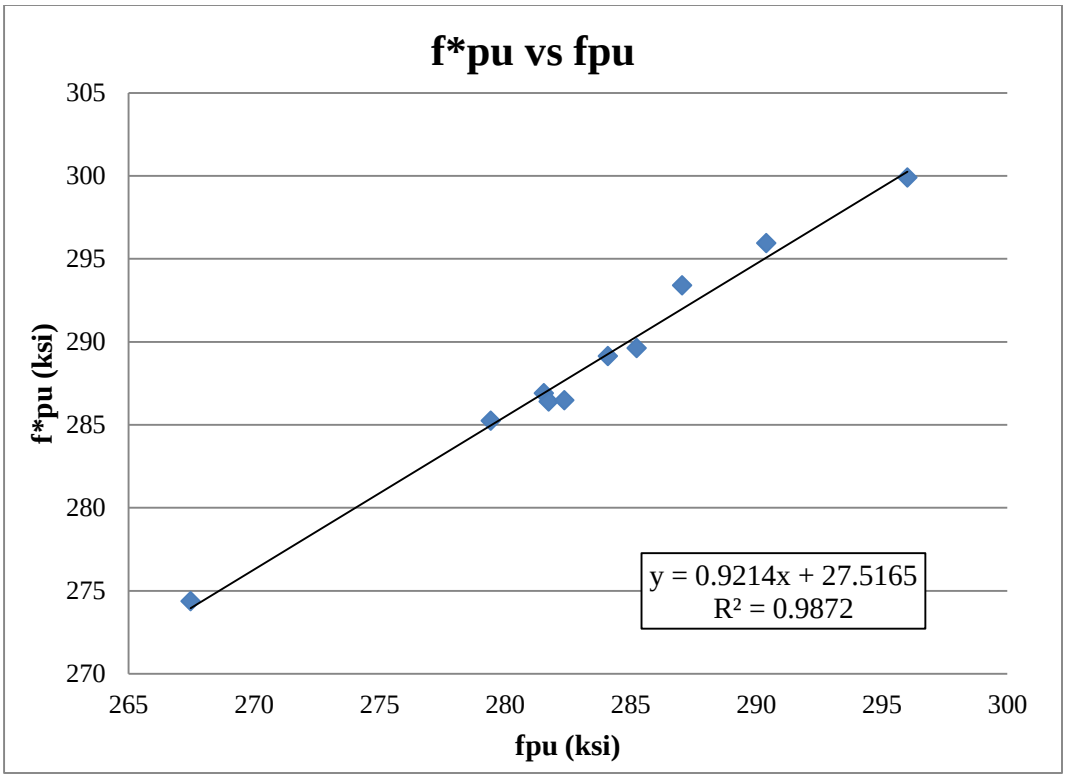


Figure 5.3 Regression relationship for constant $f^*_{pu}$

On the other hand, the value of "a" has been identified with a strong positive correlation associated to the change between the ultimate strength and yield strength with a coefficient of determination of 0.9479. The regression analysis graph is shown in Figure 5.4.

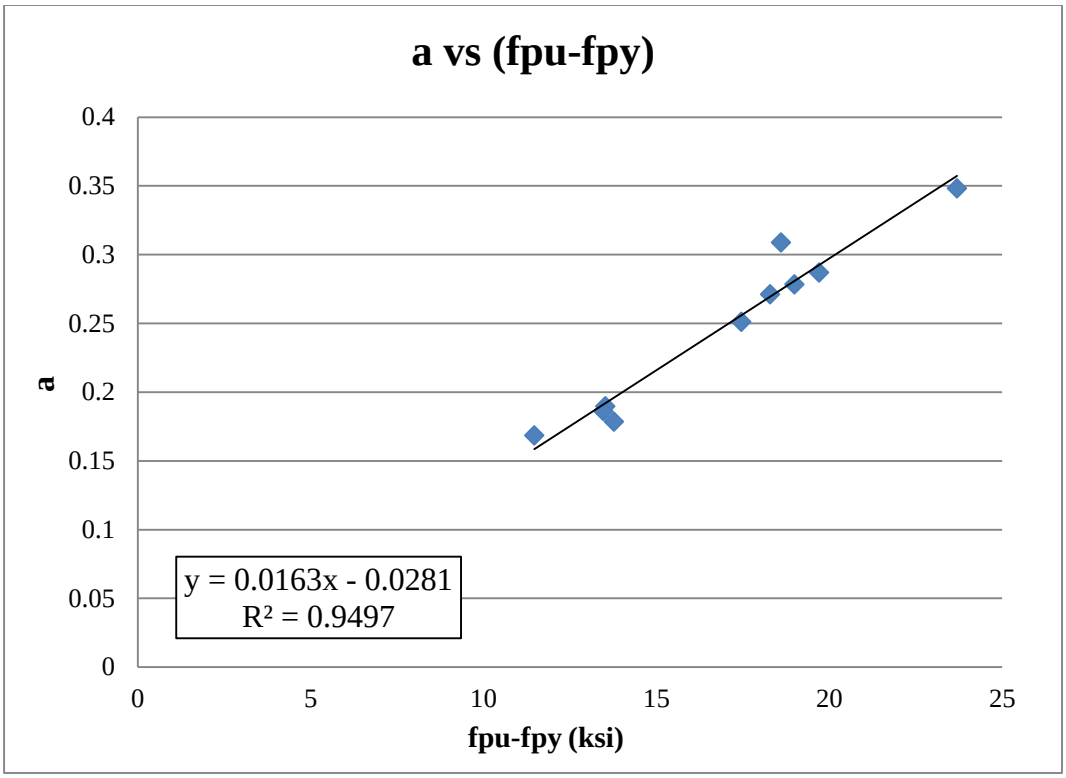


Figure 5.4 Regression relationship for constant "a"

The linear regression equation is

$$a = 0.0163(f_{pu} - f_{py}) - 0.0281 \ \ (ksi)$$ Equation (5-7)

The constant “b” could be solved through the predicted “f*pu” and “a” constants from the regression equations into the PCI wire equation evaluated at the proportional limit. The evaluated results are shown in Table 5.2, and the individual wire stress-strain curves are shown in Appendix E. In Table 5.2, the constants did not have much variation, which is the same as the experimental fitting results, and the regression analysis results maintained accuracy above 96%, which did not have significant difference than the average experimental curve-fitting maximum error. The 96% accuracy was computed through an average 28 regression analysis maximum error, and subtracted by 100%.

Table 5.2 Parameters from regression analysis and percentage of variance

| | $f_{py}$ @ 1.5% strain ,ksi [MPa] | a | b | $f^*_{pu}$ ,ksi [MPa] | Maximum error, % |
|---|---|---|---|---|---|
| **[WB]** | 282.23 [1,946] | 0.1965 | 0.0049 | 300.26 [2,070] | 2.94 |
| **[WD]** | 263.24 [1,815] | 0.2701 | 0.0036 | 286.92 [1,978] | 3.25 |
| **[WE]** | 264.27 [1,822] | 0.2564 | 0.0039 | 287.10 [1,979] | 2.76 |
| **[WF]** | 260.42 [1,796] | 0.2816 | 0.0036 | 284.97 [1,965] | 4.45 |
| **[WG]** | 248.87 [1,716] | 0.2752 | 0.0032 | 273.97 [1,889] | 3.01 |
| **[WH]** | 276.87 [1,909] | 0.1923 | 0.0046 | 295.08 [2,035] | 2.54 |
| **[WI]** | 270.88 [1,868] | 0.1589 | 0.0051 | 287.68 [1,984] | 3.36 |
| **[WJ]** | 271.76 [1,874] | 0.1915 | 0.0049 | 290.33 [2,002] | 2.33 |
| **[WL]** | 264.39 [1,823] | 0.2931 | 0.0034 | 289.28 [1,995] | 5.67 |
| **[WM]** | 263.35 [1,816] | 0.3581 | 0.0027 | 292.00 [2,013] | 4.82 |
| Average | 266.63 [1,838] | 0.2474 | 0.0040 | 288.76 [1,990] | 3.51 |

## 5.3 Design and Recommendation for a Wire Using PCI Equation

The purpose of this section was to design the PCI equation for estimating wire stress in any types of prestressing wire under the assumed wire strength. The designed PCI equation was intended for estimated $f_{ps,}$ while the wire strength was in between 250 ksi to 300 ksi. The wire strength range was determined by examining the current estimation and experimental results. The PCI equation was redefined as below:

$$f_{ps} = f'_{pu} - \frac{a'}{\hat{\varepsilon_{ps}} - b'} \qquad \text{Equation (5-8)}$$

From the experimental results, the highest wire strength capacity was near 300 ksi, such as the [WB] wire; additionally, the current PCI strand equation had the estimation in the wire stress at 250 ksi.

Minimum wire ultimate strain ($f^{\wedge}_{pu}$) was redefined at 4% strain because all the wires grew at least 0.04 inches or more; in addition, the percent of elongation satisfied the ASTM minimum requirement. In the design using the PCI equation, the wire ultimate strain was consistent with level of wire strength, which resulted in redefining the regression equation as needed. Additionally, in order to insure the precision of the designed stress-stain curve, the design produced should minimize errors from the regression analysis. For the PCI equation, the regression equation was developed to generalize the yield stress ($f^{\wedge}_{py}$) for the purpose of corresponding in terms of wire behaviors. From the results in regression analysis, the regression equation revealed a strong positive relationship between yield stress ($f^{\wedge}_{py}$) and $f^{\wedge}_{pu}$ with $R^2$ = 0.9633. The regression analysis graph is shown in Figure 5.5.

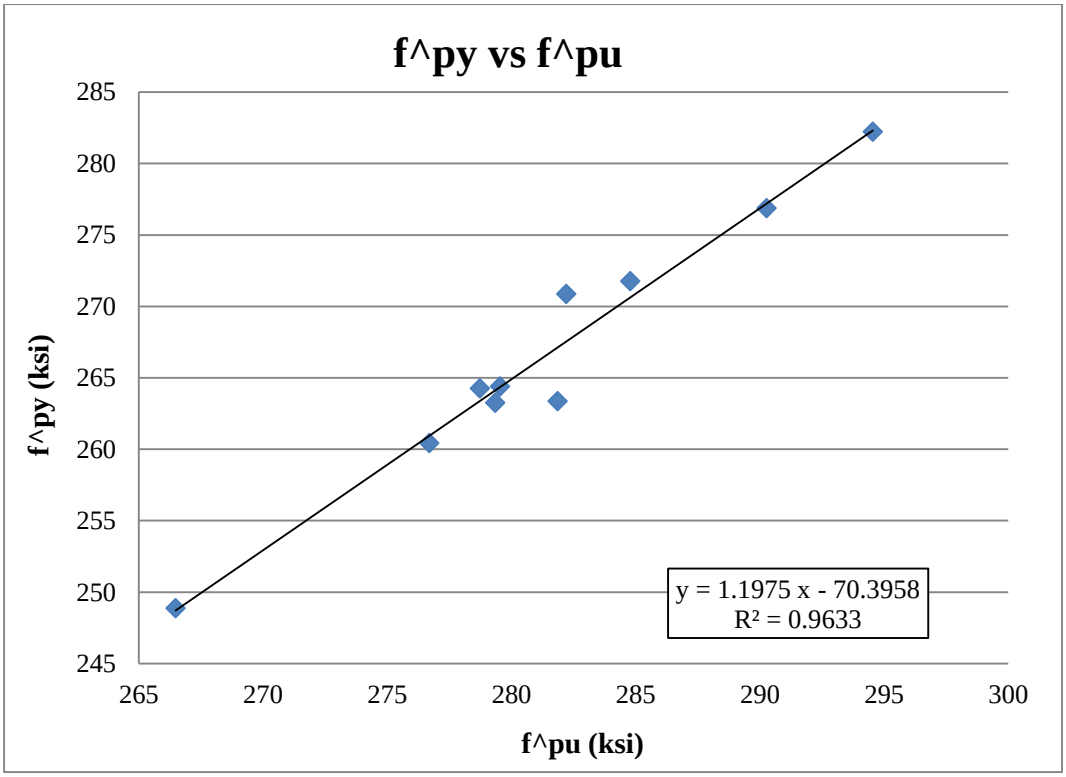


Figure 5.5 Regression relationship for yield stress, $f^{\wedge}_{py}$

The linear regression equation is shown as follows:

$$f^{\wedge}_{py} = 1.19975 f^{\wedge}_{pu} - 70.3958 \qquad \text{Equation (5-9)}$$

Under the assumption that constant $f'_{pu}$ was consistent at any point of the design curve, constants a and b will be resolved when wire stress is at $\varepsilon^{\wedge}_{ps} E_p, f^{\wedge}_{py}$, and $f^{\wedge}_{pu}$. Then equilibrium equations

could be written as

$$f'_{pu} = f^{\wedge}_{pu} + \frac{a'}{\varepsilon^{\wedge}_{pu} - b'} = f^{\wedge}_{py} + \frac{a'}{\varepsilon^{\wedge}_{py} - b'} = \varepsilon^{\wedge}_{ps} E_p + \frac{a'}{\varepsilon^{\wedge}_{ps} - b'} \qquad \text{Equation (5-10)}$$

$\varepsilon^{\wedge}_{pu}$ is ultimate strain at 4%.
$\varepsilon^{\wedge}_{py}$ is yield strain at 1.5%.
$\varepsilon^{\wedge}_{ps}$ is percent of elongation at proportional limit point.
$E_p$ is 29,376.04 ksi, which is the average of 28 experimental results.

The constant a' is found when the stress in the prestressing wire ($f^{\wedge}_{ps}$) at ultimate is equal to yield point, and the equilibrium equation is

$$f^{\wedge}_{pu} - f^{\wedge}_{py} = a' \left( \frac{1}{\varepsilon^{\wedge}_{ps} - b'} - \frac{1}{0.04 - b'} \right) \qquad \text{Equation (5-11)}$$

The equilibrium equation can be presented as

$$f^{\wedge}_{pu} - f^{\wedge}_{py} = a' \left( \frac{0.04 - \varepsilon^{\wedge}_{ps}}{\left(\varepsilon^{\wedge}_{ps} - b'\right)(0.04 - b')} \right) \qquad \text{Equation (5-12)}$$

Substitution of Equation (5-9) into Equation (5-13) can be represented as

$$f^{\wedge}_{pu} - (1.19975 f^{\wedge}_{pu} - 70.3958) = a' \left( \frac{0.04 - \varepsilon^{\wedge}_{ps}}{\left(\varepsilon^{\wedge}_{ps} - b'\right)(0.04 - b')} \right) \qquad \text{Equation (5-13)}$$

Value a' may be written

$$a' = \frac{\left(\varepsilon^{\wedge}_{ps} - b'\right)(0.04 - b')\left(-0.19975 f^{\wedge}_{pu} + 70.3958\right)}{0.025} \qquad \text{Equation (5-14)}$$

Continually constant b' could be computed when $f^{\wedge}_{ps}$ at yield point is equal to proportional limit, and the equilibrium equation is

$$\left(f^{\wedge}_{py} - \varepsilon^{\wedge}_{ps} E_p\right) = a' \left( \frac{1}{\varepsilon^{\wedge}_{ps} - b'} - \frac{1}{0.015 - b'} \right) \qquad \text{Equation (5-15)}$$

Substitution of Equation (5-14) into Equation (5-15), and the equation can be written as

$$\left(f_{py}^{\wedge} - \varepsilon_{ps}^{\wedge} E_p\right) = \left(\frac{(0.015 - b\ ´)(0.04 - b\ ´)(f_{pu}^{\wedge} - f_{py}^{\wedge})}{0.025}\right)\left(\frac{0.015 - \varepsilon_{ps}^{\wedge}}{(\varepsilon_{ps}^{\wedge} - b\ ´)(0.015 - b\ ´)}\right) \quad \text{Equation (5-16)}$$

$$\left(f_{py}^{\wedge} - \varepsilon_{ps}^{\wedge} E_p\right) = \frac{0.015 - \varepsilon_{ps}^{\wedge}}{0.025}\left(f_{pu}^{\wedge} - f_{py}^{\wedge}\right)\left(\frac{(0.04 - b')}{\left(\varepsilon_{ps}^{\wedge} - b'\right)}\right) \quad \text{Equation (5-17)}$$

$$\left(\frac{0.025}{0.015 - \varepsilon_{ps}^{\wedge}}\right)\left[\left(f_{py}^{\wedge} - \varepsilon_{ps}^{\wedge} E_p\right)\varepsilon_{ps}^{\wedge} - \left(f_{py}^{\wedge} - \varepsilon_{ps}^{\wedge} E_p\right)b'\right] = \left(f_{pu}^{\wedge} - f_{py}^{\wedge}\right)0.04 - \left(f_{pu}^{\wedge} - f_{py}^{\wedge}\right)b' \quad \text{Equation (5-18)}$$

$$b'\left(f_{pu}^{\wedge} - f_{py}^{\wedge} - \left(\frac{0.025}{0.015 - \varepsilon_{ps}^{\wedge}}\right)f_{py}^{\wedge} + \left(\frac{0.025}{0.015 - \varepsilon_{ps}^{\wedge}}\right)\varepsilon_{ps}^{\wedge} E_p\right) = \left(f_{pu}^{\wedge} - f_{py}^{\wedge}\right)0.04 - \left(\frac{0.025}{0.015 - \varepsilon_{ps}^{\wedge}}\right)\varepsilon_{ps}^{\wedge}\left(f_{py}^{\wedge} - \varepsilon_{ps}^{\wedge} E_p\right) \quad \text{Equation (5-19)}$$

Then value b' may be written as

$$b' = \frac{\left(f_{pu}^{\wedge} - f_{py}^{\wedge}\right)0.04 - \left(\frac{0.025}{0.015 - \varepsilon_{ps}^{\wedge}}\right)\varepsilon_{ps}^{\wedge}\left(f_{py}^{\wedge} - \varepsilon_{ps}^{\wedge} E_p\right)}{\left(f_{pu}^{\wedge} - f_{py}^{\wedge} - \left(\frac{0.025}{0.015 - \varepsilon_{ps}^{\wedge}}\right)f_{py}^{\wedge} + \left(\frac{0.025}{0.015 - \varepsilon_{ps}^{\wedge}}\right)\varepsilon_{ps}^{\wedge} E_p\right)} \quad \text{Equation (5-20)}$$

Substituting Equation (5-9) into Equation (5-20) solved constant b' with corresponding proportional limit ($\varepsilon_{ps}^{\wedge}$) in Table 5.3. Then $f'_{pu}$ can be found by substituting Equation (2-14), Equation (2-20), and the proper value of the proportional limit point ($\varepsilon_{ps}^{\wedge}$) into Equation (5-10). The strain at proportional limited ($\varepsilon^{\wedge}_{ps}$) was varied because the yield evolution was influenced by level of wire ultimate strength. The yielding evolution happened earlier with lower wire strength, opposing higher wire ultimate stress. Hence, $\varepsilon^{\wedge}_{ps}$ was classified in three regions as shown in Table 5.3.

Table 5.3 Proportional limit point ($\varepsilon^{\wedge}_{ps}$) with corresponding wire strength ($f^{\wedge}_{pu}$)

| $\boldsymbol{\varepsilon_{ps}^{\wedge}}$ | $\boldsymbol{f_{pu}^{\wedge}}$ **(ksi)** |
|---|---|
| 0.8% | 290 and 300 |
| 0.7% | 280 and 270 |
| 0.6% | 260 and 250 |

Then constant $f'_{pu}$ could be obtained by substituting constant a' and b' from Equation (5-14) and Equation (5-20), and using either yield, ultimate, or proportional limited points to solve it. The stress-strain curve could be plotted by substituting Equation (5-10), Equation (5-14), and Equation (5-20) into Equation (5-8). The computation for constants is presented in Table 5.4, and the designed stress-strain curves are presented in Figure 5.6. From Figure 5.6, the stress at 4% strain did not exceed assumed wire ultimate stress, and terms of the proportional limit made the yielding behavior more appropriate in level of wire strength.

Table 5.4 Parameters for designed PCI equation

| $\hat{f_{pu}}$, ksi [MPa] | $\hat{\varepsilon_{ps}}$, % | $\hat{f_{py}}$, ksi [MPa] | $f'_{pu}$, ksi [MPa] | $a'$ | $b'$ |
|---|---|---|---|---|---|
| 250 [1,724] | 0.6 | 228.98 [1,579] | 304.00 [2,096] | 0.491 | 3.02E-4 |
| 260 [1,793] | 0.6 | 240.95 [1,661] | 295.29 [2,036] | 0.378 | 1.97E-3 |
| 270 [1,862] | 0.7 | 252.93 [1,744] | 286.60 [1,976] | 0.314 | 2.69E-3 |
| 280 [1,931] | 0.7 | 264.90 [1,827] | 278.41 [1,920] | 0.237 | 4.07E-3 |
| 290 [2,000] | 0.8 | 276.88 [1,909] | 269.93 [1,861] | 0.186 | 4.92E-3 |
| 300 [2,068] | 0.8 | 288.85 [1,992] | 262.36 [1,809] | 0.136 | 6.03E3 |

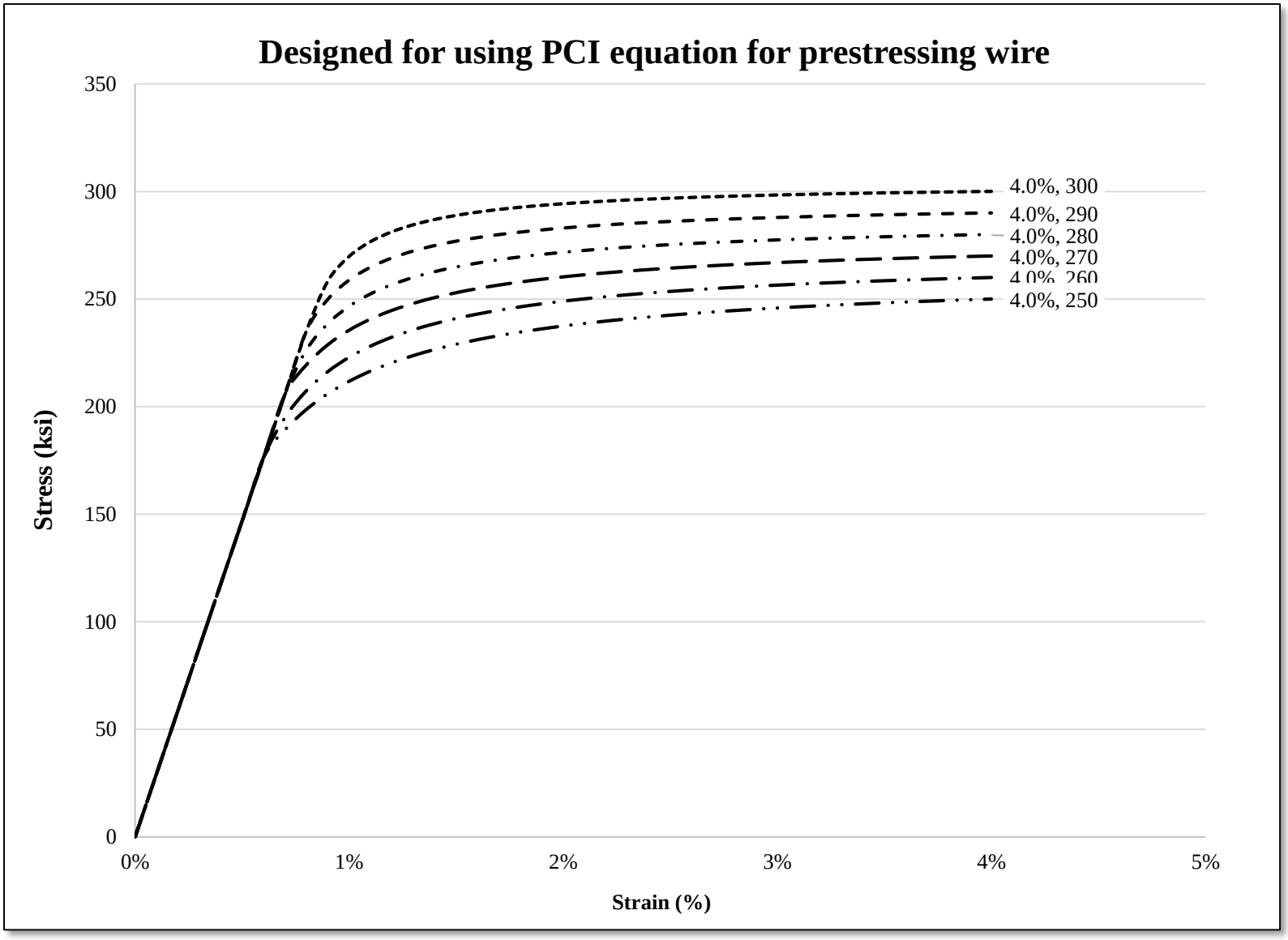


Figure 5.6 Stress-strain curves plotted by redesigned PCI equation

## 5.4 Conclusion

Prestressing wire is internationally used in the manufacture of concrete railroad ties, with ASTM A881 often used as the standard for design and quality control. During specimen tensile testing, differences in wire properties have been discovered. A majority of actual wire properties showed a slight difference from the mill cert data, and also did not reach upwards of ASTM A881 minimum requirements. Additionally the wires' mechanic behavior satisfied ASTM A881 but overall wire experimental results indicated a higher behavior in stress with longer minimum elongation. Compared to ASTM minimum requirements, even wires with the lowest tensile strength and percent elongation showed significant differences.

For predicting stress in prestressing wire, several equations exist, but those estimations are not precise and underestimate a wire's true strength. This research captured the completed stress-strain development behavior experimentally, and evaluated coefficients in the PCI equation through fitting individual experimental results. The modeling stress-strain curves improved the accuracy of the response when the yield point was at 1.5% strain and the proportional limit at 0.7% strain; consequently, the average error out of 28 curves was reduced to 5%.

PCI strand equations are commonly using for estimating stress in prestressing wire even though the equation was designed for prestressing strand. However, the PCI strand equation is not appropriate to estimate the stress in prestressing wire because it overestimated the stress before the end of yield evolution. The regression analysis was developed to generate PCI equations when the basic wire type and properties are known. The regression equations were developed to generalize the constants in the PCI equation based on experimental fitting results and accuracy of the wire behaviors maintained.

For future demand, the designed PCI equation may be used in practical application for estimating the ultimate strength of prestressing wire. A wire's ultimate strength corresponding to minimum elongation is unified at 4% strain, and yield stress is generalized by the linear regression equation. Hence, the design equation provided efficient utilization of wire material behavior, and also the calibrated design equation was accurate, reliable, and slightly conservative. A closer estimation could effectively reduce unnecessary prestressing wire involved in the design and result in huge savings.

# Chapter 6 Recommendations Using Equations

This research discovered a more accurate response to experimental outputs through several stages of analysis. First, constants were redefined through finding the best-fit experimental curves. Second, the constants were correlated to the strongest independent variable by generating linear regression equations. In this step, the newly developed equations could be applied while the prestressing wire types and grades were known. Last, the equations were re-developed for design-oriented computations. To offer convenience applying the equations in practical applications, the parameters were correlated to the wire grade, which is a common assumption in prestressing or reinforcement concrete design. Thus the equation could be used when specific or assumed ultimate prestressing strength was given.

Re-developed “power formula” and PCI equations had different responses on the transition part of the curve when specific prestressing wire grade was applied, as shown in Figure 6.1. Figure 6.1 presents the stress-strain curves computed by the re-developed equations (PCI and power formula), fitting to the WG wire experimental curve. No significant differences showed after yielding in the re-developed curves. The re-developed power formula curve had a smaller radius and closer yielding achievement than the PCI equation when the yield point was at 1% strain. On the other hand, the redeveloped PCI equation had good agreement at 1.5% strain. The redeveloped equations had different responses to the transition of the curve, indicating that yield point should be considered as a key factor when selecting an equation.

There are some recommendations for applying the newly developed PCI equation and power formula. For the prestressing wire type when grade is recognized, the difference for applying the newly developed equations was the yield strain, which was 0.1% for the power formula, and 0.15% for the PCI equation. For using the PCI equation, Table 5.2 defined the detail constants for implementing the stress-strain curve or particular strength in the wire with the corresponding strain. For using the power formula, Table 6.1 offers the required parameters to construct stress in prestressing wire. On the other hand, the common design grade in prestressing concrete is 250 ksi and 270 ksi, and Table 6.2 indicates the parameters and detail-fitting constraints for using re-developed equations.

Table 6.1 Newly developed power formula design parameter for specific prestressing wire type and grade

| Type of wire | Modulus of elasticity ($E_p$), ksi [MPa] | Yield strength ($f_{py}$), ksi [MPa] | Ultimate strength ($f_{py}$), ksi [MPa] | Ultimate strain ($\varepsilon_{pu}$), % | K | Q | R |
|---|---|---|---|---|---|---|---|
| **[WB]** | 29,419 [202,840] | 269.24 [1,856] | 296.01 [2,041] | 4.99 | 1.044 | 0.013 | 10.662 |
| **[WD]** | 29,763 [205,210] | 253.19 [1,746] | 281.54 [1,941] | 5.39 | 1.040 | 0.014 | 7.779 |
| **[WE]** | 29,057 [200,340] | 251.73 [1,736] | 281.73 [1,942] | 5.57 | 1.040 | 0.015 | 8.472 |
| **[WF]** | 28,778 [198,420] | 252.00 [1,737] | 279.42 [1,927] | 5.20 | 1.040 | 0.014 | 8.884 |
| **[WG]** | 28,890 [199,190] | 240.47 [1,658] | 267.47 [1,844] | 4.84 | 1.037 | 0.016 | 6.795 |
| **[WH]** | 30,882 [212,930] | 264.81 [1,826] | 290.39 [2,002] | 4.06 | 1.043 | 0.015 | 8.188 |
| **[WI]** | 292.55E2 [201,710] | 257.57 [1,776] | 282.35 [1,947] | 4.25 | 1.041 | 0.015 | 9.138 |
| **[WJ]** | 282.98E2 [195,110] | 258.62 [1,783] | 285.23 [1,967] | 4.55 | 1.042 | 0.016 | 10.530 |
| **[WL]** | 29,696 [204,750] | 258.76 [1,784] | 284.09 [1,959] | 5.98 | 1.042 | 0.010 | 8.755 |
| **[WM]** | 29,722 [204,920] | 254.95 [1,758] | 287.05 [1,979] | 6.10 | 1.041 | 0.014 | 8.118 |
| Yield strain is 0.1% | | | | | | | |

Table 6.2 Parameters or re-designed equations

| Stress-strain relationship | Fitting constraints | Prestressing wire | |
|---|---|---|---|
| | | 250 ksi [1,723.69 MPa] | 270 ksi [1,861.58 Mpa] |
| Power Formula | $\varepsilon_{py} = 0.01$<br>$\varepsilon_{pu} = 0.04$ | $f_{py}^{*} = 224.65$<br>$K^{*} = 1.0246$<br>$Q^{*} = 0.0210$<br>$R^{*} = 6.2949$ | $f_{py}^{*} = 244.68$<br>$K^{*} = 1.0355$<br>$Q^{*} = 0.0180$<br>$R^{*} = 7.4270$ |
| PCI equation | $\varepsilon_{py} = 0.015$<br>$\varepsilon_{py} = 0.04$<br>$\varepsilon_{ps} = 0.007^{*}$<br>$\varepsilon_{ps} = 0.006^{**}$ | $f'_{pu} = 304.0$<br>$a' = 0.491$<br>$b' = 29.20\text{E-}5$ | $f'_{pu} = 286.6$<br>$a' = 0.314$<br>$b' = 26.81\text{E} - 5$ |
| *for $f_{pu}$=270 ksi<br>**for $f_{pu}$=250 ksi<br>Modulus of elasticity ($E_p$) is 2,937.04 ksi (20,250.18 MPa) for both equations. | | | |

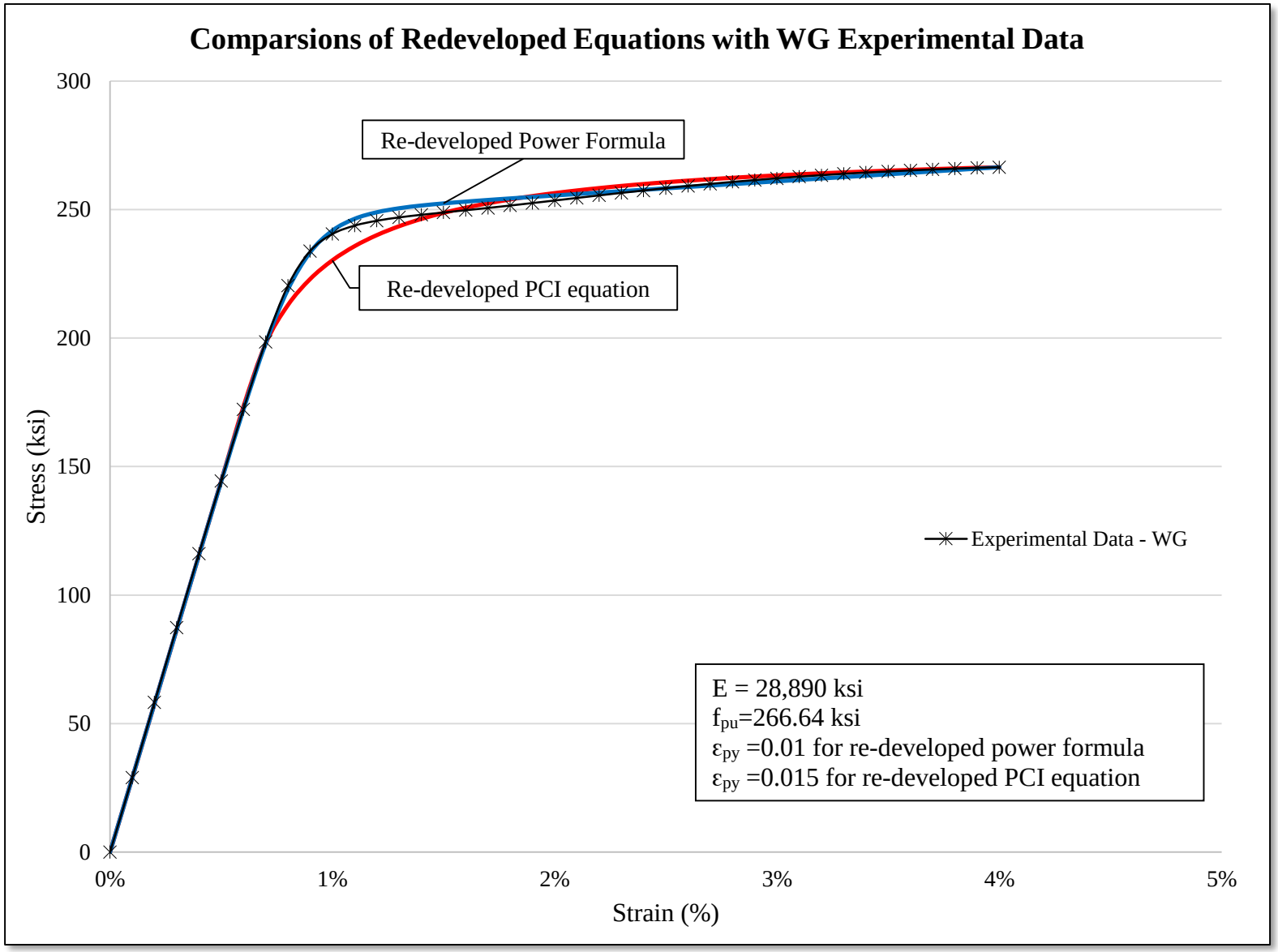


Figure 6.1 Comparisons of WG wire experimental results and re-developed equations

# References


Abdella, K. (2012). A three-stage, full-range,stress–strain inversion for stainless steel. *Thin-Walled Structures*(53), 9-14.

Albanesi, T., & Nuti, e. (2007). *Reinforcing Steel Bar Model.* Rome: University Roma Tre. Retrieved 02 28, 2016, from file:///F:/prestressed%20wire%20test/papers/1970.pdf

American Concrete Institute. (2014). *Building Code Requairments for Structural Concrete (ACI 318-11) and Commentary.* Farmington Hills.

ASTM A370. (2014). Standard Test Methods and Definitions for Mechanical Testing of Steel Products. In *Annual Book of ASTM Standards.* West Conshohocken, PA: ASTM International. Retrieved from www.astm.org

ASTM A416. (2015). Standard Specification for Low-Relaxation, Seven-Wire, Stress-Relieved Strand for Prestressed Concrete. In *Annual Book of ASTM Standard.* West Conshohocken, PA: ASTM International. Retrieved from www.astm.org

ASTM A881/A881M. (2015). Standard Specification for Steel Wire, Indented, Low-Relaxation for Prestressed Concrete Railroad Ties. In *Annual Book of ASTM Standards.* West Conshohocken, PA: ASTM International. Retrieved from www.astm.org

ASTM E8/E8M. (2015). Standard Test Methods for Tension Testing of Metallic Materials. In *Annual Book of ASTM Standards.* West Conshohocken, PA: ASTM International. Retrieved from http://compass.astm.org/download/E8E8M.10237.pdf

ASTM International. (2004). Tensile Testing - Chapter 1 : Introduction to Tensile Testing. (Second). Materuals Park, OH, USA. Retrieved 09 2015, from http://www.asminternational.org/documents/10192/3465262/05105G_Chapter_1.pdf/e13396e8-a327-490a-a414-9bd1d2bc2bb8

Beer, F. P., Johnston, E. R., DeWolf, J. T., & Mazurek, D. F. (2015). *Mechanics of Materials.* (Seventh, Ed.) New York: Mc Graw Hill Education.

Bosco, M., Ferrara, E., Ghersi, A., Marino, E. M., & Rossi, P. P. (2014). Improvement of the model proposed by Menegotto and Pinto for steel. *Second European Conference on Earthquake Engineering and Seismology* . Istanbul. Retrieved from file:///E:/prestressed%20wire%20test/papers/Menegott%20and%20pinto%201970.pdf

Byars, E. F., Snyder, R. D., & Plants, H. L. (1925). *Engineering Mechanics of Deformable*

*Bodies.* New York: Harper & Row.

Callister, D. W. (2007). *Materials Science and Engineering — An Introduction.* New York: John Wiley $ Sons, Inc. Retrieved from http://jpkc.fudan.edu.cn/picture/article/255/ba/c4/ceea01074b18aa612e67c5c8ed3d/14e79255-e194-4093-98f3-c1317c2adc73.pdf

Devalapura, R. K., & Tadros, M. K. (1992, March-April). Stress-Strain Modeling of 270 ksi Low-Relaxation Prestressing Strands. *PCI Journal, 37*(2), 100-106. Retrieved from http://www.pci.org/uploadedFiles/Siteroot/Publications/PCI_Journal/1992/DOI_Articles/jl-92-march-april-8.pdf

Goldberg, J. E., & Richard, R. M. (1963, August). Analysis of Nonlinear Structures. *Journal of the Structure Division: Proceeding of the American Society of Civil Engineers*, 333-351.

Haynes, M. D. (2015). *Improving Pre-Stressed Reinforcement for Concrete Railroad Ties via Geometrical Dimensioning and Tolerancing.* Manhattan: Kansas State University.

Haynes, M., Wu, C.-H., Peterman, R. J., & Beck, T. B. (2014). Prestressing Steel Reinforcement Wire Measurement Protocol. Colorado Spring: American Society if Mechanical Engineers.

Loov, R. E. (1988, November-December). A General Equatioin for the Steel Stress for Bonded Prestressed Concrete Members. *PCI Journal, 33*(6), 108-137. Retrieved from http://www.pci.org/uploadedFiles/Siteroot/Publications/PCI_Journal/1988/DOI_Articles/jl-88-november-december-6.pdf

Mattock, A. H. (1979, January-February). Flexural Strength of Prestressed Concrete Sections by Programmable Calculator. *PCI Journal, 24*(1), pp. 32-54.

Menegotto, M., & Pinto, P. E. (1973). Method of anaysis for cyclically loaded, reinforced concrete plane frames including changes in geometry and non-elastic behavior of elements under combined normal force and bending. *13*, 15-22.

Naaman, A. E. (1977, January-Februrary). Ultimate Analysis of Prestressed and Partially Prestressed Sections by Strain Compatibility. *PCI Journal, 22*(1), 32-51. Retrieved from http://www.pci.org/uploadedFiles/Siteroot/Publications/PCI_Journal/1977/DOI_Articles/jl-77-january-february-3.pdf

Naaman, A. E. (1985, November-December). Partially Prestressed Concrete:Review and Recommendations. *PCI Journal, 30*(5), 30-70.

Podolny, W. J. (1967, October). Understanding the Steel in Prestressing. *PCI Journal, 12*(5), 54-66. Retrieved from http://www.pci.org/uploadedFiles/Siteroot/Publications/PCI_Journal/1967/DOI_Articles/jl-67-october-5.pdf

Precast / Prestressed Concrete Institute. (2010). PCI Dessign Handbook 7th Edition. *PCI Dessign Handbook 7th Edition*. Chicage, IL: Precast / Prestressed Concrete Institute.

Ramberg, W., & Osgood, W. R. (1943). *Description of stress-strain curves by three parameters.* NASA Scientific and Technical Information Facility. Washington: National Advisory Committee of Aeronautics. Retrieved from http://ntrs.nasa.gov/archive/nasa/casi.ntrs.nasa.gov/19930081614.pdf

Rasmussen, K. J. (2006). *Full-Range Stress-Strain Curve for Stainless Steel Alloys.*Sydney: University of Sydney-Department of Civil Engineering. Retrieved from http://sydney.edu.au/engineering/civil/publications/2001/r811.pdf

Shimadzu. (2009). *Trapezium X User's Guide.* Tokyo: Shimadzu Corporation.

Skongman, B. C., Tadros, M. K., & Grasmick, R. (1988). Flexural Strength of Prestressed Concrete Members. *PCI Journal, 33*(5), 96-123. Retrieved from http://www.pci.org/uploadedFiles/Siteroot/Publications/PCI_Journal/1988/DOI_Articles/jl-88-september-october-4.pdf

University of Colorado Boulder. (2015). *Lecture 5 : Stress-Strain Material Law.* Retrieved from University of Colorado Boulder engineering: http://www.colorado.edu/engineering/CAS/courses.d/Structures.d/IAST.Lect05.d/IAST.Lect05.pdf

Whitney, C. S. (1937, March-April). Design of Reinforced Concrete Member under Flexure and Combined Flexure and Direct Compression. *ACI Journal, 33*, 483-498.

# Appendix A. Wire Measurement

Appendix A. 1 Wire specimen length measurement for WA

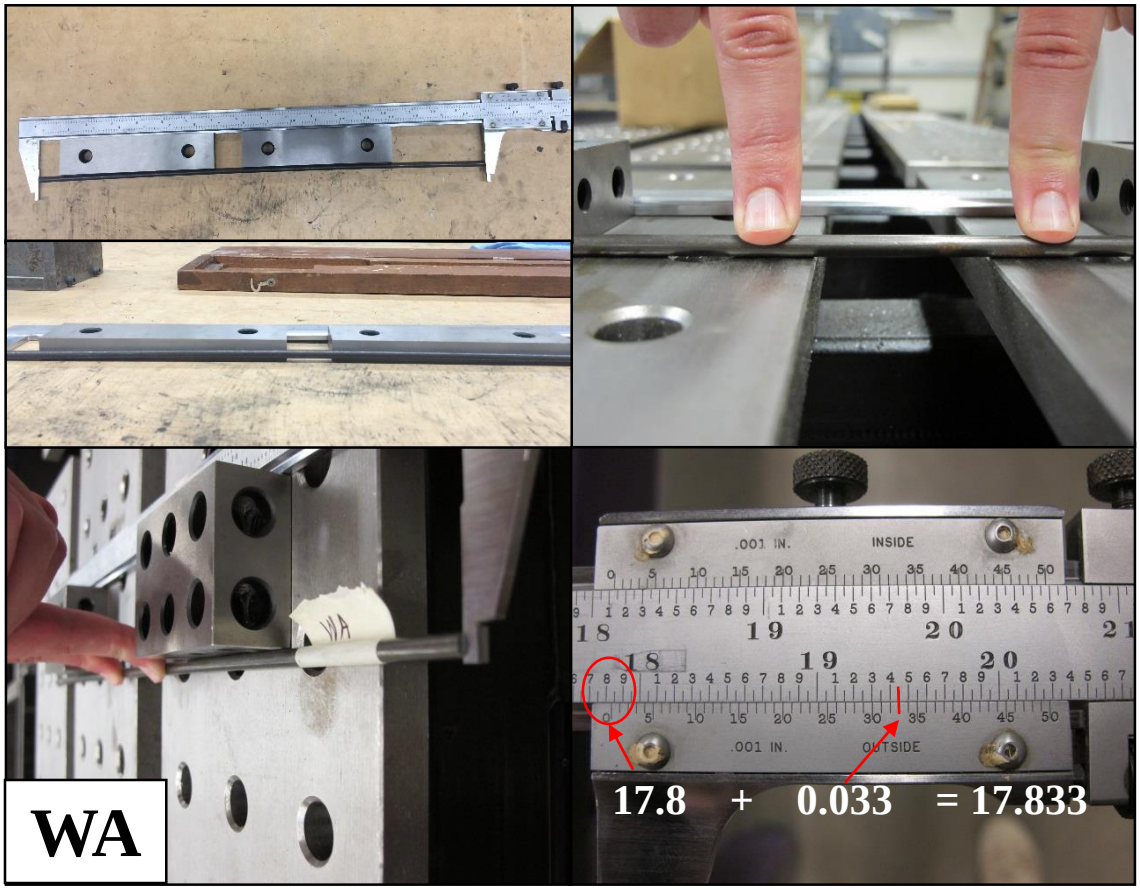

Appendix A. 2. Wire specimen length measurement for WB

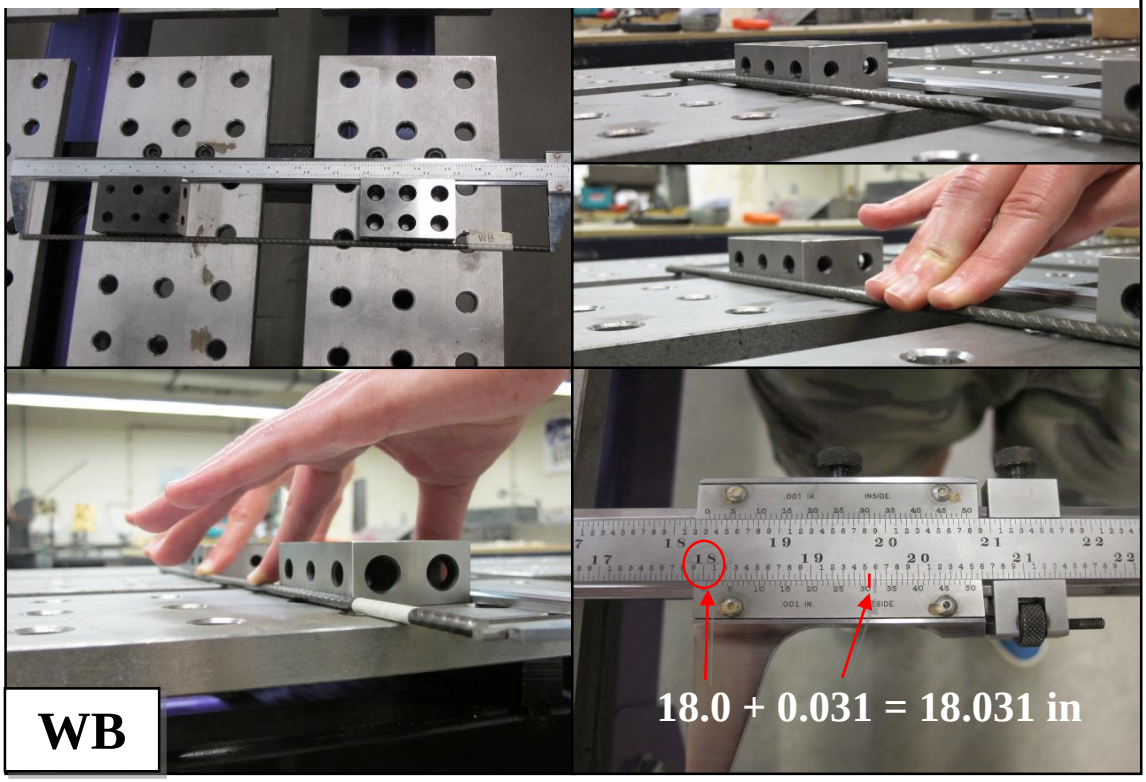


Appendix A. 3. Wire specimen length measurement for WC

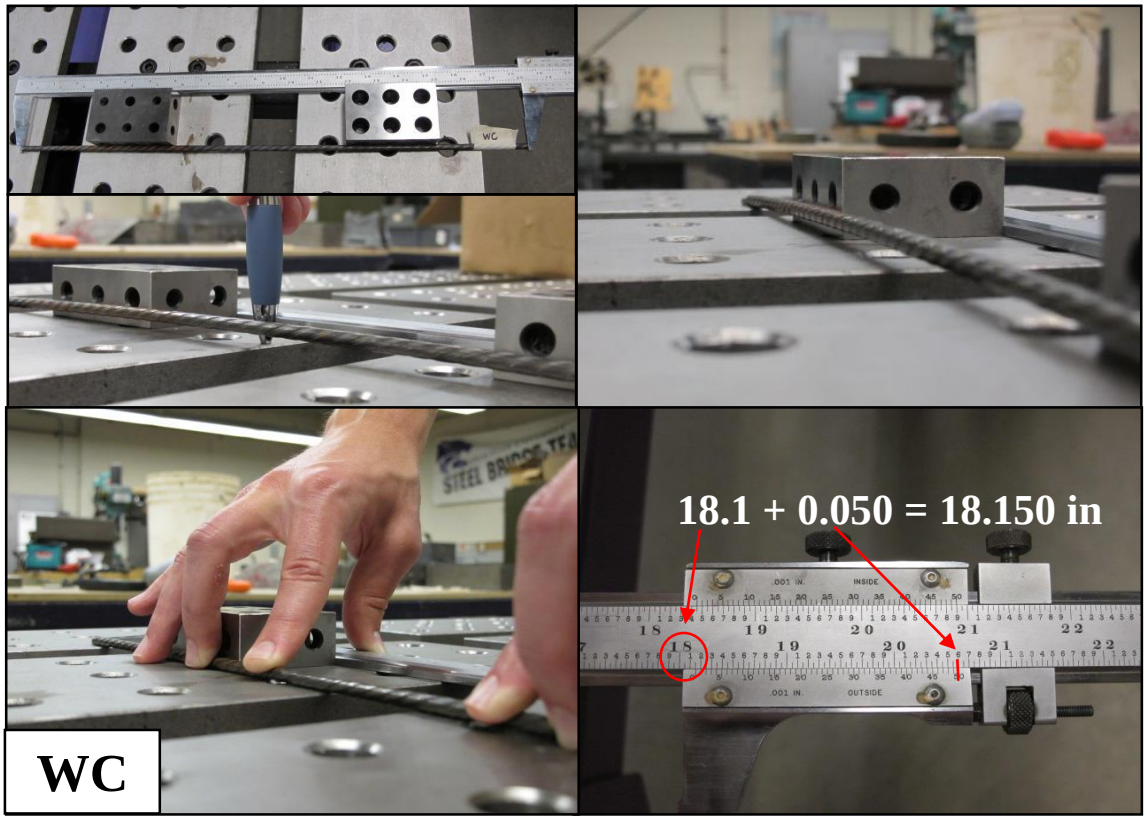

Appendix A. 4. Wire specimen length measurement for WD

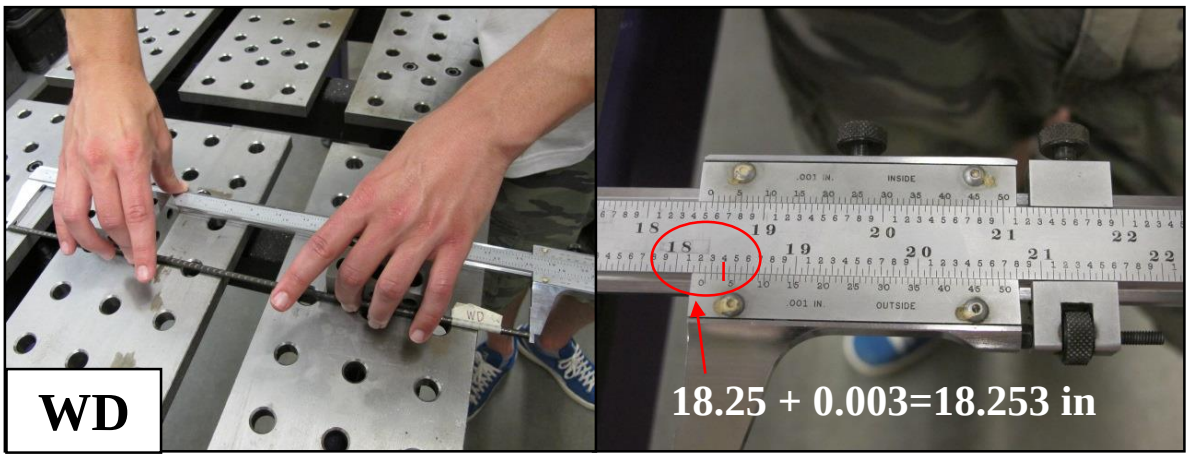


Appendix A. 5. Wire specimen length measurement for WE

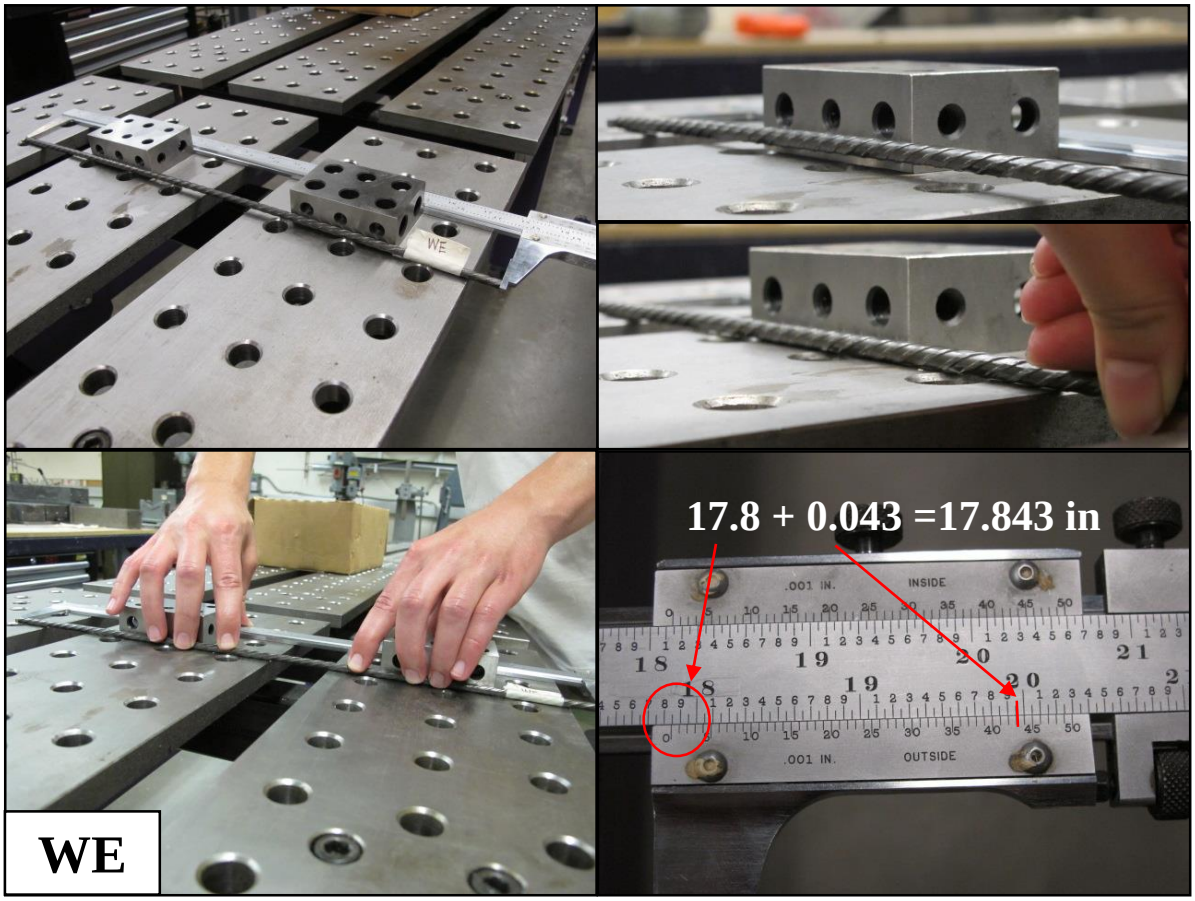

Appendix A. 6. Wire specimen length measurement for WF

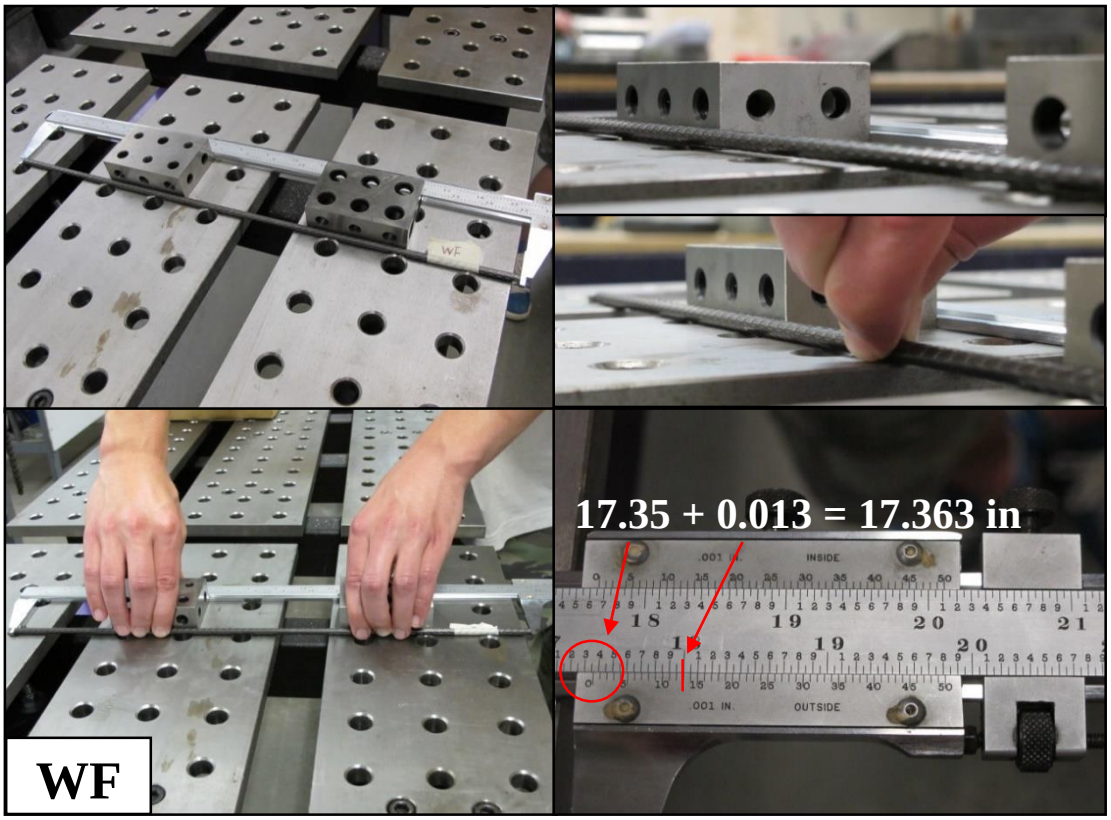


Appendix A. 7. Wire specimen length measurement for WG

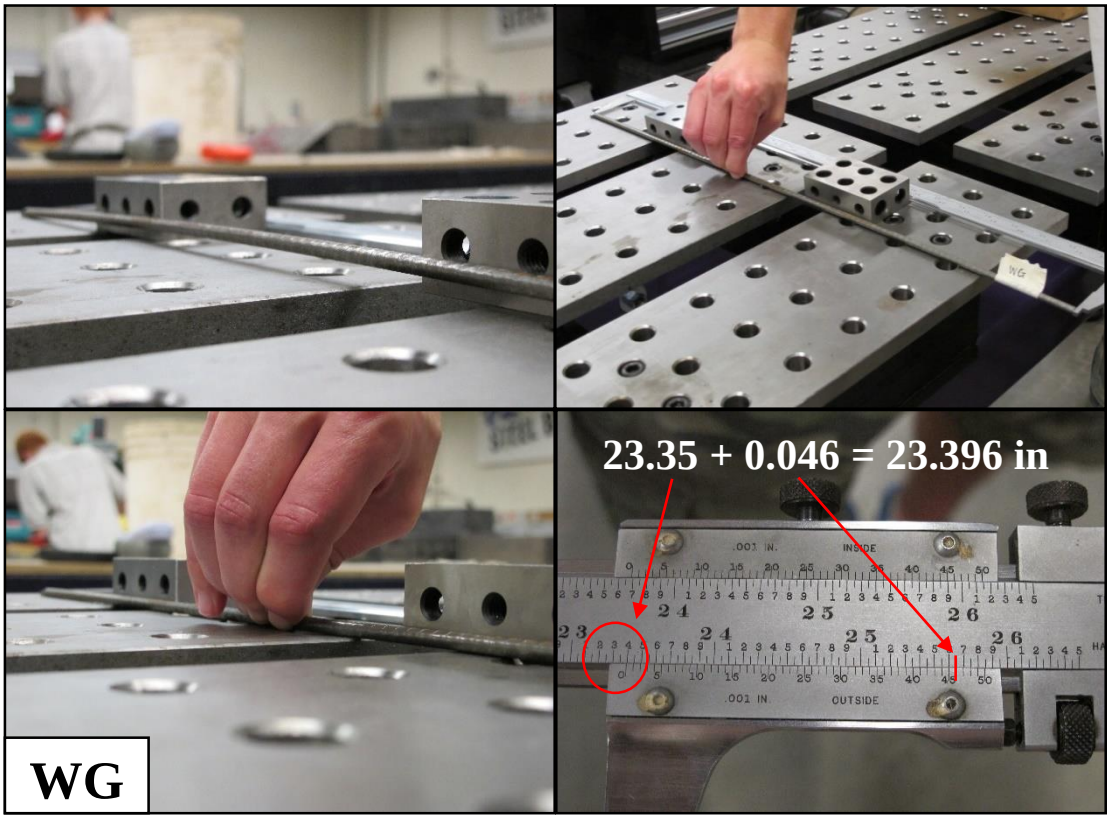

Appendix A. 8. Wire specimen length measurement for WH

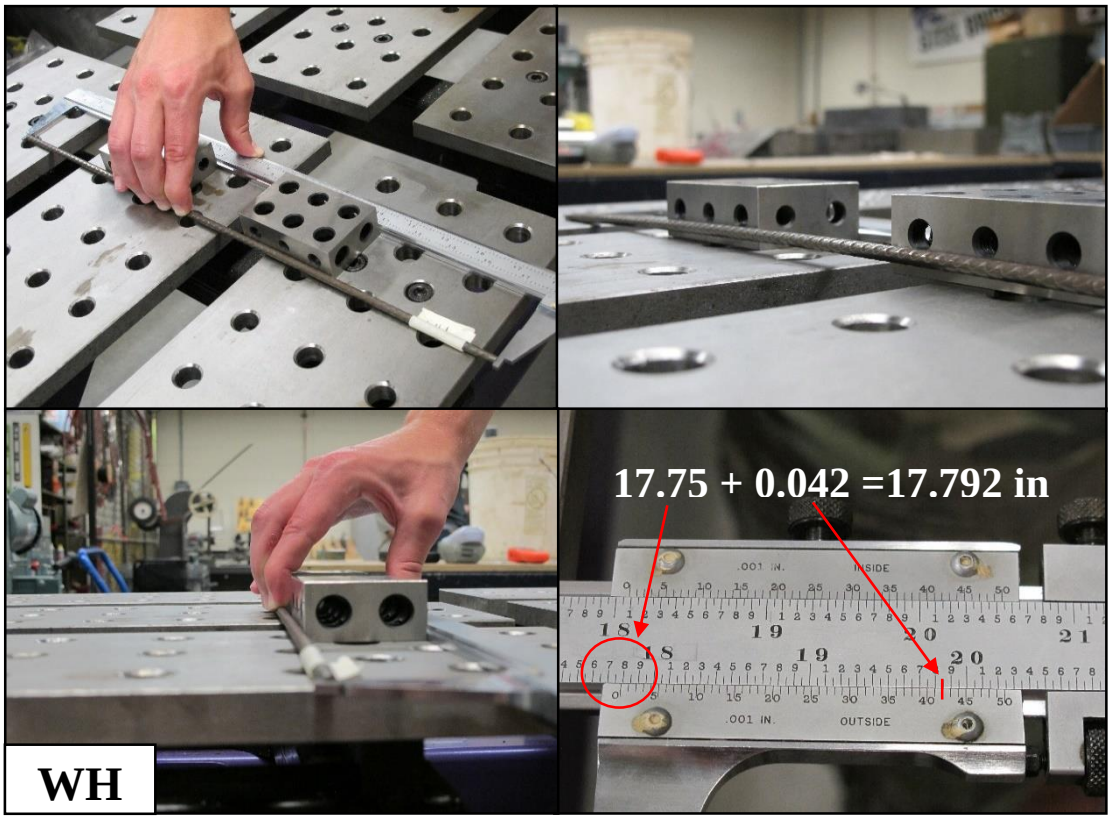


Appendix A. 9. Wire specimen length measurement for WI

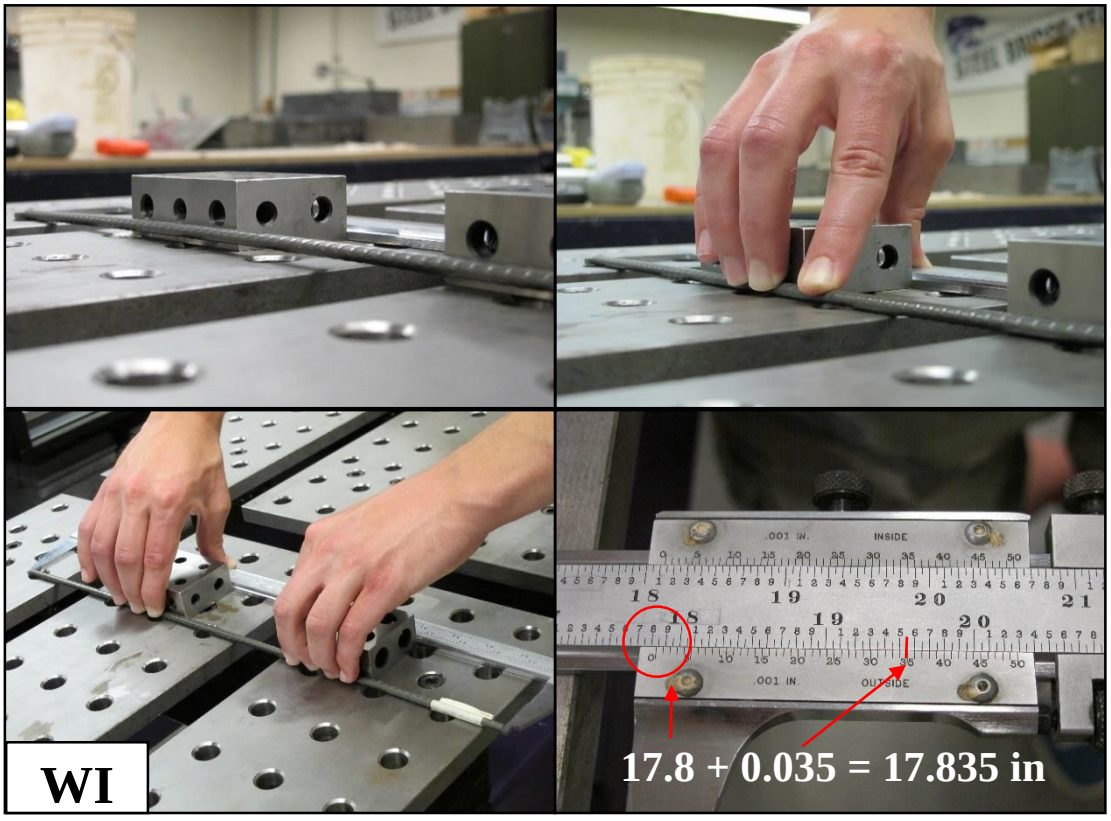

Appendix A. 10. Wire specimen length measurement for WJ

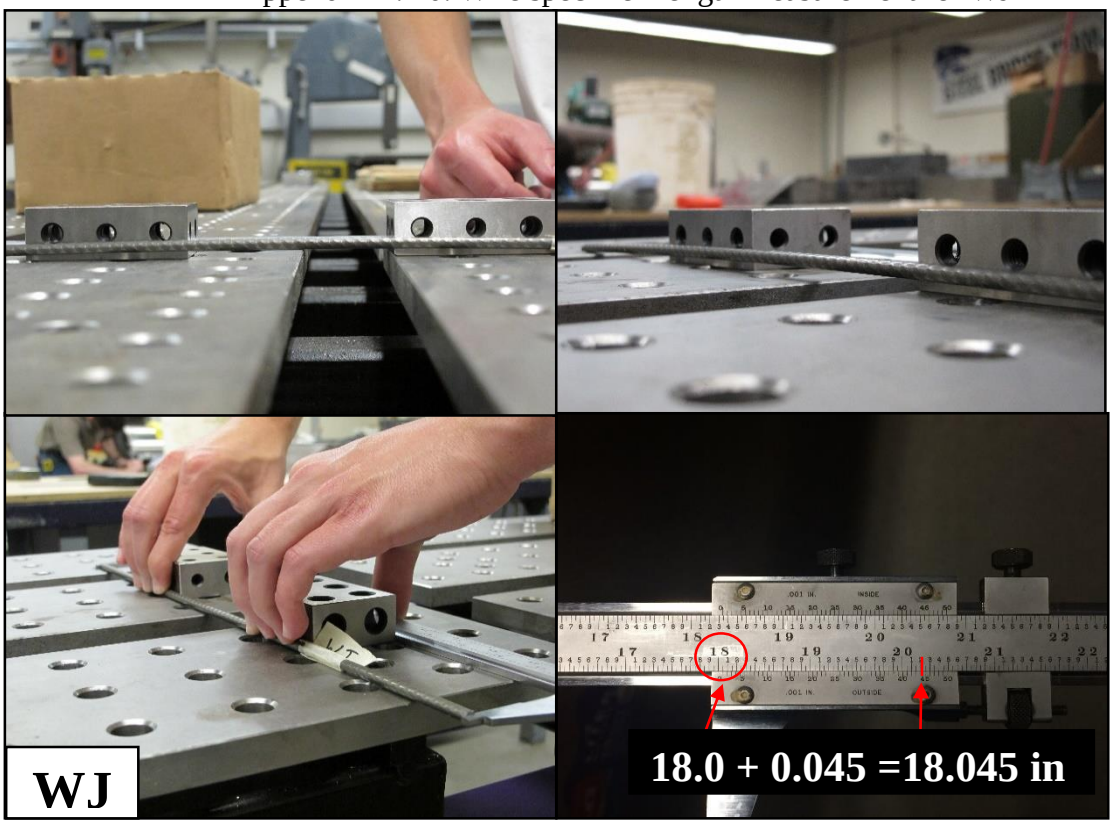


Appendix A. 11. Wire specimen length measurement for WK

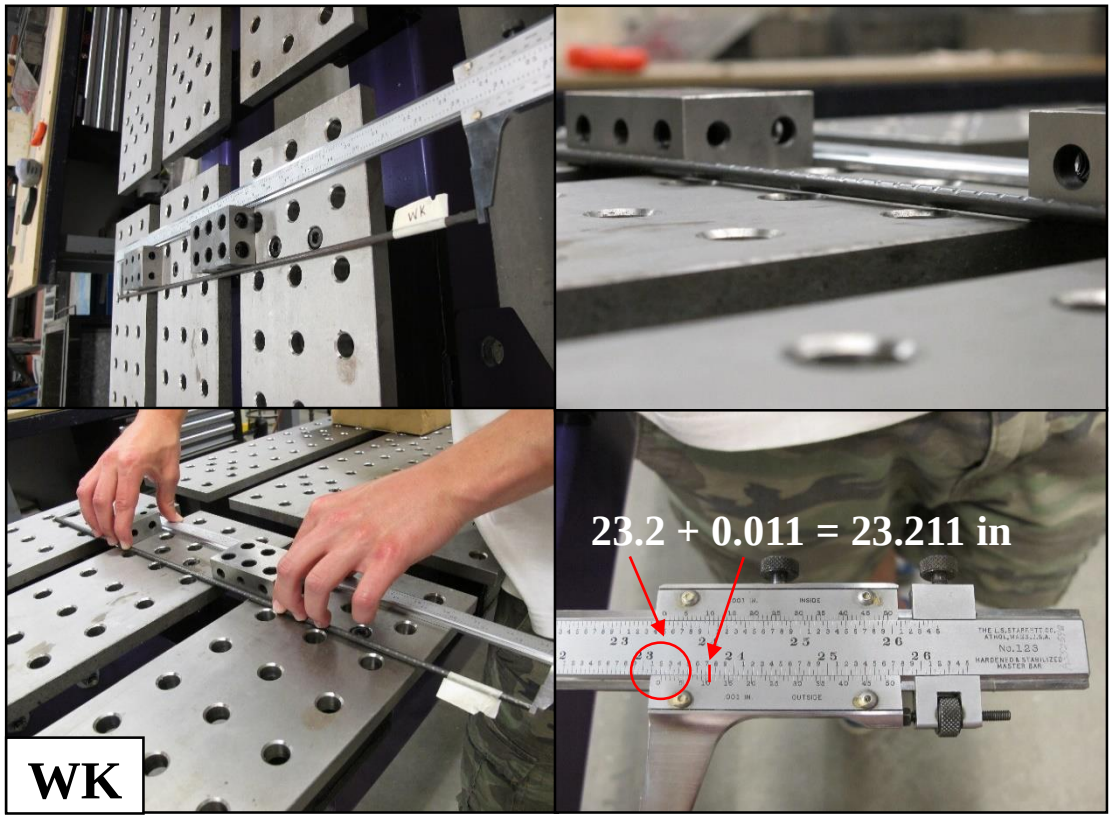

Appendix A. 12. Wire specimen length measurement for WL

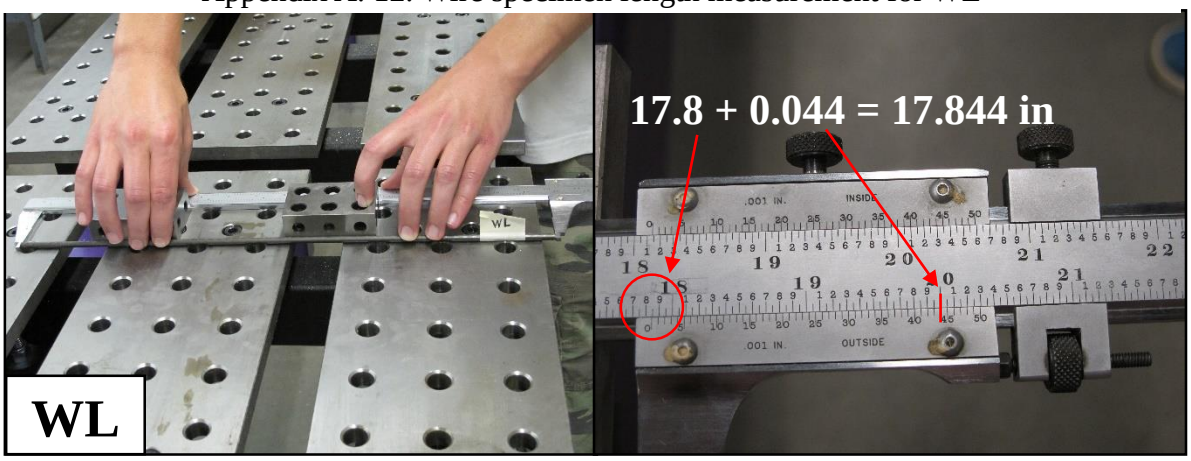


Appendix A. 13. Wire specimen length measurement for WM

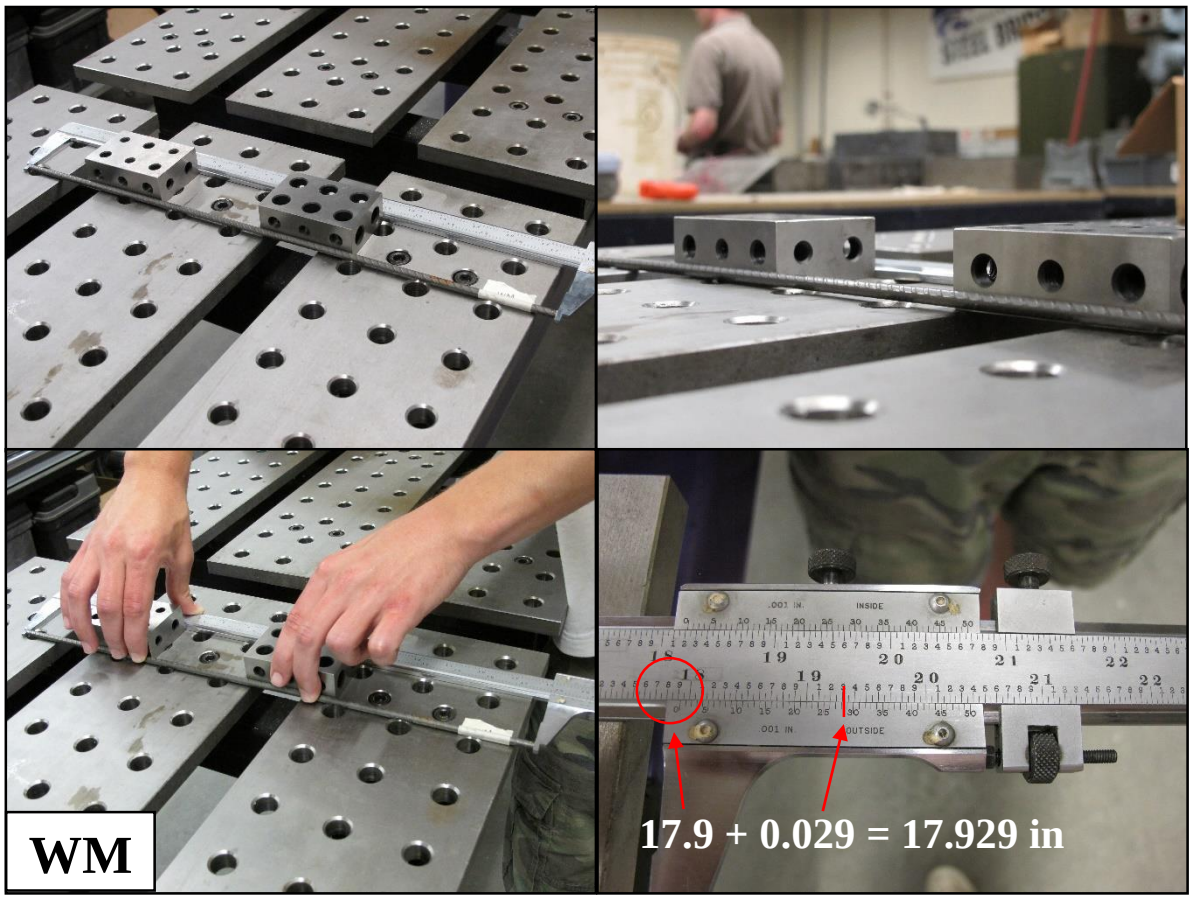

# Appendix B. Schematic of Tensile Testing Machine

This is a schematic of the universal testing machine with movable chuck jaw head and two single-point extensometers on each side of the testing specimen. This machine was used for the testing at Kansas State University documented in this research.

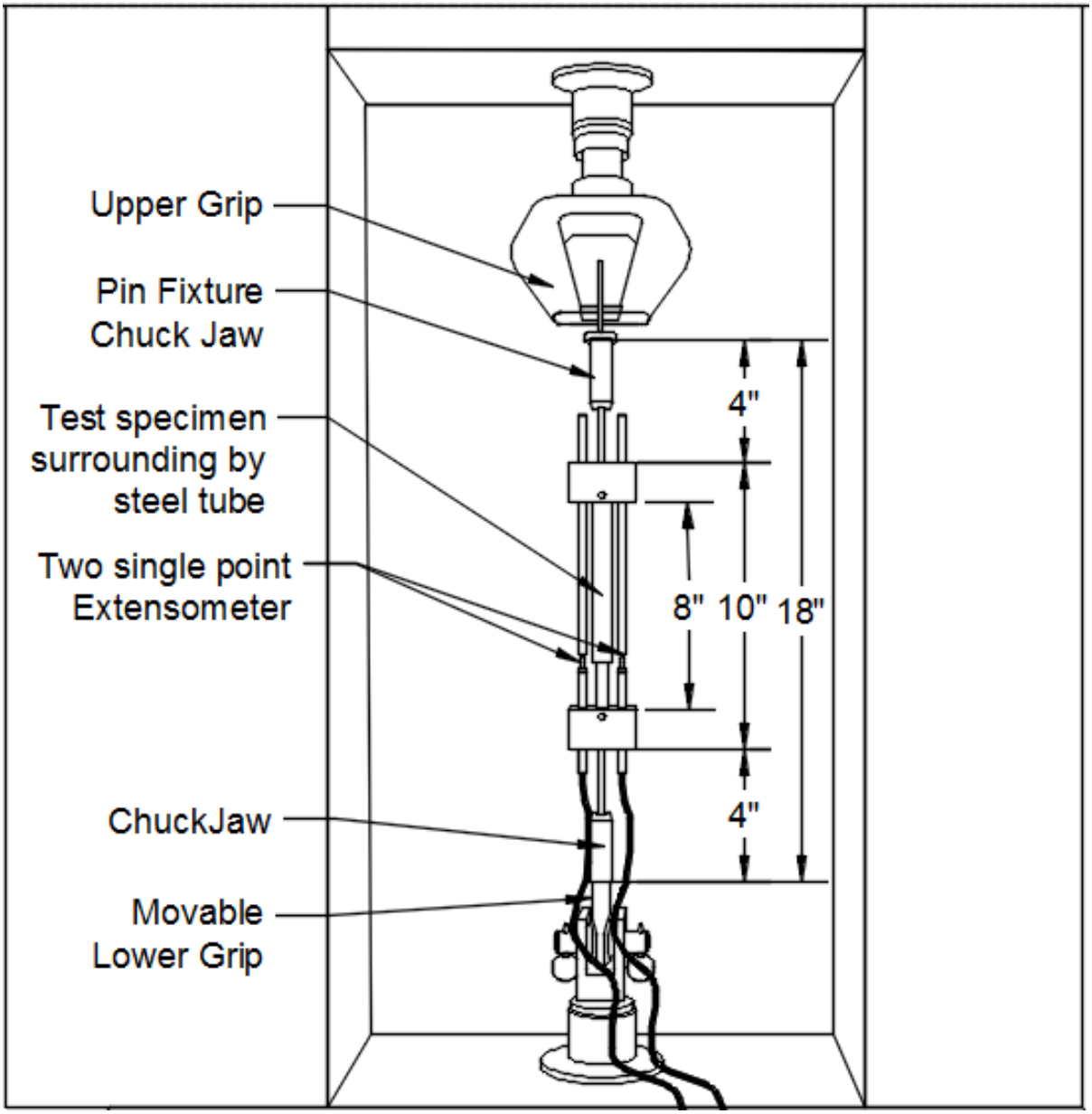

# Appendix C. Tensile Testing Results

Appendix C. 1. Experimental stress-strain curve and average curve for WB wire

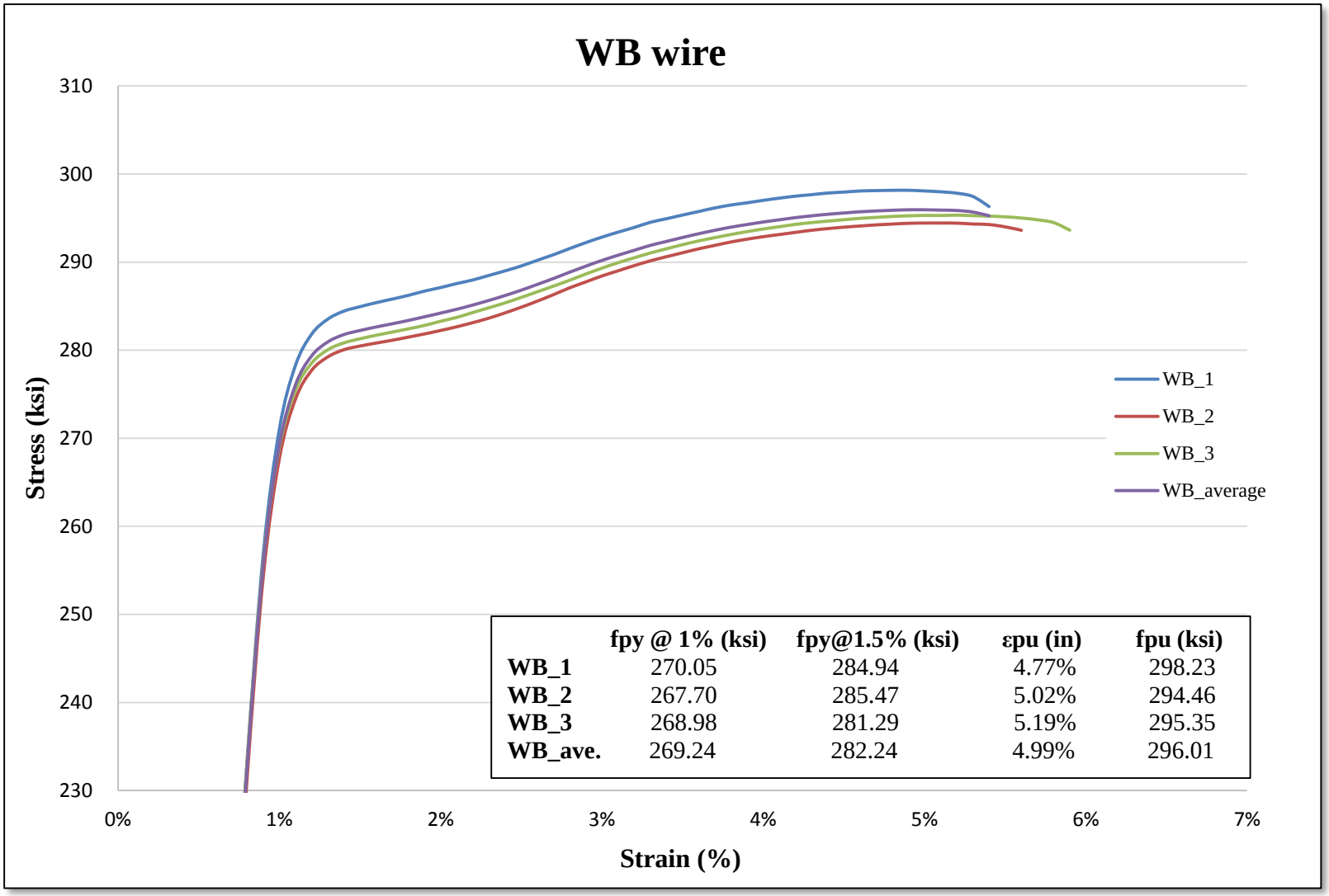


| | fpy @ 1% (ksi) | fpy@1.5% (ksi) | εpu (in) | fpu (ksi) |
|---|---|---|---|---|
| **WB_1** | 270.05 | 284.94 | 4.77% | 298.23 |
| **WB_2** | 267.70 | 285.47 | 5.02% | 294.46 |
| **WB_3** | 268.98 | 281.29 | 5.19% | 295.35 |
| **WB_ave.** | 269.24 | 282.24 | 4.99% | 296.01 |

Appendix C. 2. Experimental stress-strain curve and average curve for WD wire

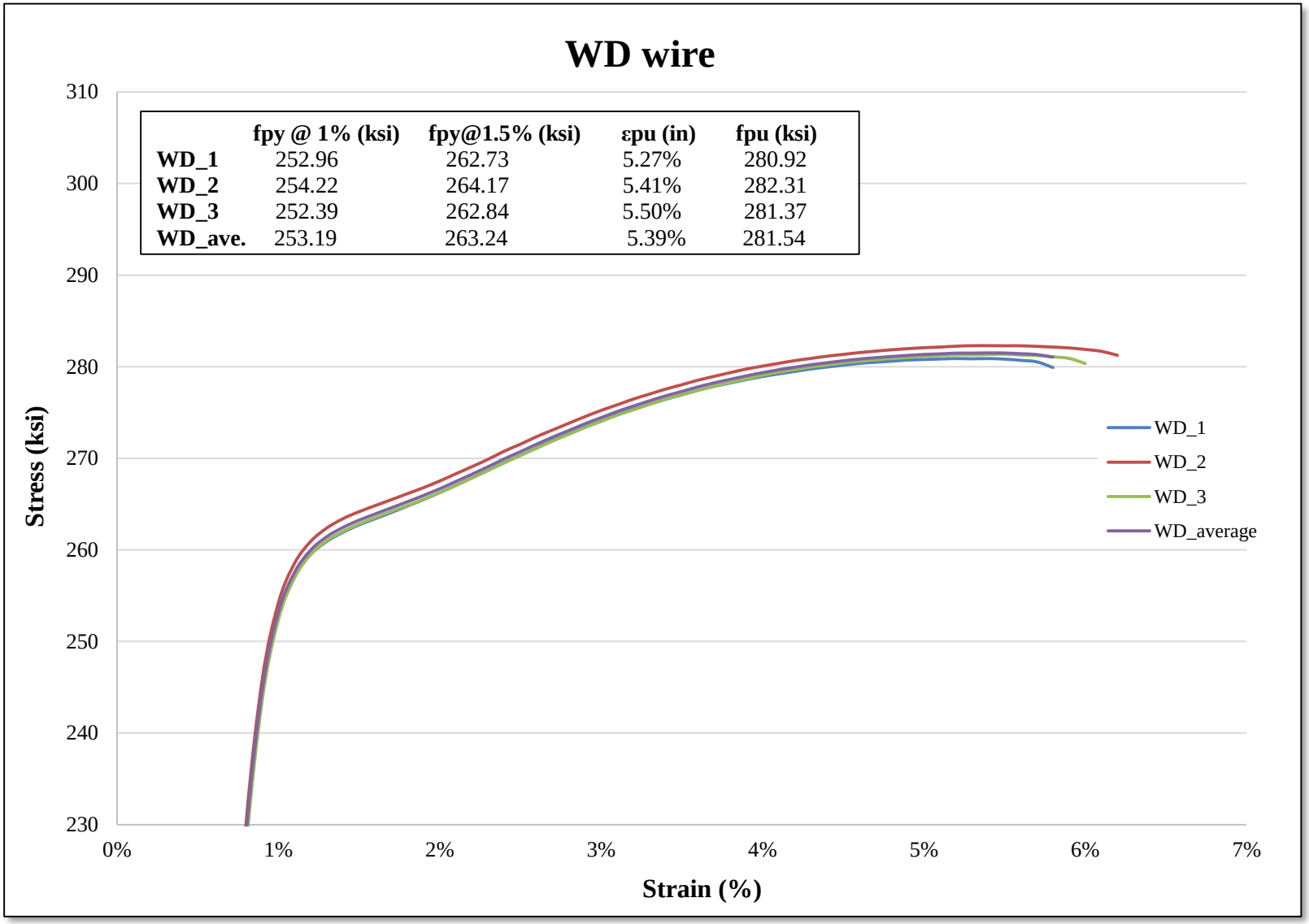

Appendix C. 3. Experimental stress-strain curve and average curve for WE wire

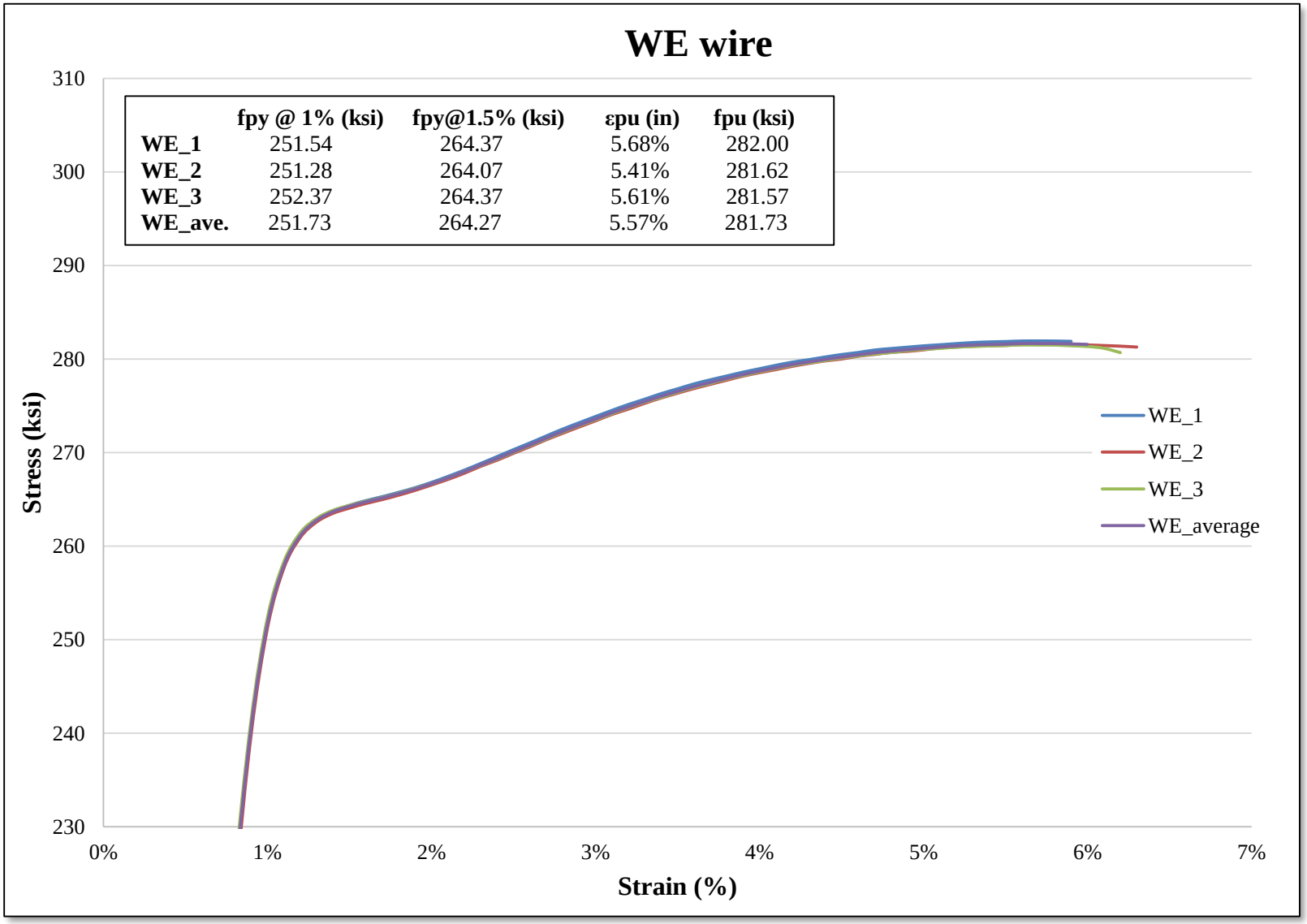

Appendix C. 4. Experimental stress-strain curve, and average curve for WF wire

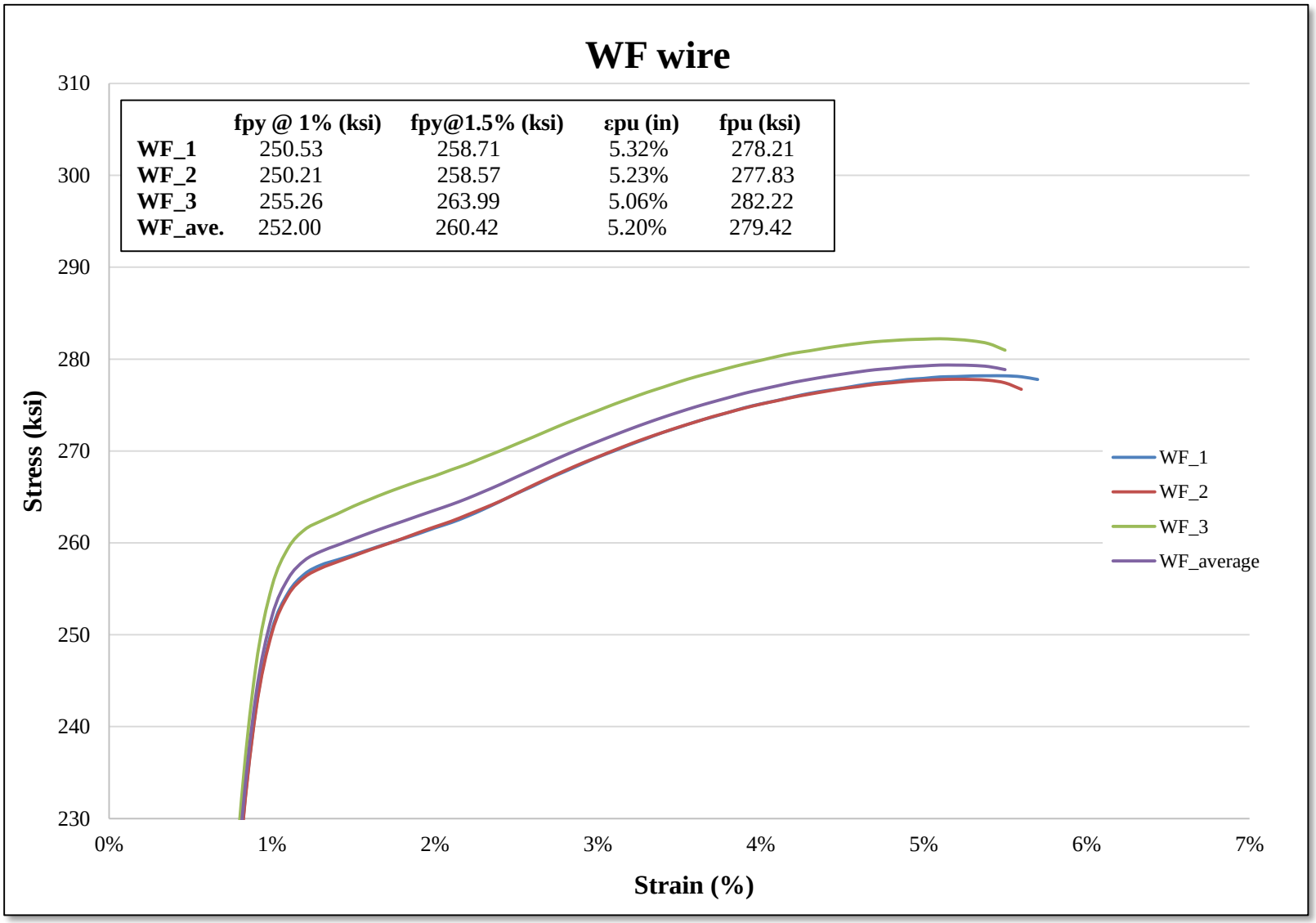

Appendix C. 5. Experimental stress-strain curve and average curve for WG wire

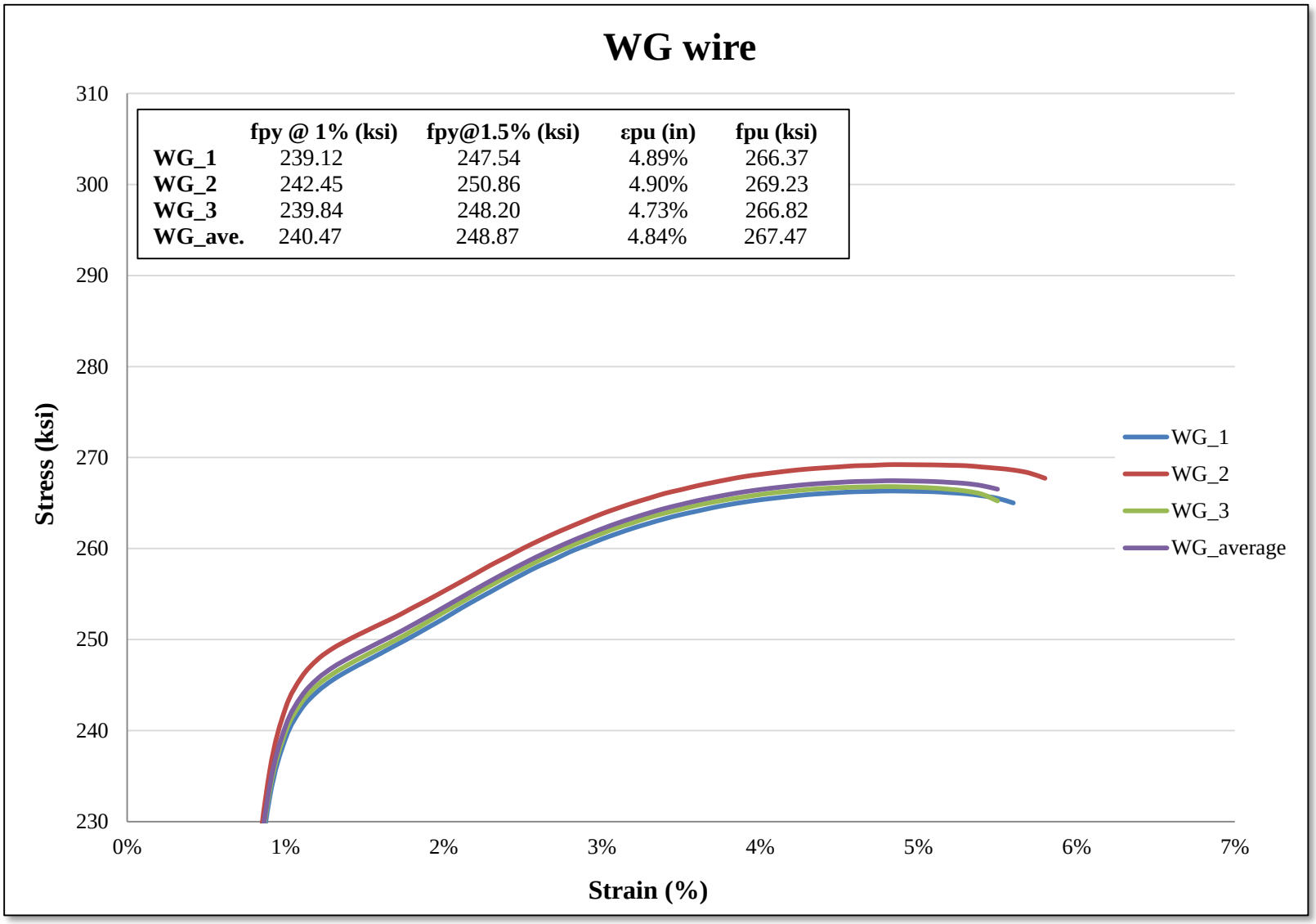

Appendix C. 6. Experimental stress-strain curve and average curve for WH wire

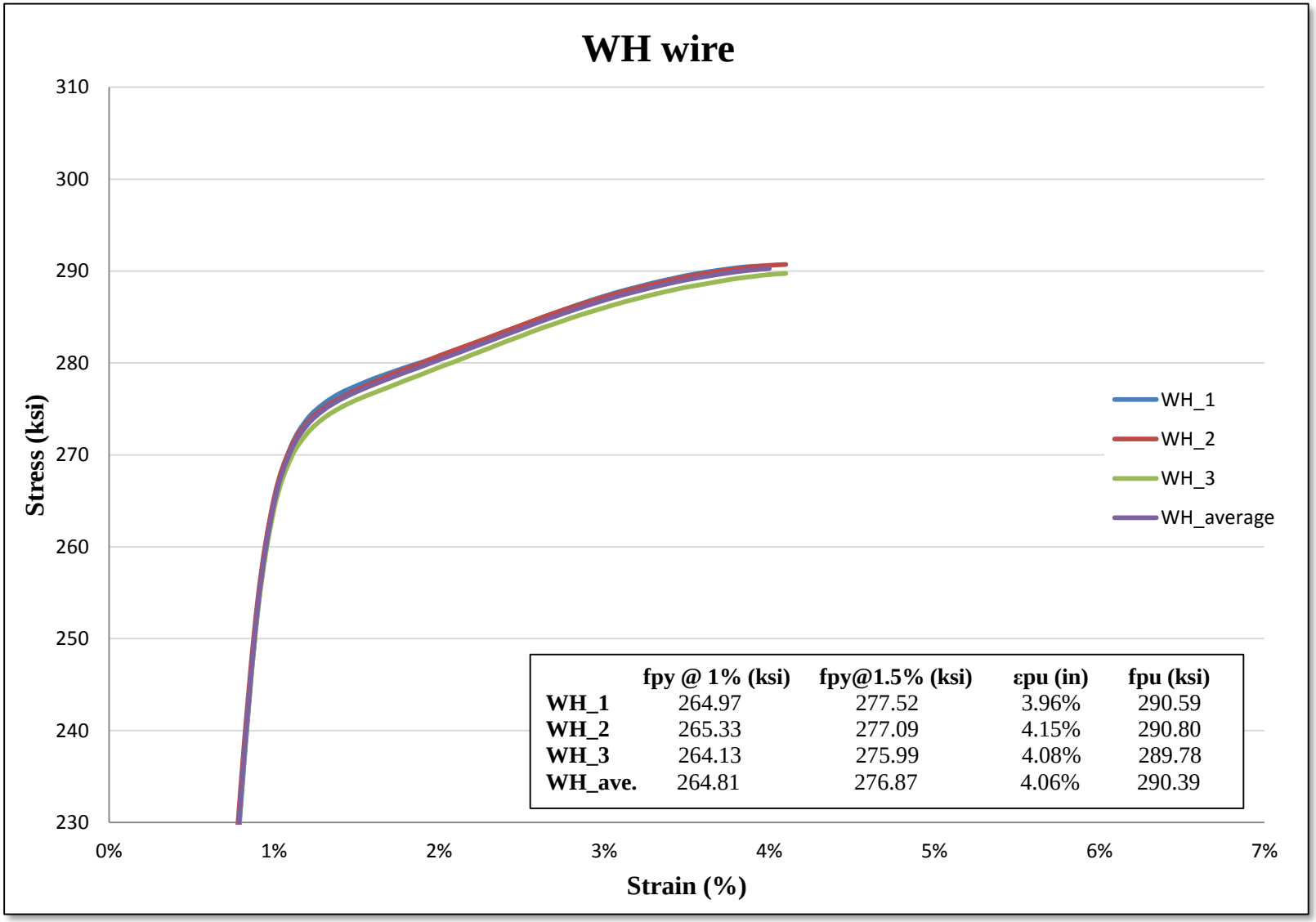


| | fpy @ 1% (ksi) | fpy@1.5% (ksi) | εpu (in) | fpu (ksi) |
|---|---|---|---|---|
| **WH_1** | 264.97 | 277.52 | 3.96% | 290.59 |
| **WH_2** | 265.33 | 277.09 | 4.15% | 290.80 |
| **WH_3** | 264.13 | 275.99 | 4.08% | 289.78 |
| **WH_ave.** | 264.81 | 276.87 | 4.06% | 290.39 |

Appendix C. 7. Experimental stress-strain curve and average curve for WI wire

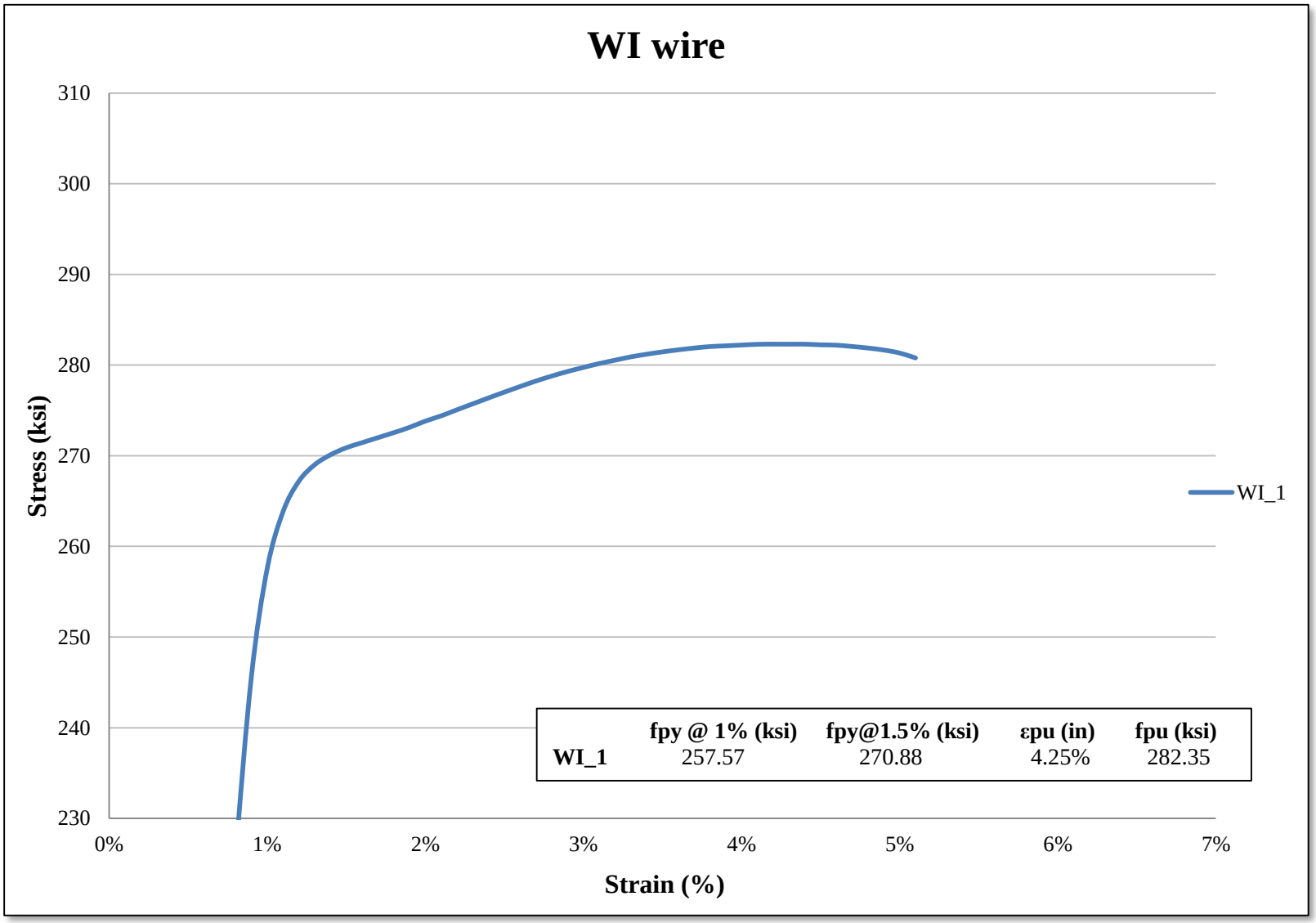

Appendix C. 8. Experimental stress-strain curve and average curve for WJ wire

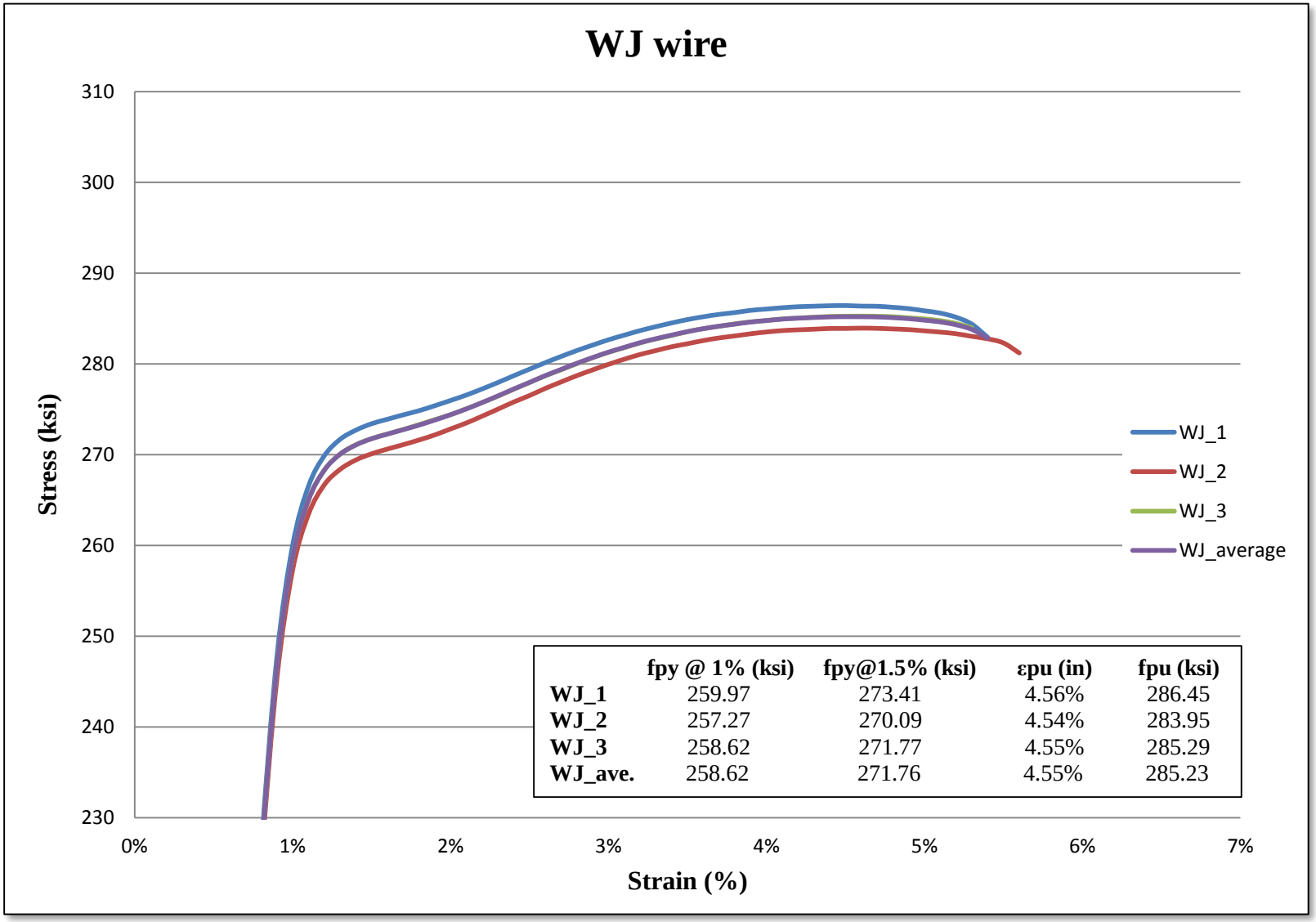


| | fpy @ 1% (ksi) | fpy@1.5% (ksi) | εpu (in) | fpu (ksi) |
|---|---|---|---|---|
| **WJ_1** | 259.97 | 273.41 | 4.56% | 286.45 |
| **WJ_2** | 257.27 | 270.09 | 4.54% | 283.95 |
| **WJ_3** | 258.62 | 271.77 | 4.55% | 285.29 |
| **WJ_ave.** | 258.62 | 271.76 | 4.55% | 285.23 |

Appendix C. 9. Experimental stress-strain curve and average curve for WL wire

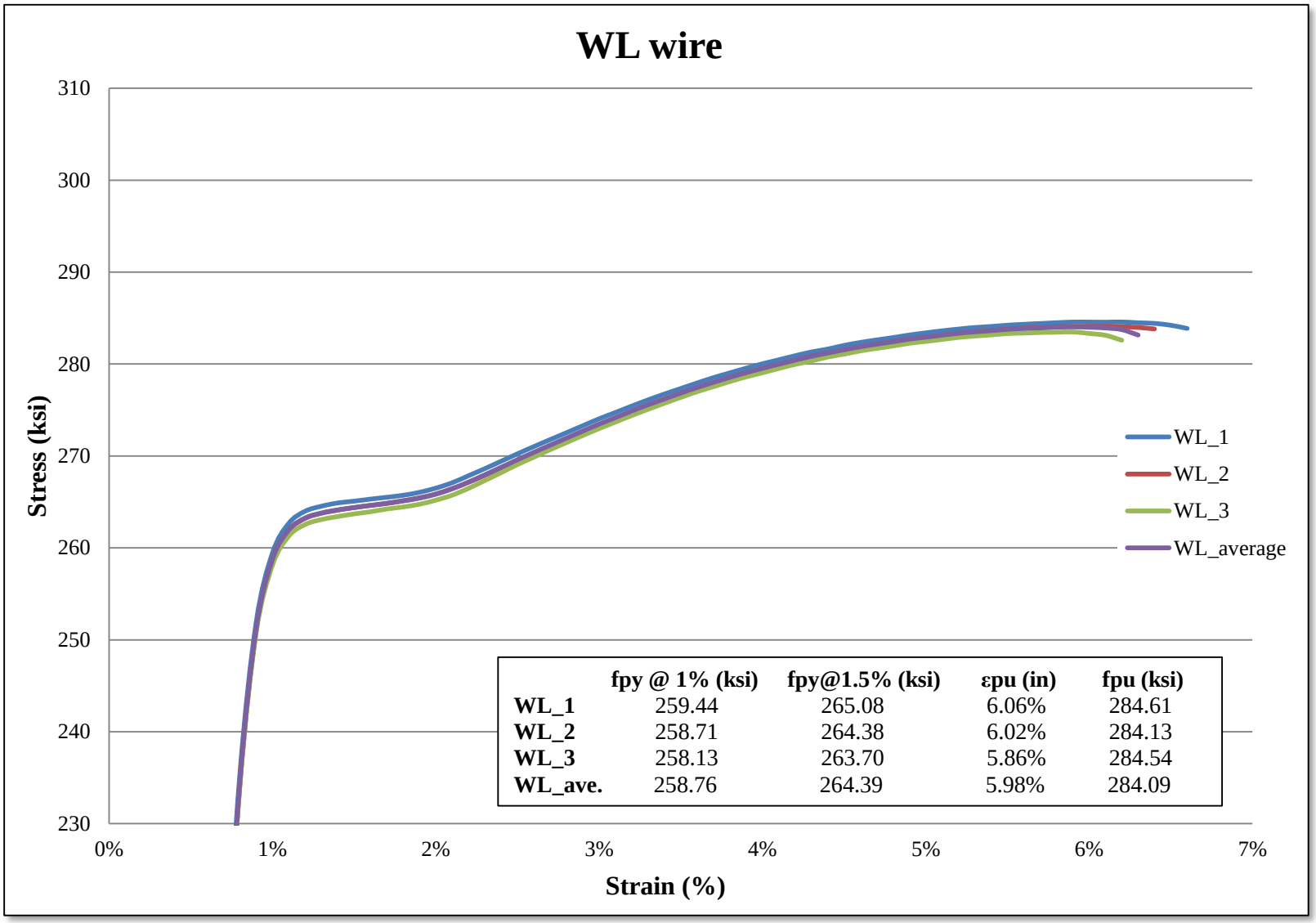


| | fpy @ 1% (ksi) | fpy@1.5% (ksi) | εpu (in) | fpu (ksi) |
|---|---|---|---|---|
| **WL_1** | 259.44 | 265.08 | 6.06% | 284.61 |
| **WL_2** | 258.71 | 264.38 | 6.02% | 284.13 |
| **WL_3** | 258.13 | 263.70 | 5.86% | 284.54 |
| **WL_ave.** | 258.76 | 264.39 | 5.98% | 284.09 |

Appendix C. 10. Experimental stress-strain curve and average curve for WM wire

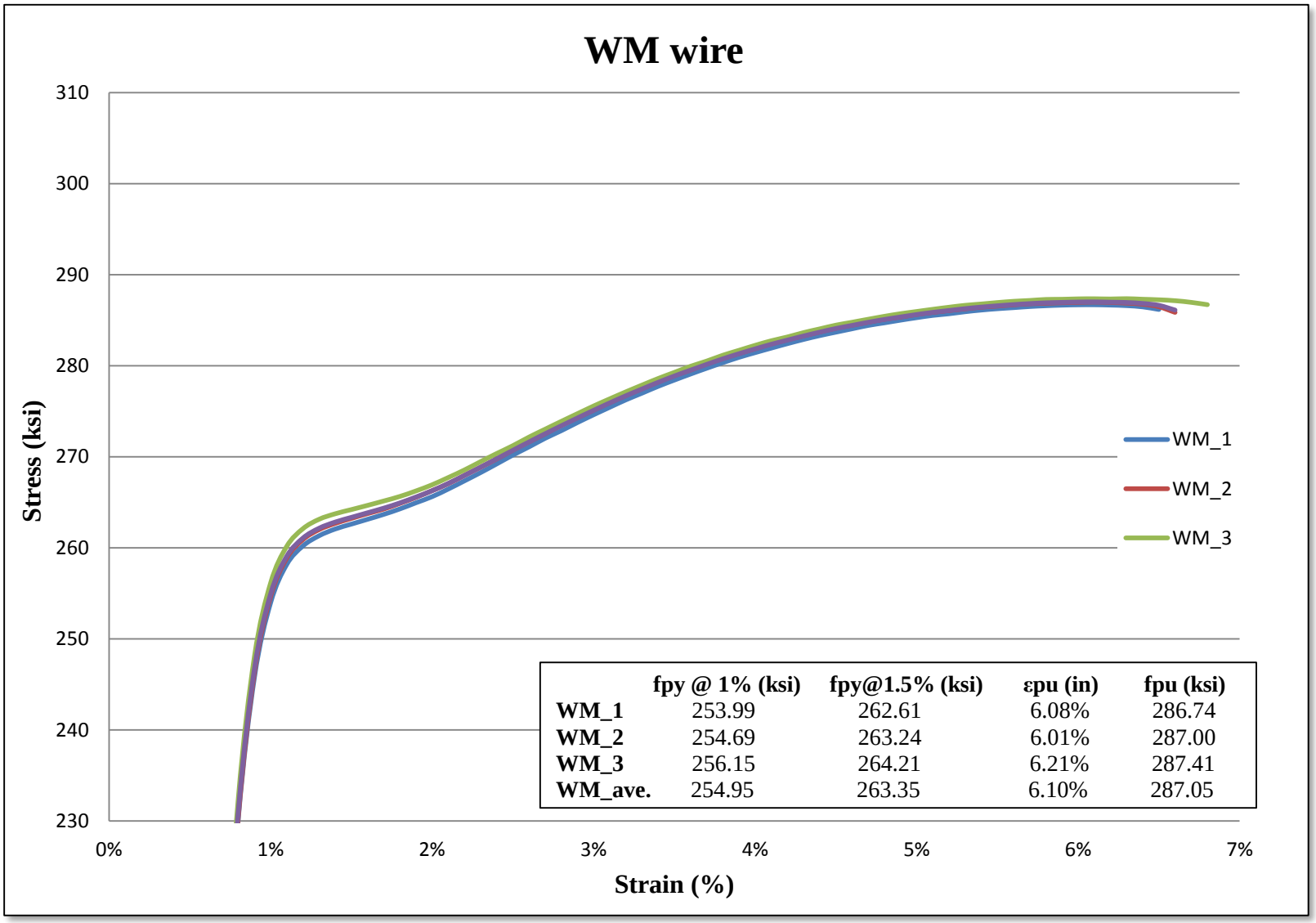


| | fpy @ 1% (ksi) | fpy@1.5% (ksi) | εpu (in) | fpu (ksi) |
|---|---|---|---|---|
| **WM_1** | 253.99 | 262.61 | 6.08% | 286.74 |
| **WM_2** | 254.69 | 263.24 | 6.01% | 287.00 |
| **WM_3** | 256.15 | 264.21 | 6.21% | 287.41 |
| **WM_ave.** | 254.95 | 263.35 | 6.10% | 287.05 |

## Appendix D. Analytical and Modeling Curves by Power Formula

Appendix D. 1. Comparing modeling power formula curves to experimental curve for WB wire

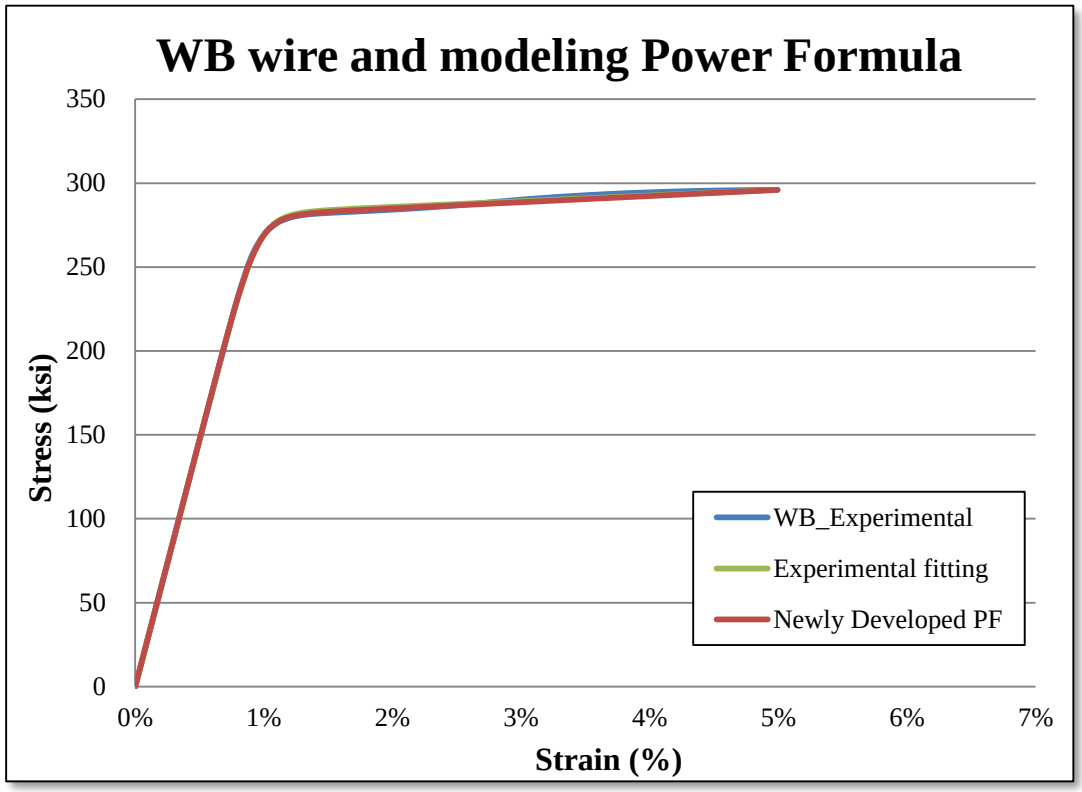


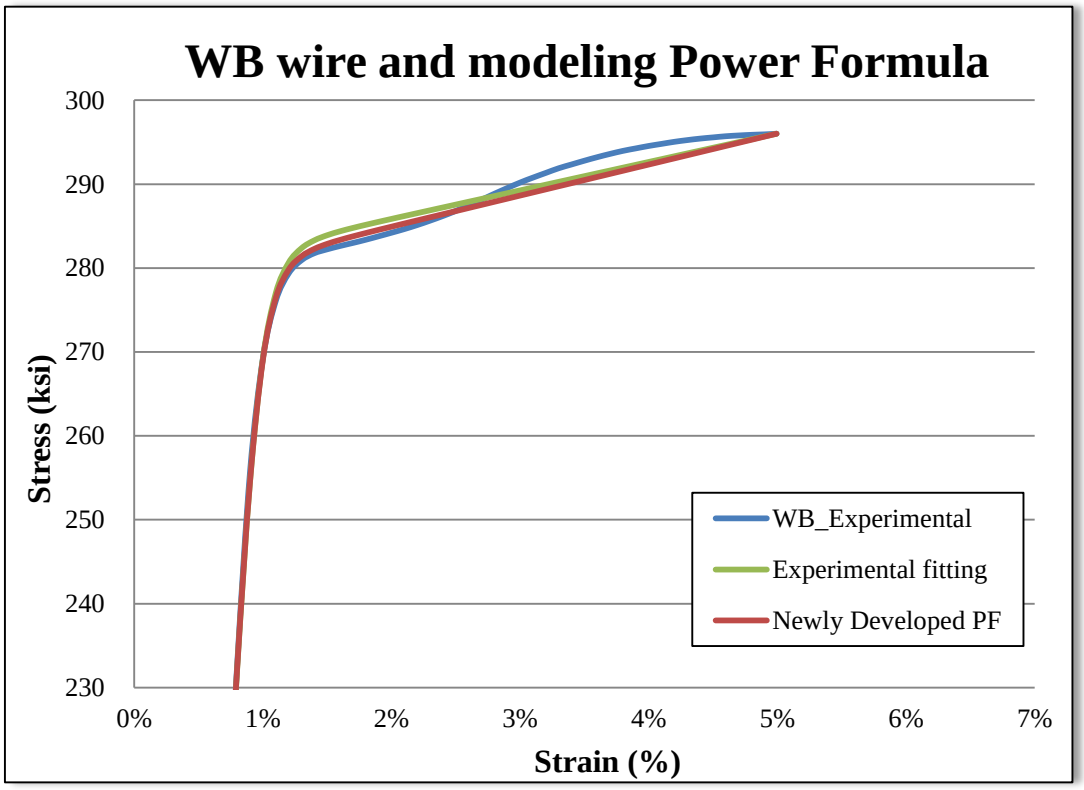

Appendix D. 2. Comparing modeling power formula curves to experimental curve for WD wire

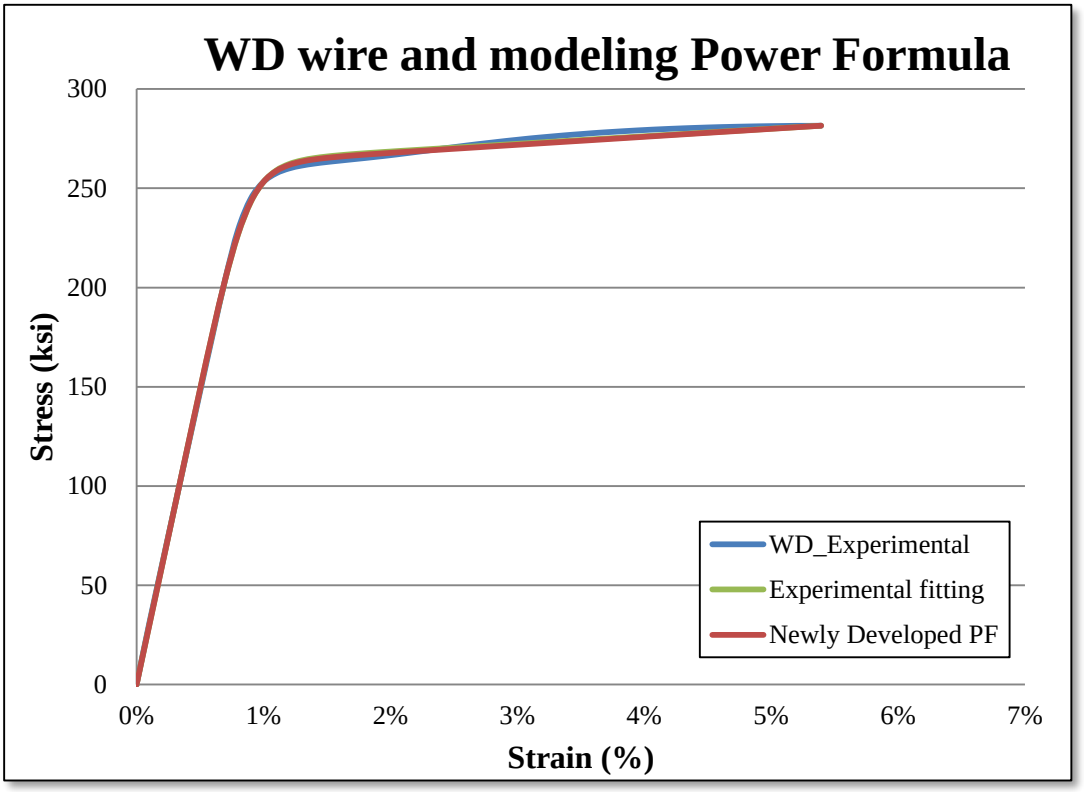


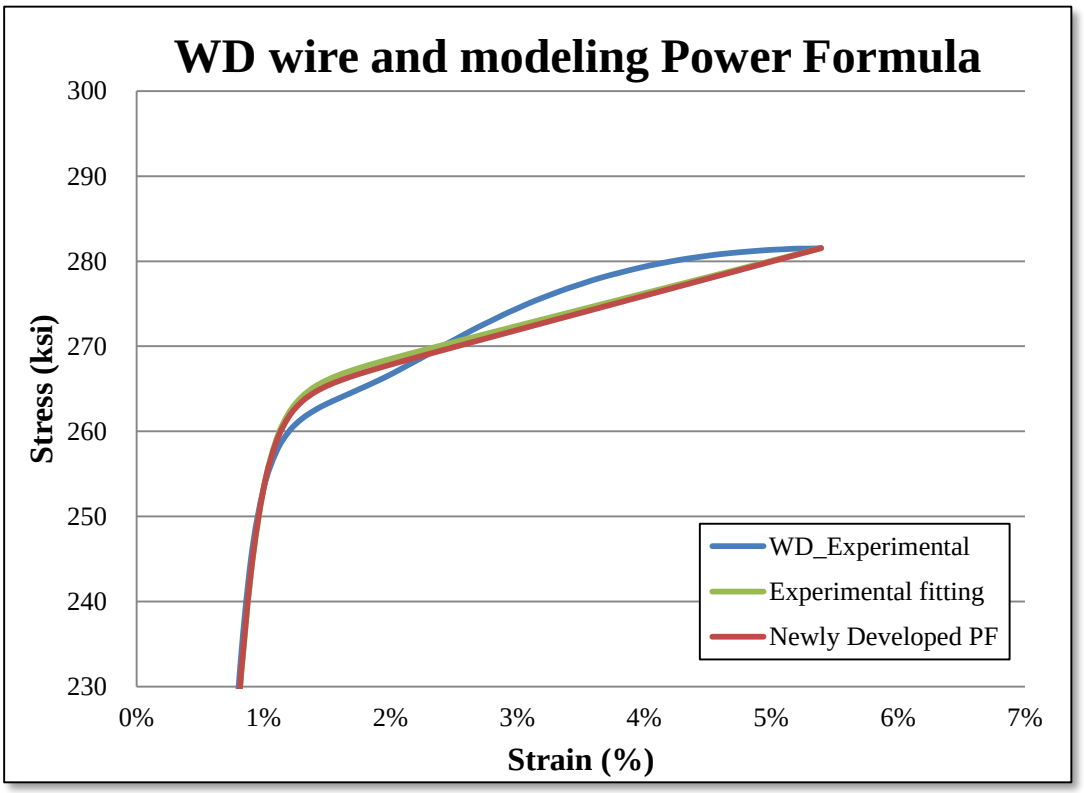

Appendix D. 3. Comparing modeling power formula curves to experimental curve for WE wire

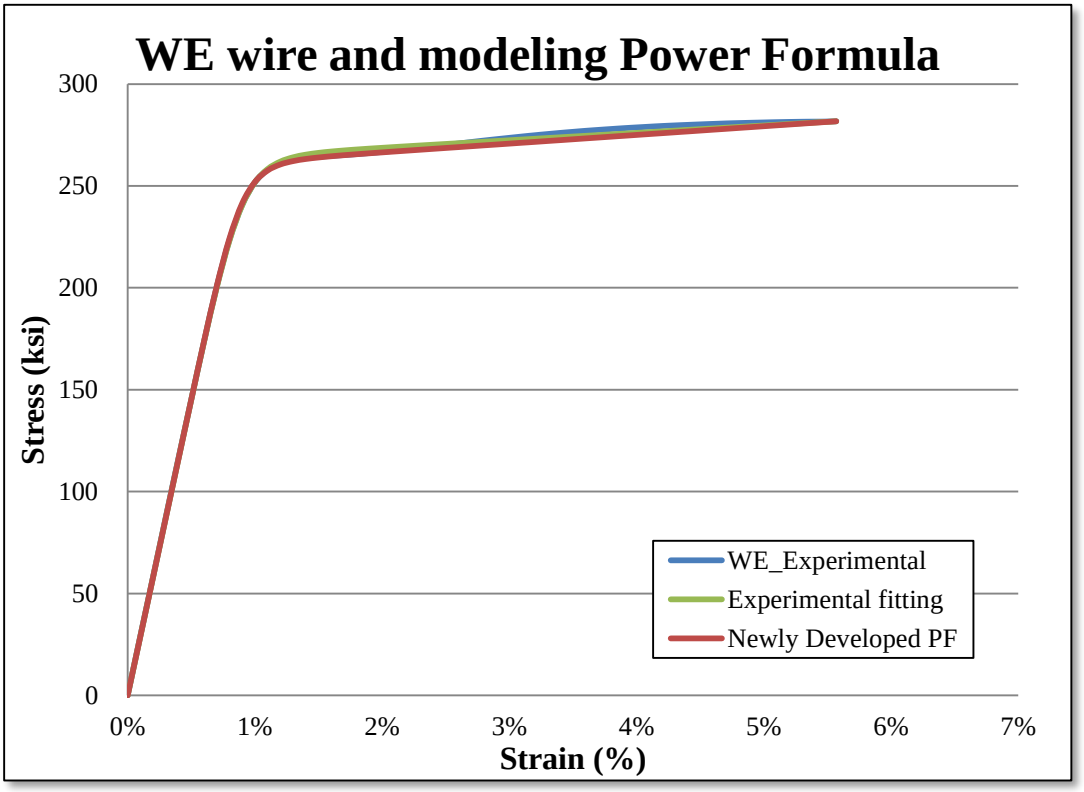


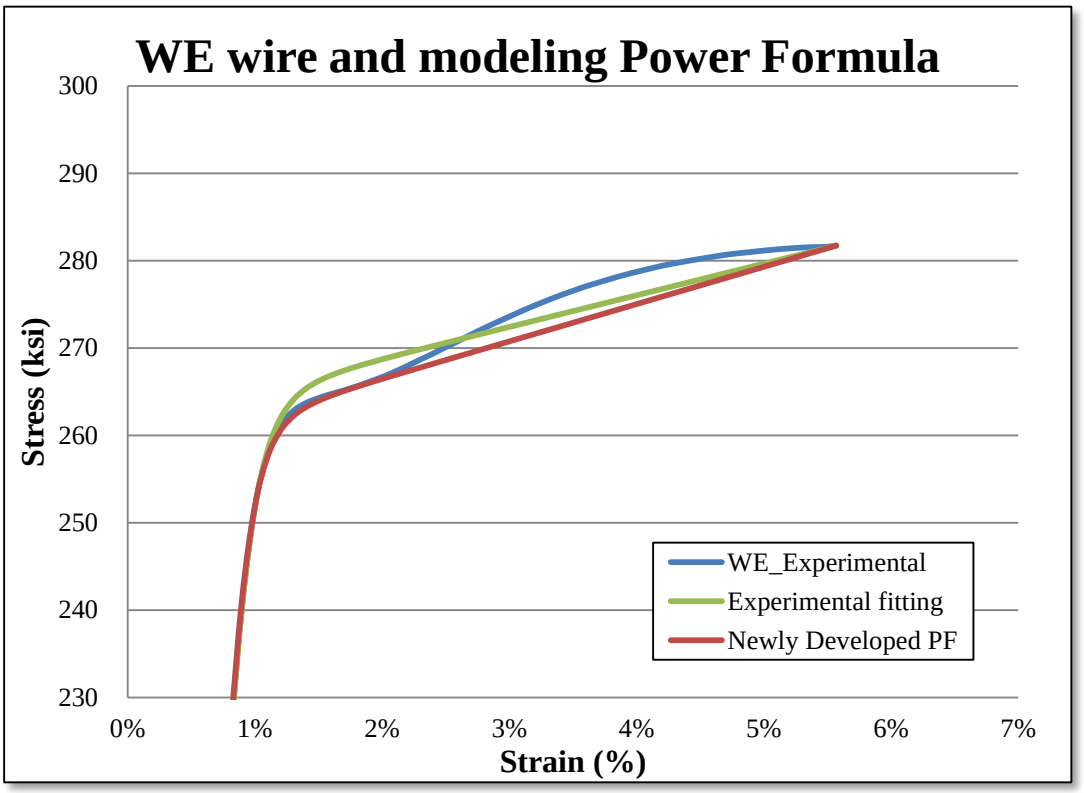

Appendix D. 4.Comparing modeling power formula curves to experimental curve for WF wire

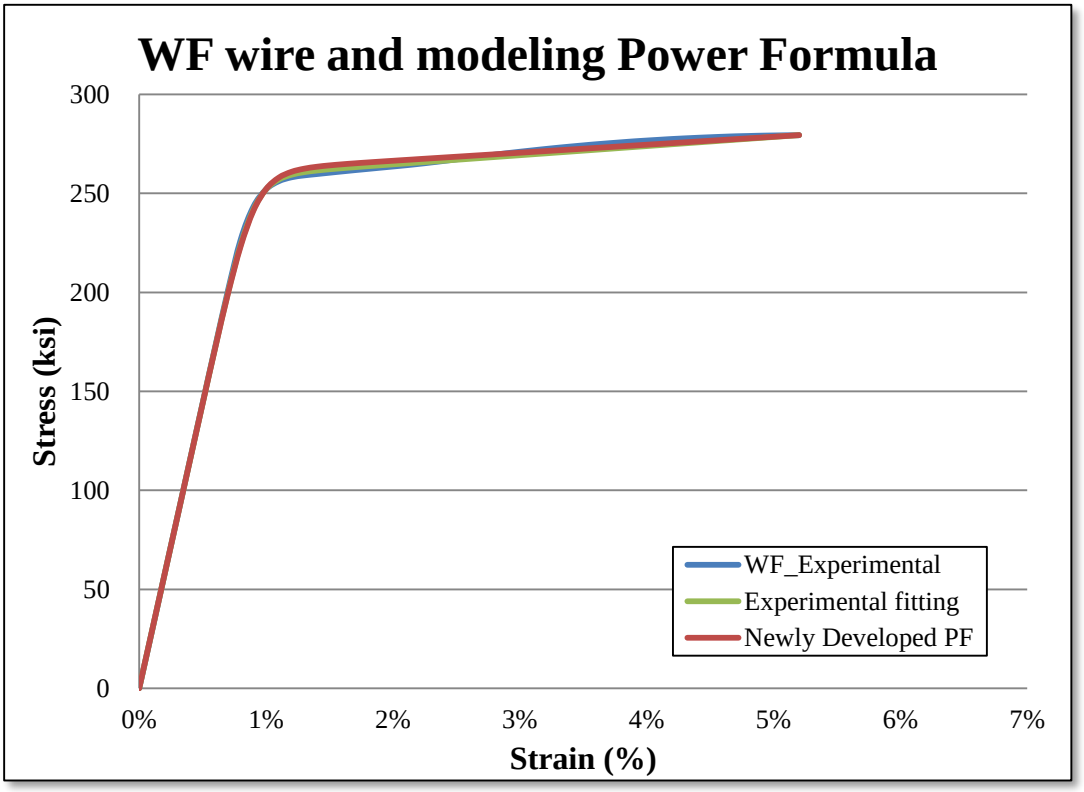


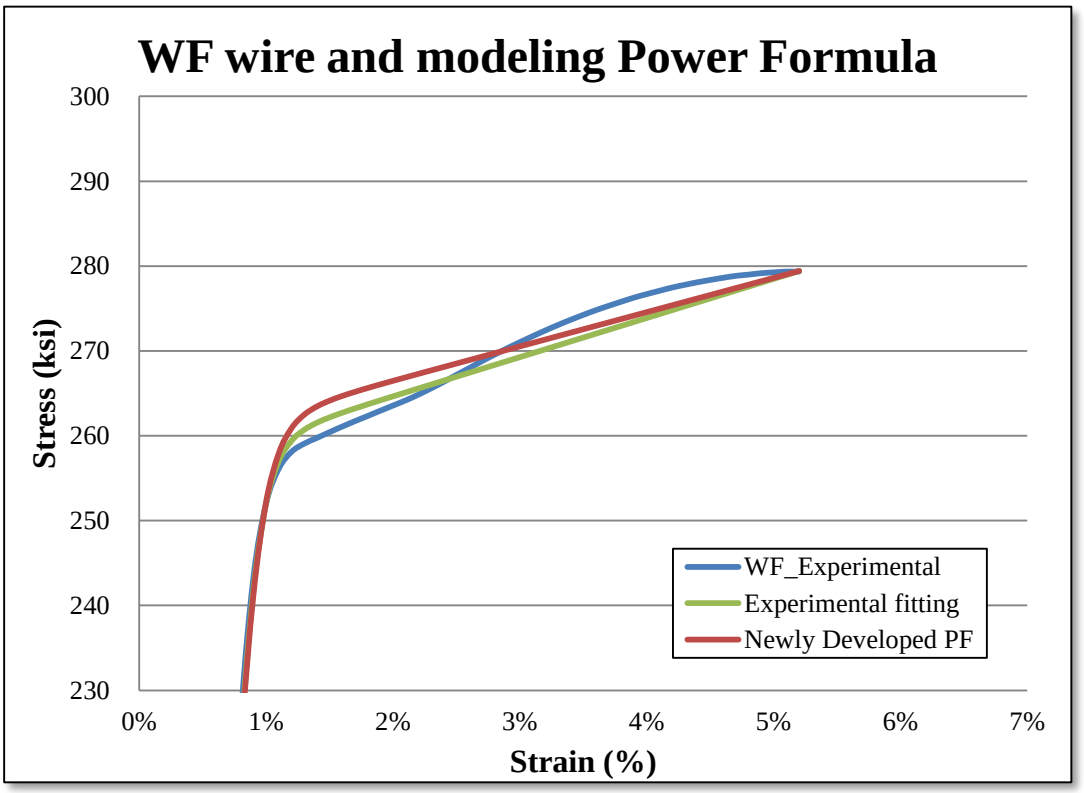

Appendix D. 5. Comparing modeling power formula curves to experimental curve for WG wire

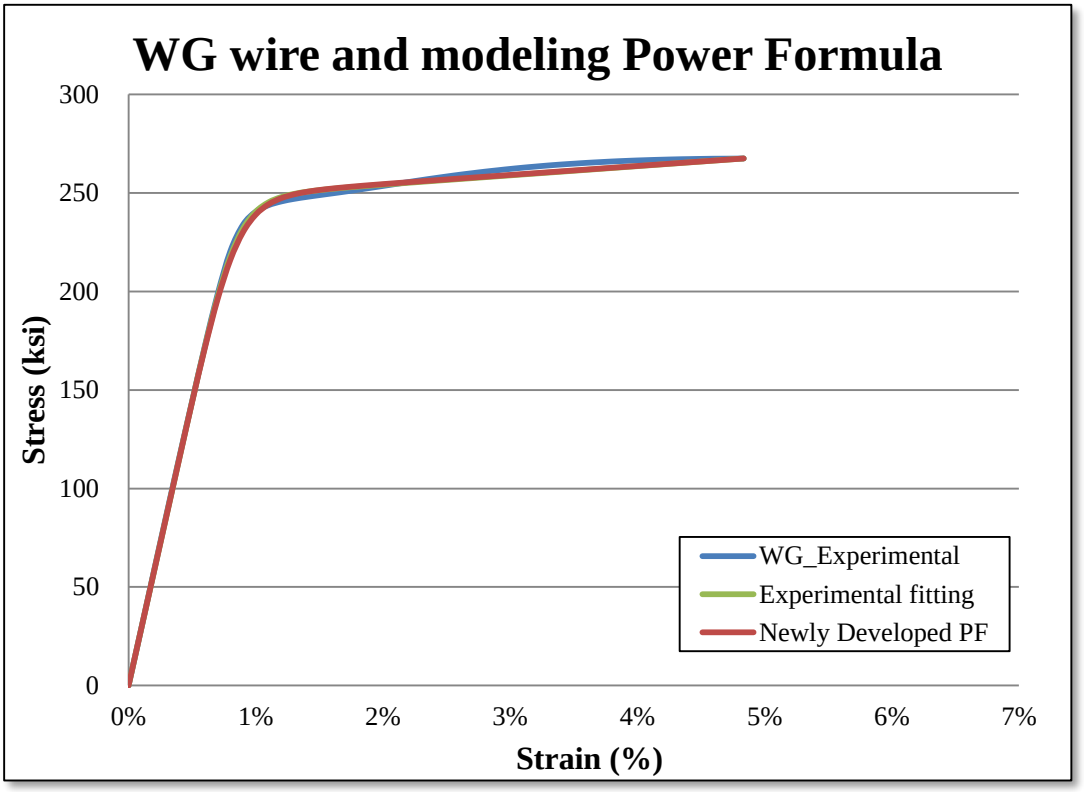


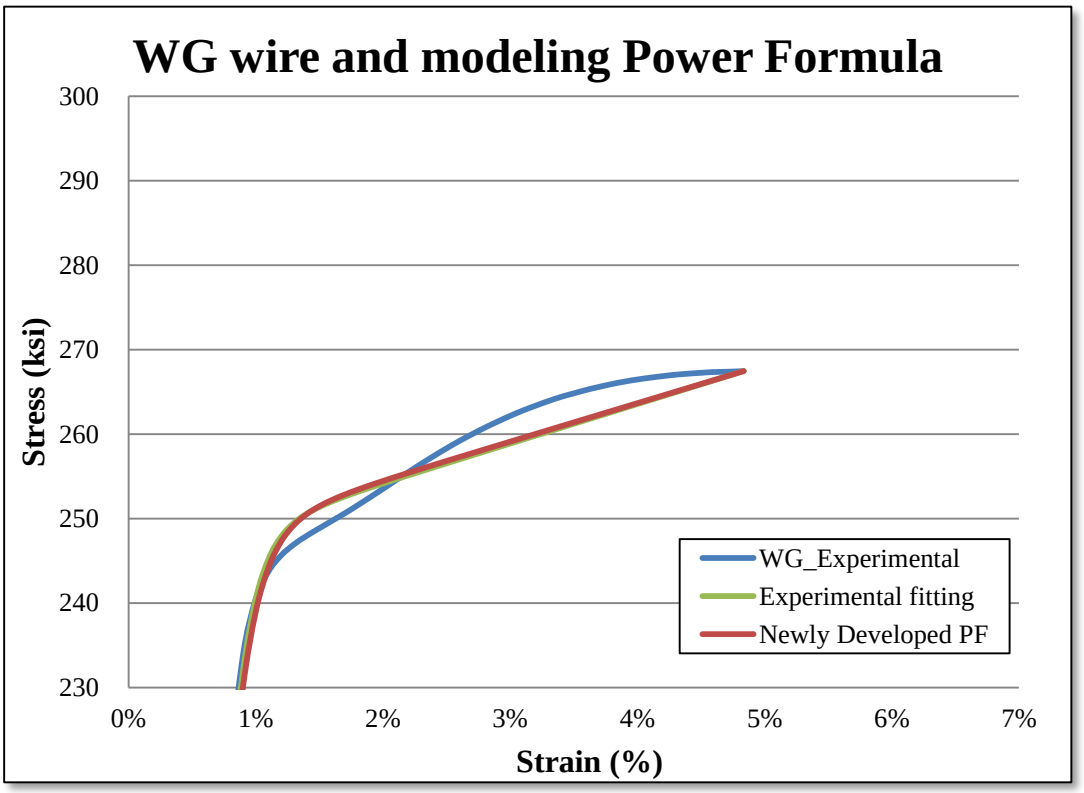

Appendix D. 6. Comparing modeling power formula curves to experimental curve for WH wire

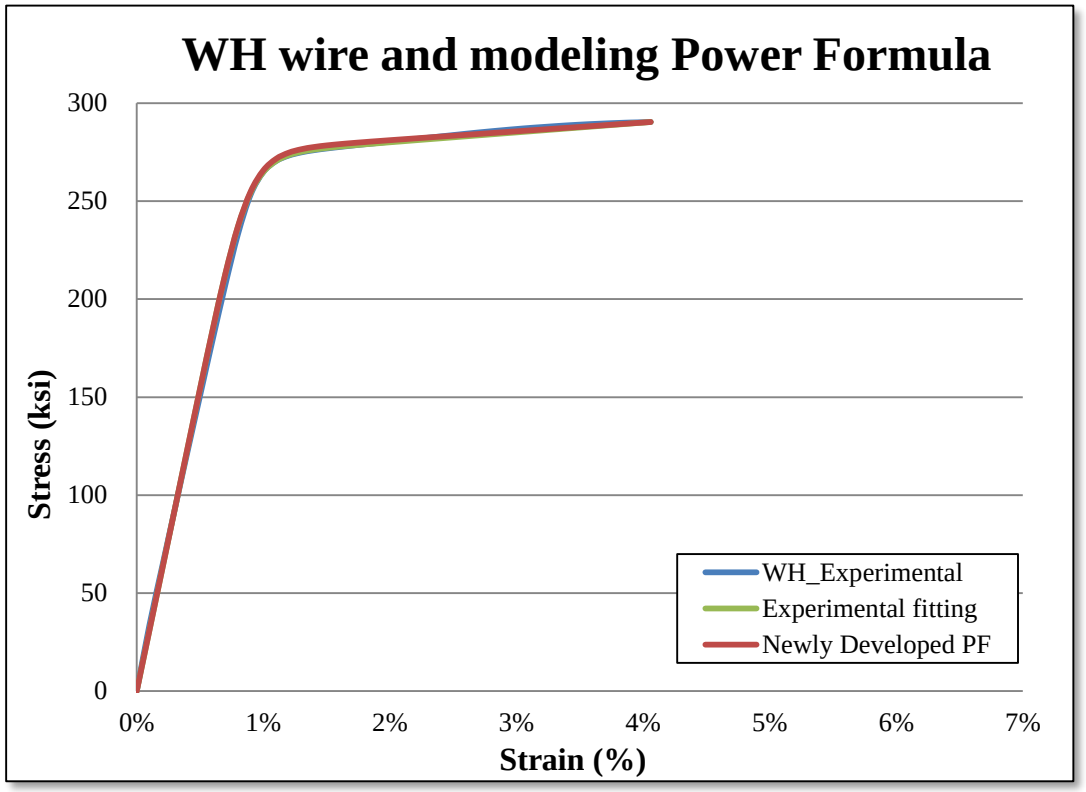


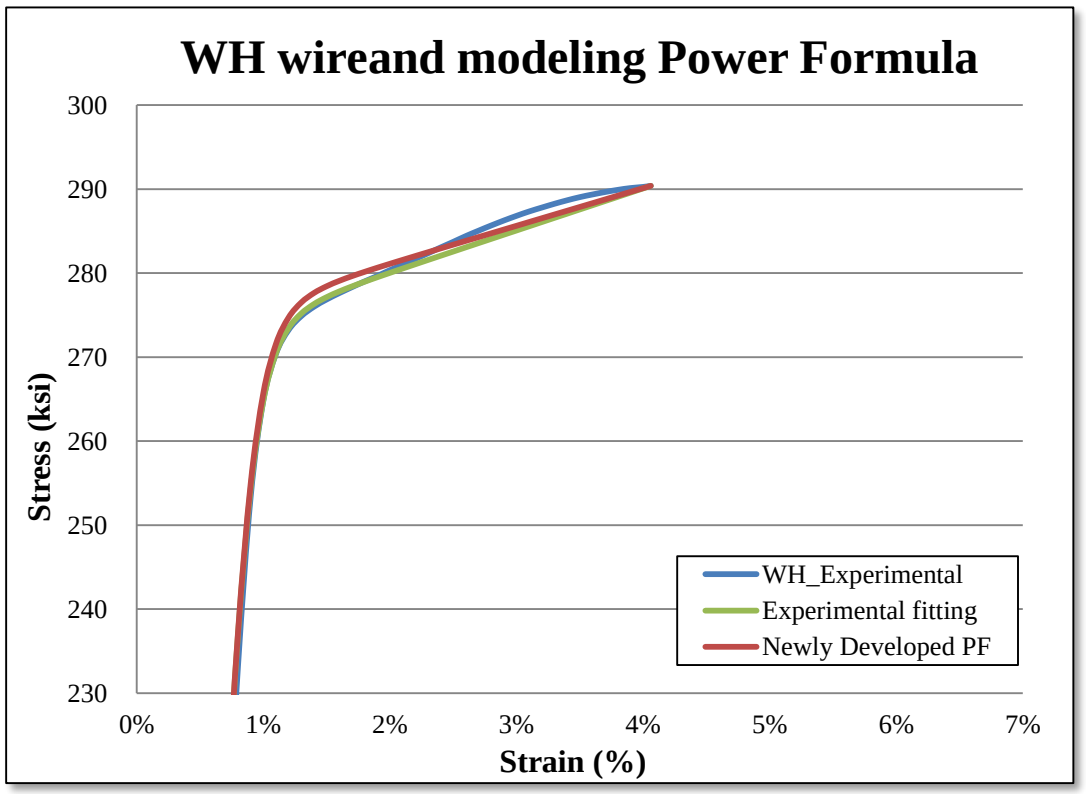

Appendix D. 7. Comparing modeling power formula curves to experimental curve for WI wire

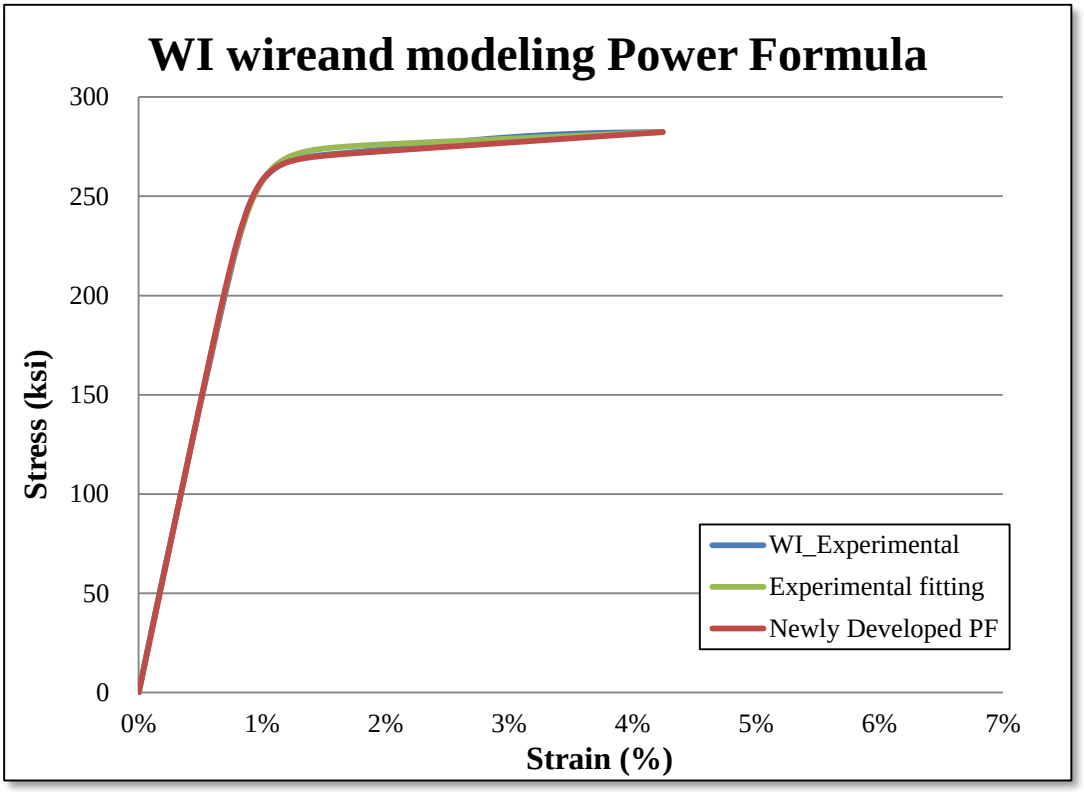


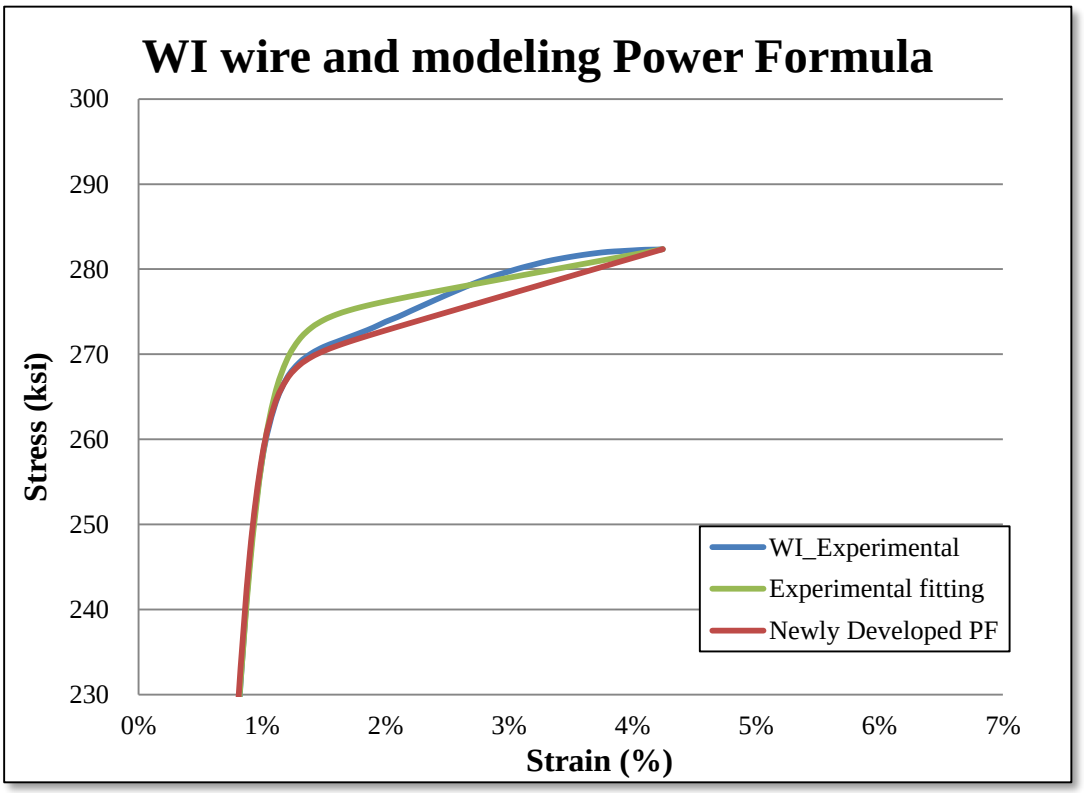

Appendix D. 8. Comparing modeling power formula curves to experimental curve for WJ wire

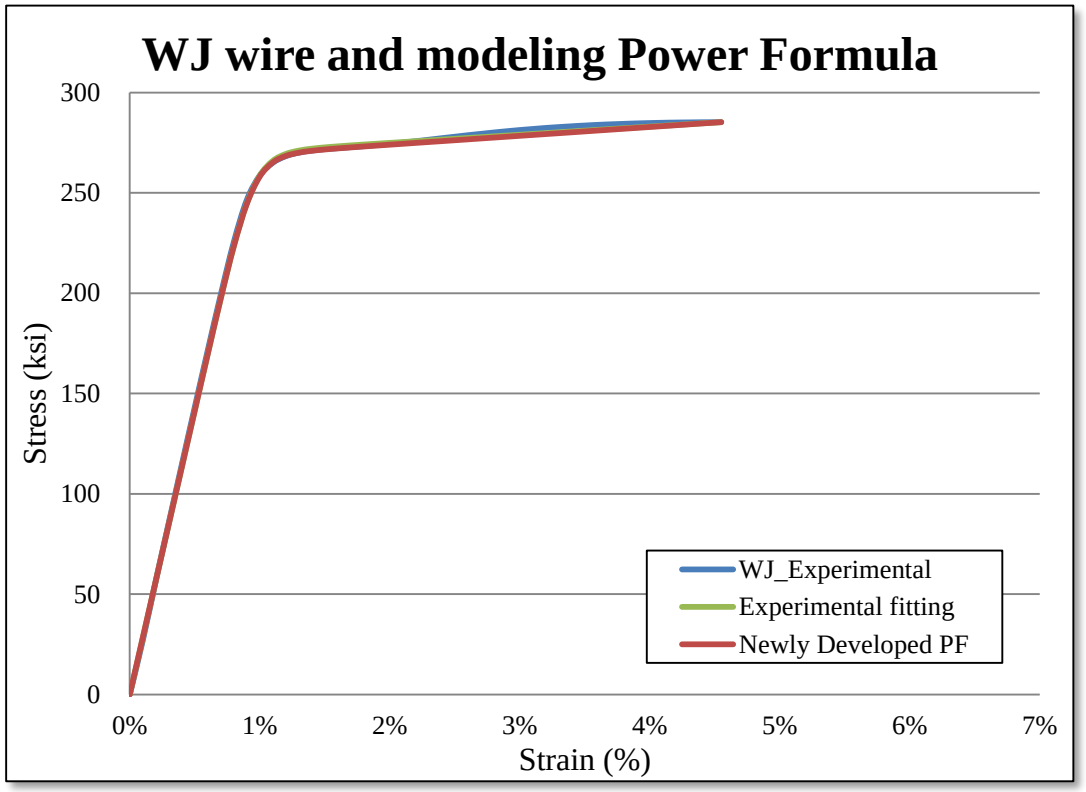


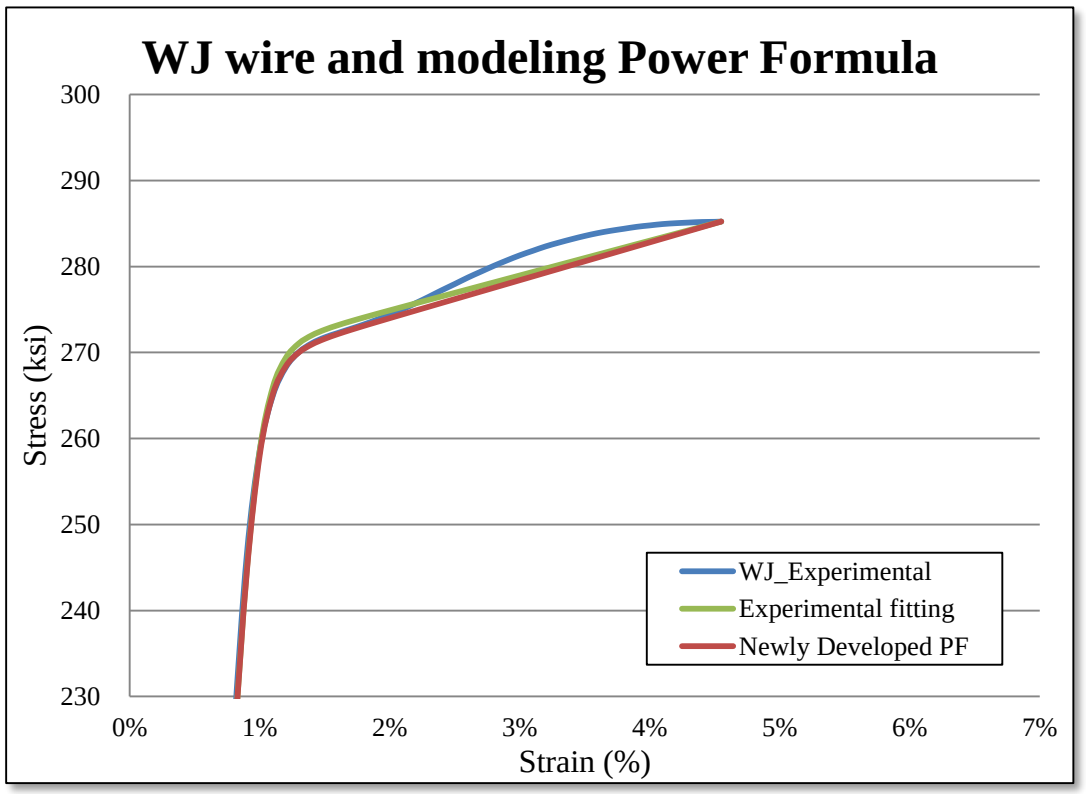

Appendix D. 9. Comparing modeling power formula curves to experimental curve for WL wire

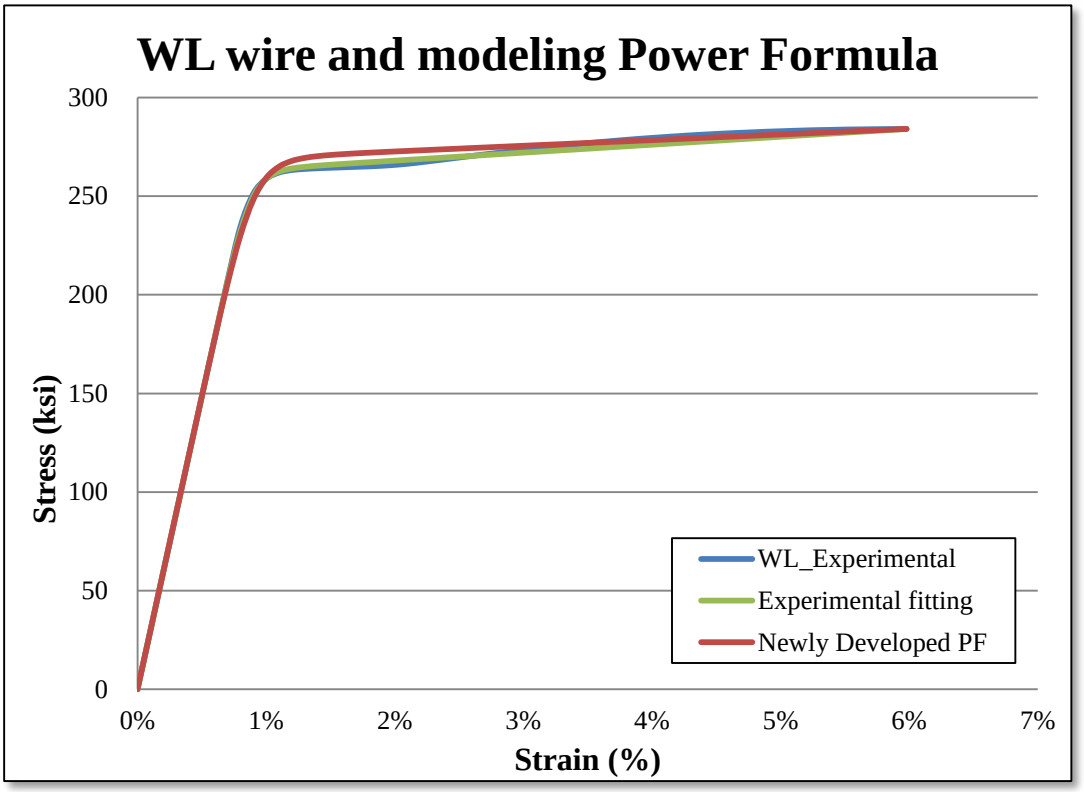


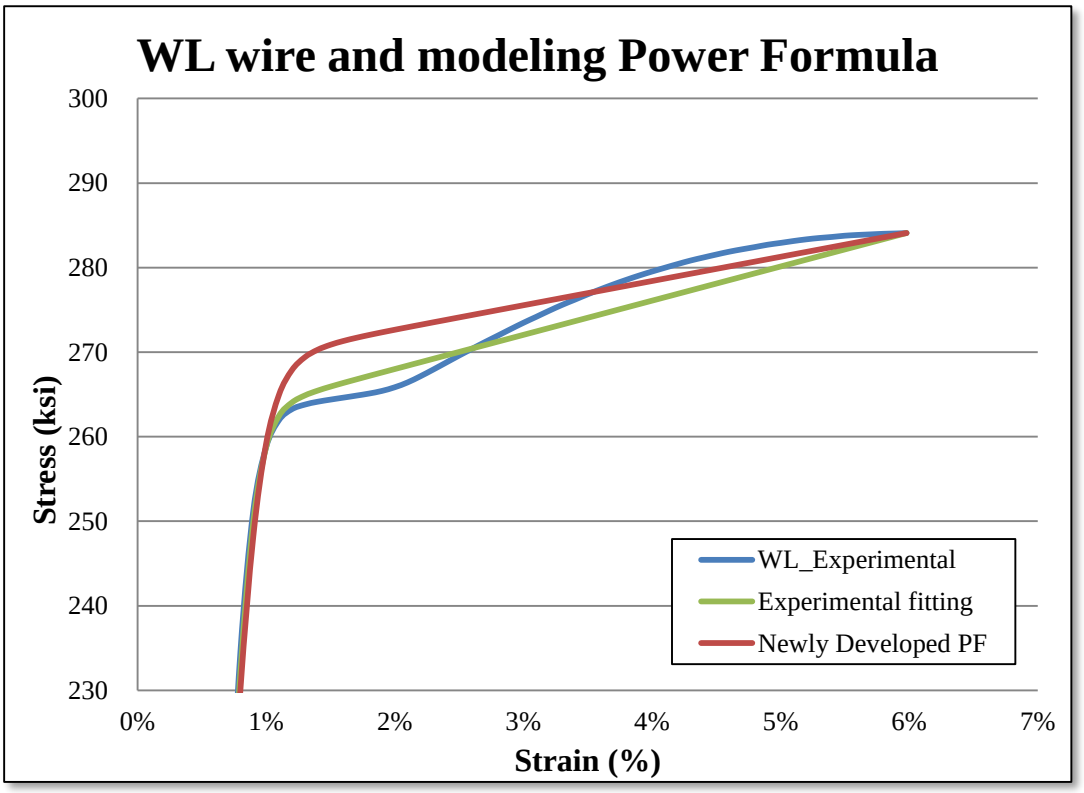

Appendix D. 10. Comparing modeling power formula curves to experimental curve for WM wire

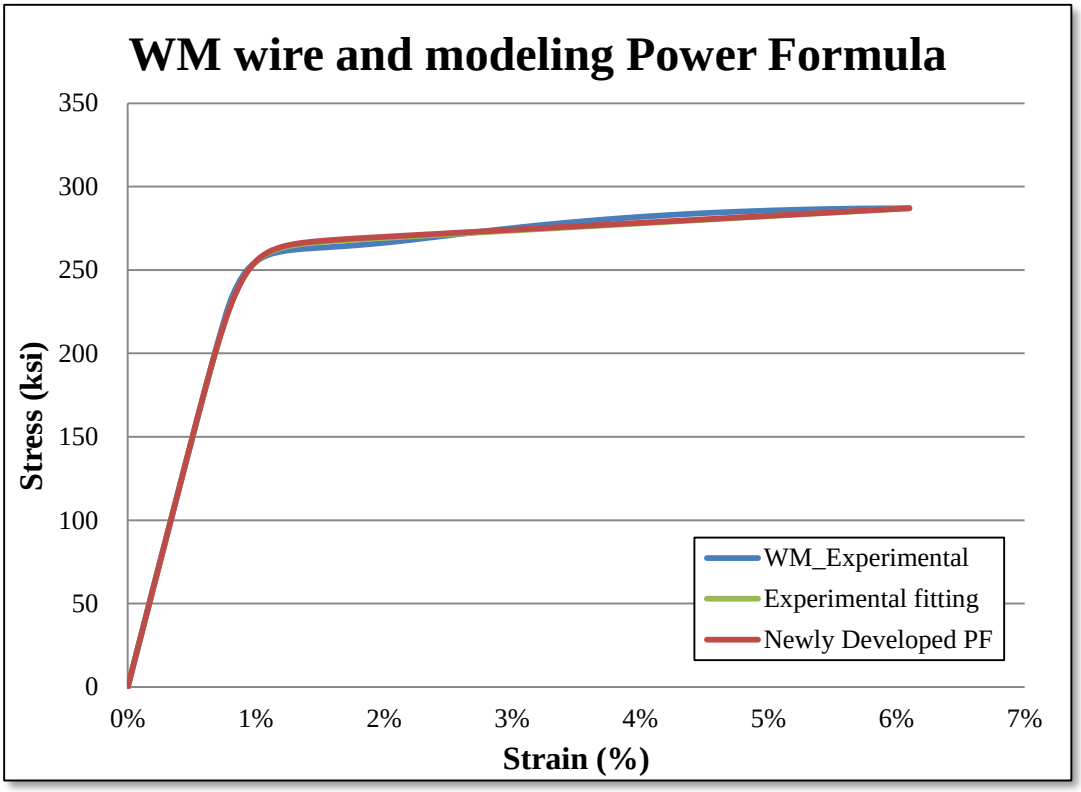


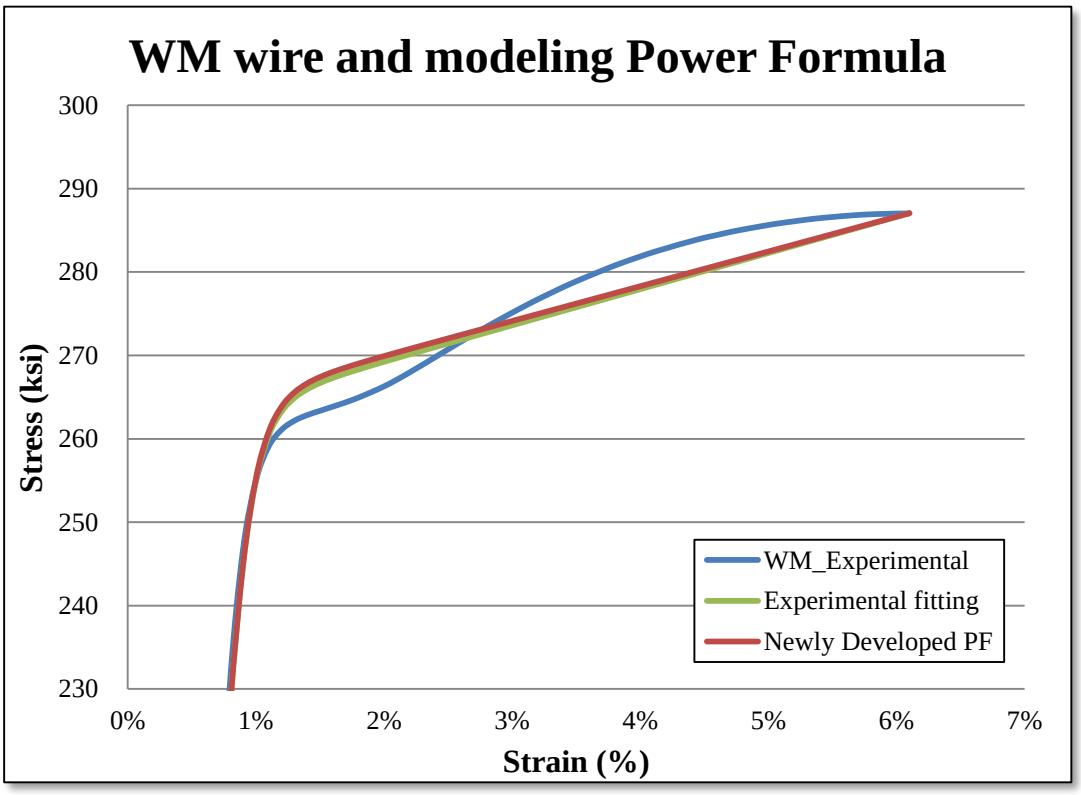

## Appendix E. Analytical and Modeling Curves by PCI Equation

Appendix E. 1. Comparing modeling PCI equation curves to experimental curve for WB wire

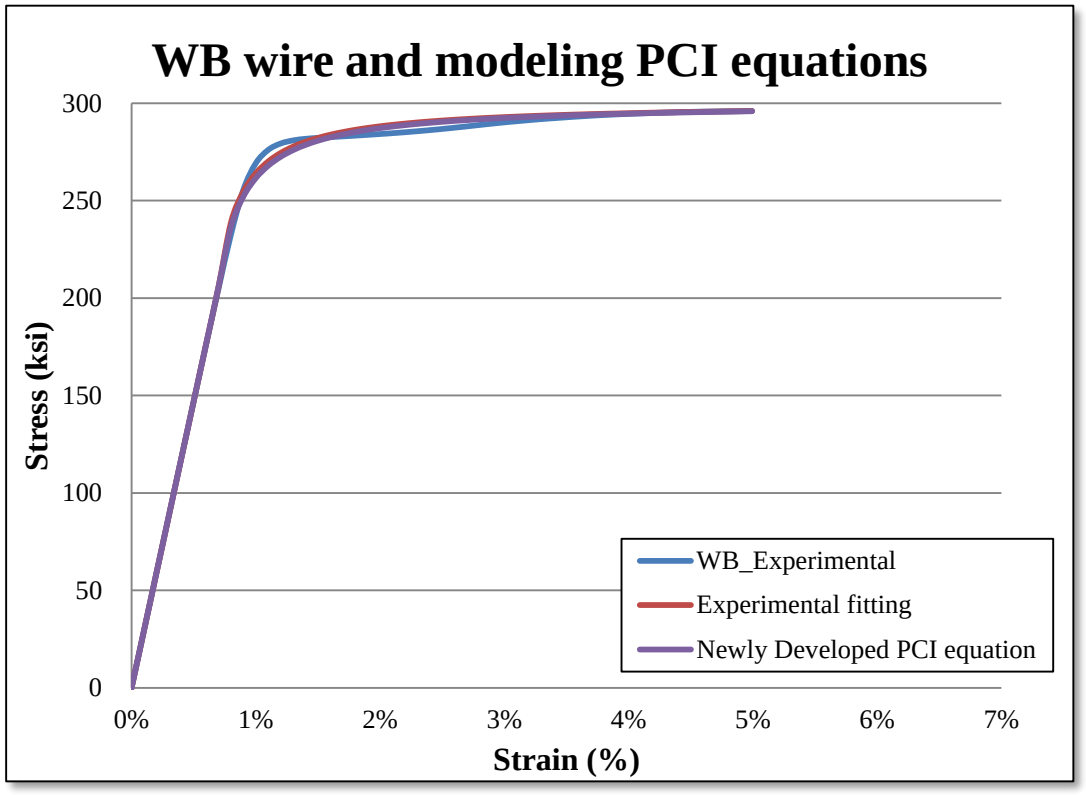


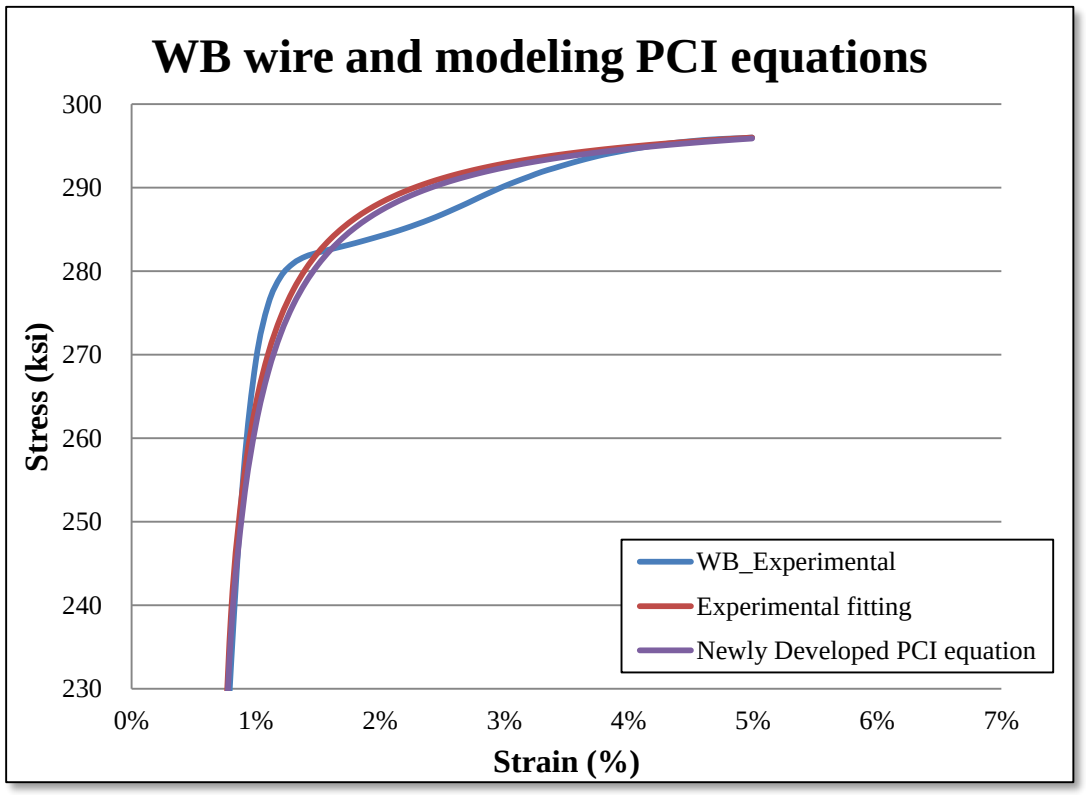

Appendix E. 2. Comparing modeling PCI equation curves to experimental curve for WD wire

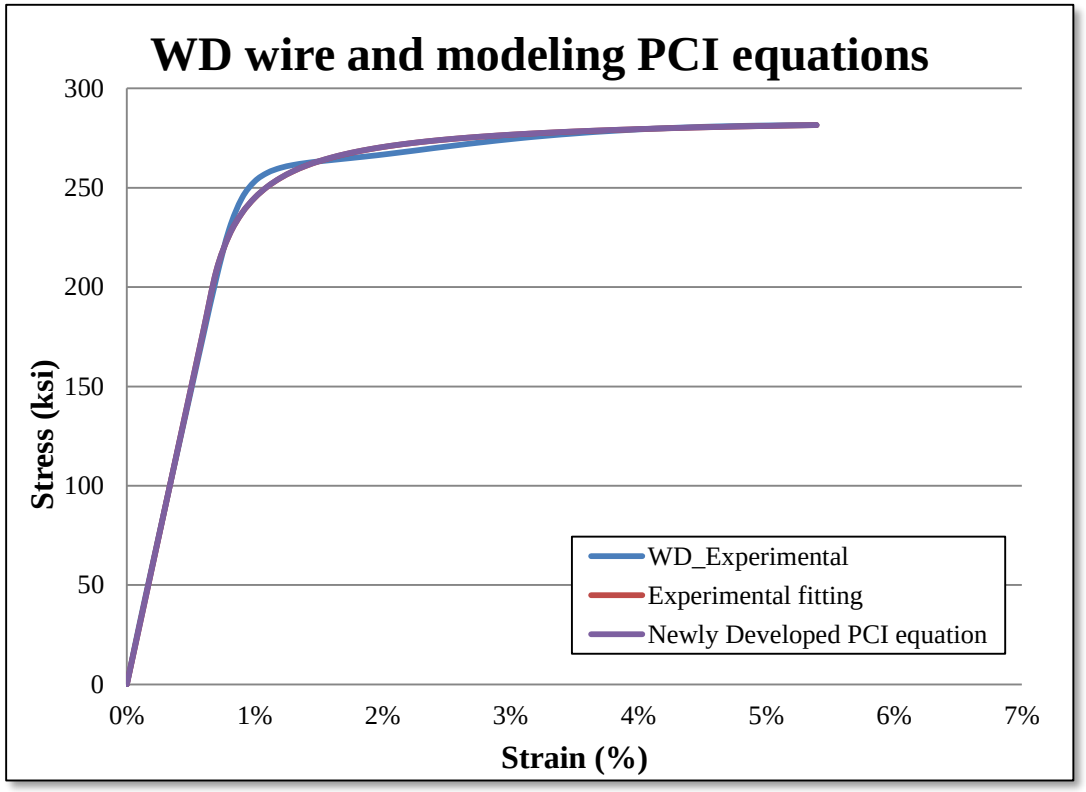


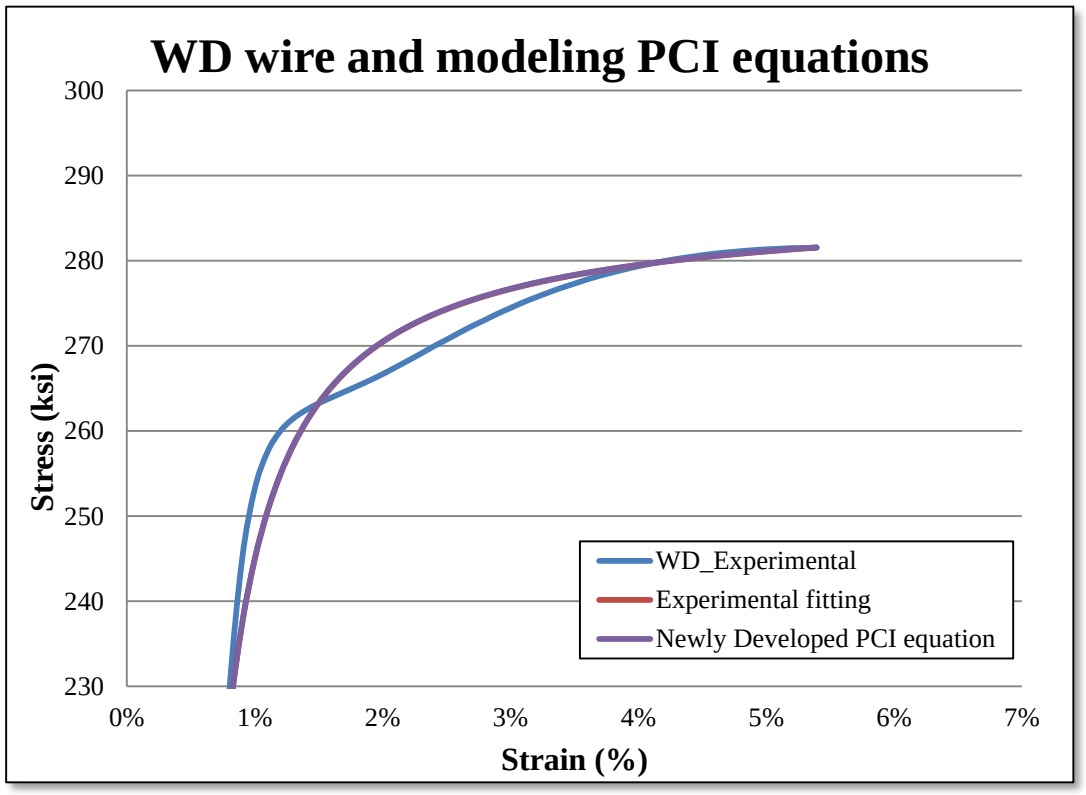

Appendix E. 3. Comparing modeling PCI equation curves to experimental curve for WE wire

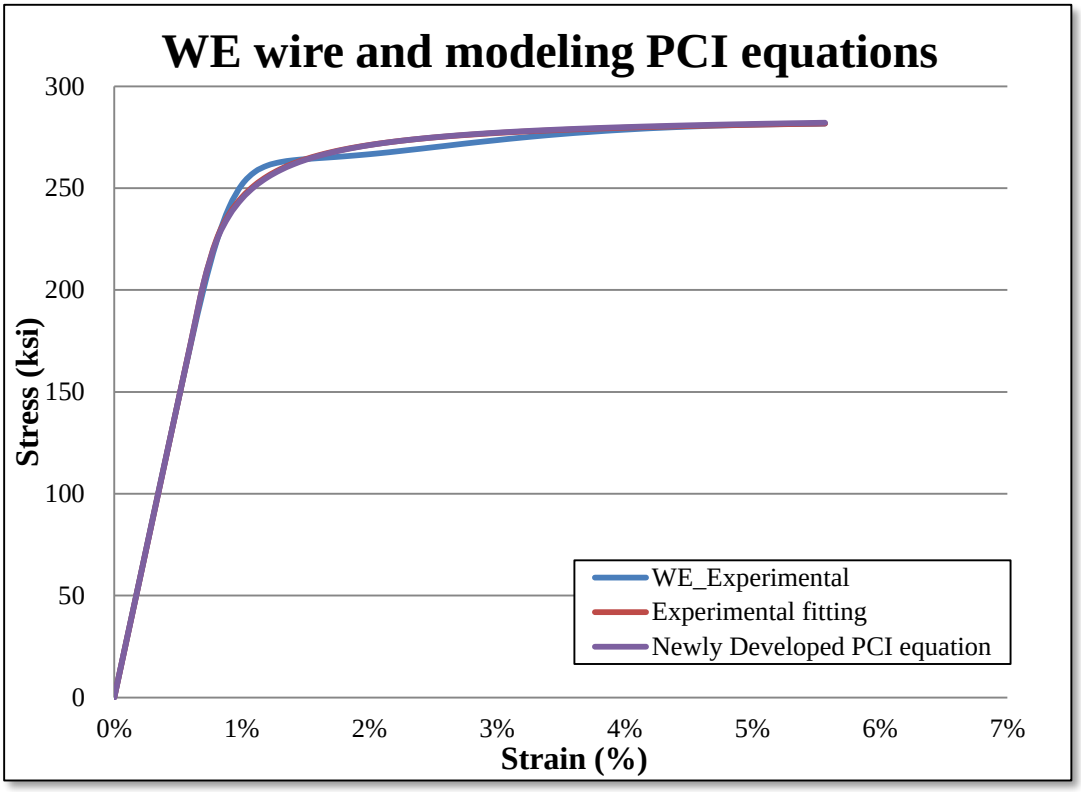


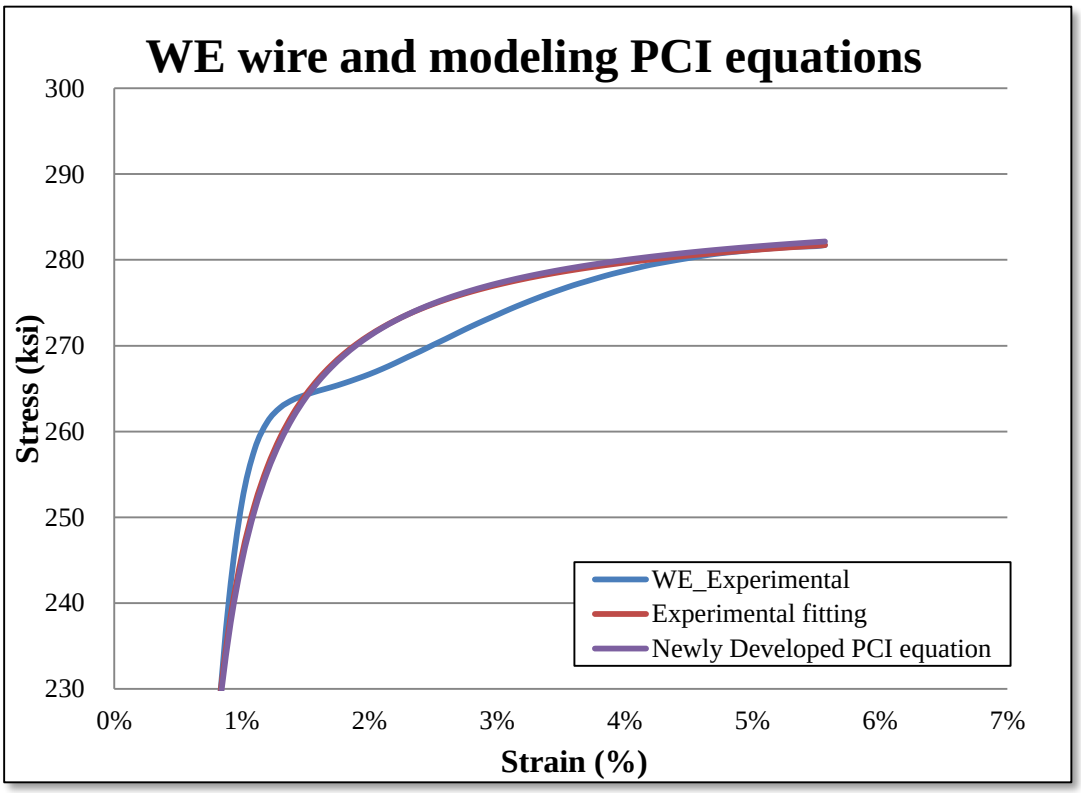

Appendix E. 4. Comparing modeling PCI equation curves to experimental curve for WF wire

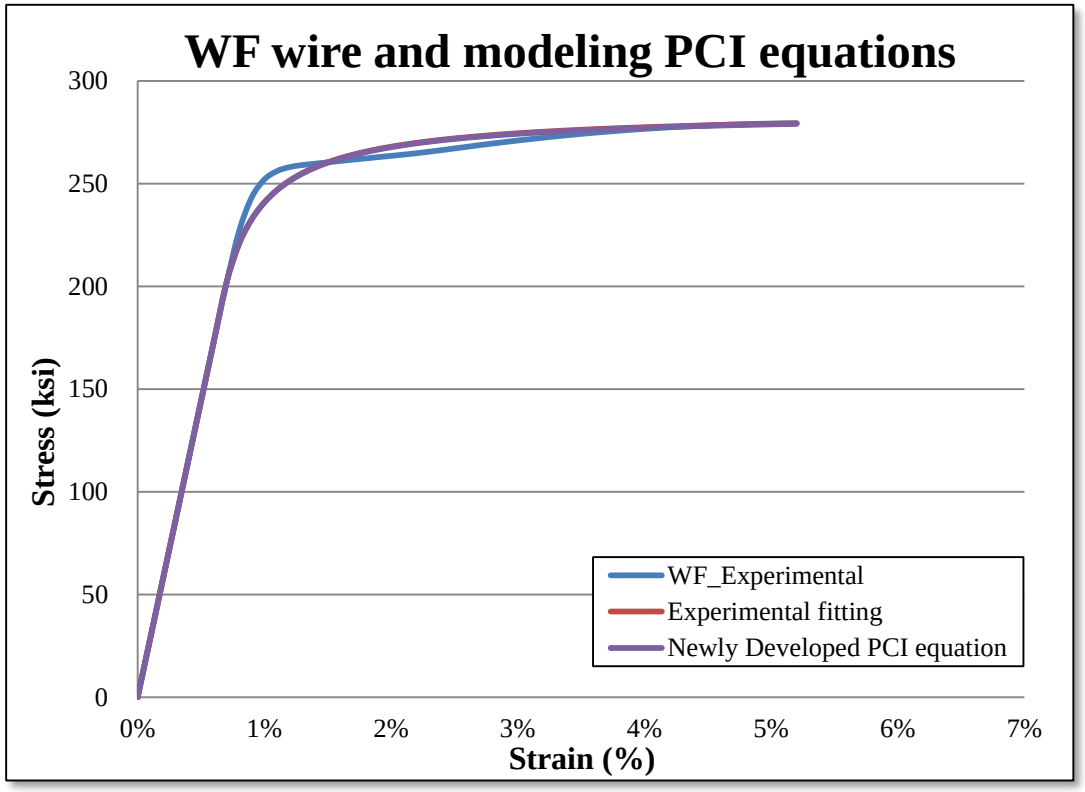


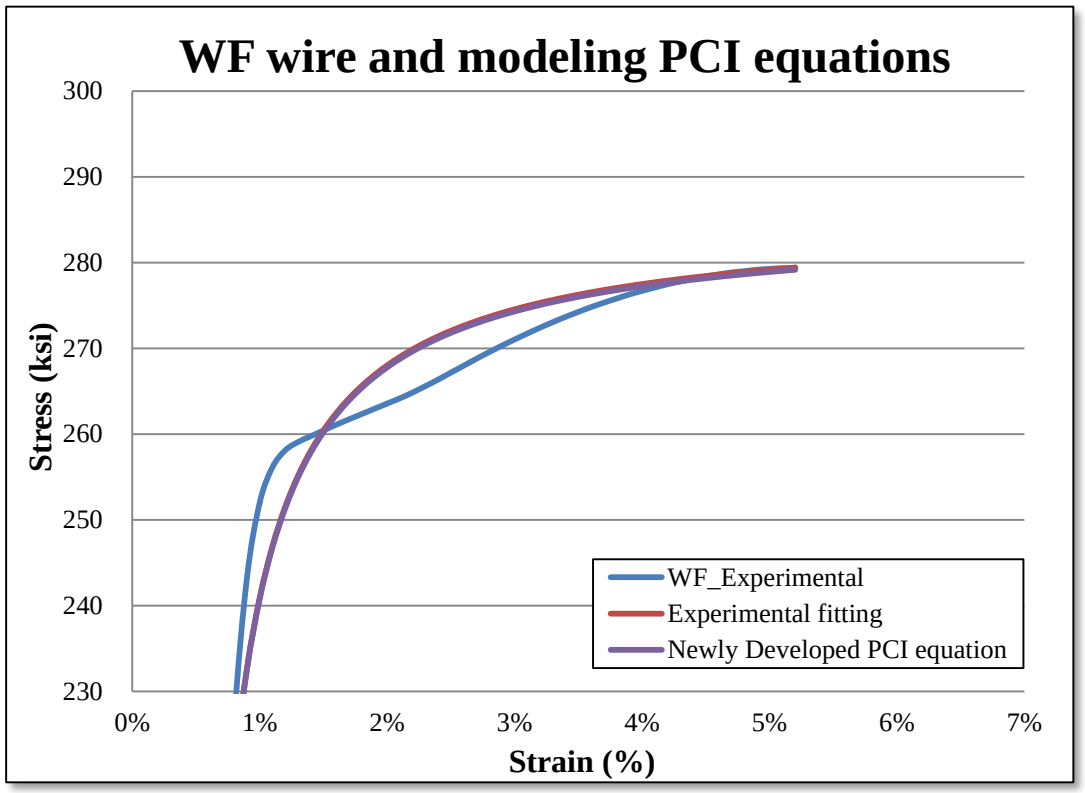

Appendix E. 5. Comparing modeling PCI equation curves to experimental curve for WG wire

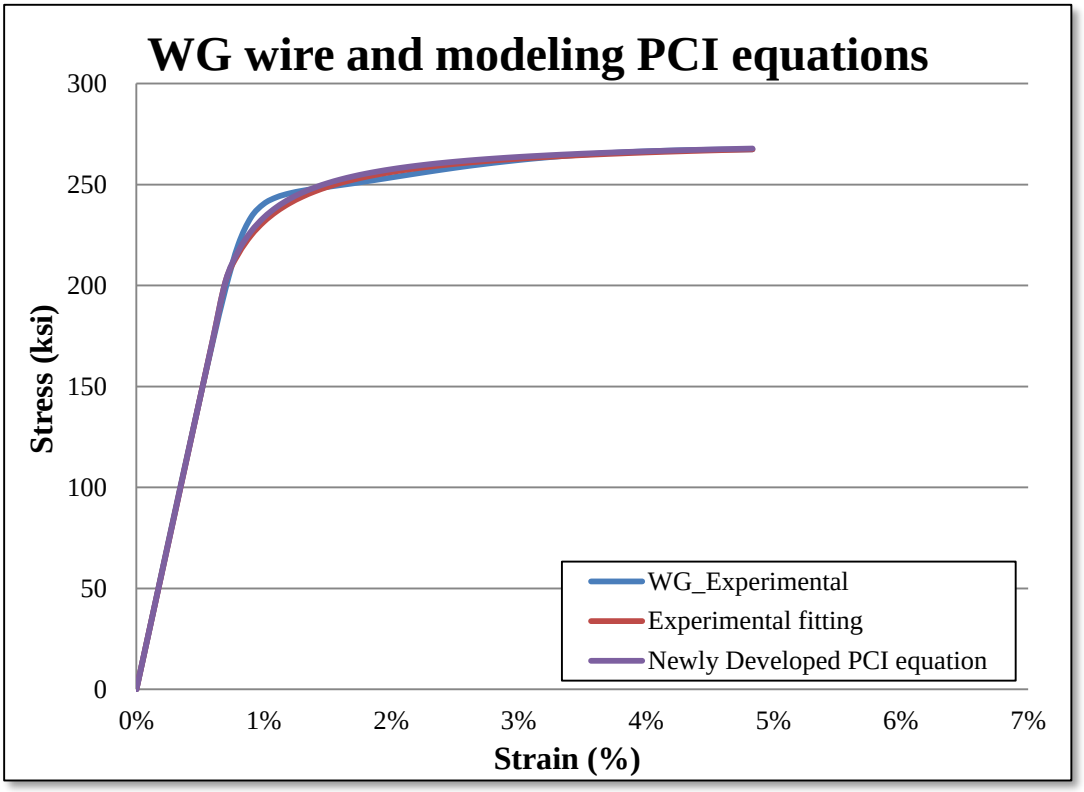


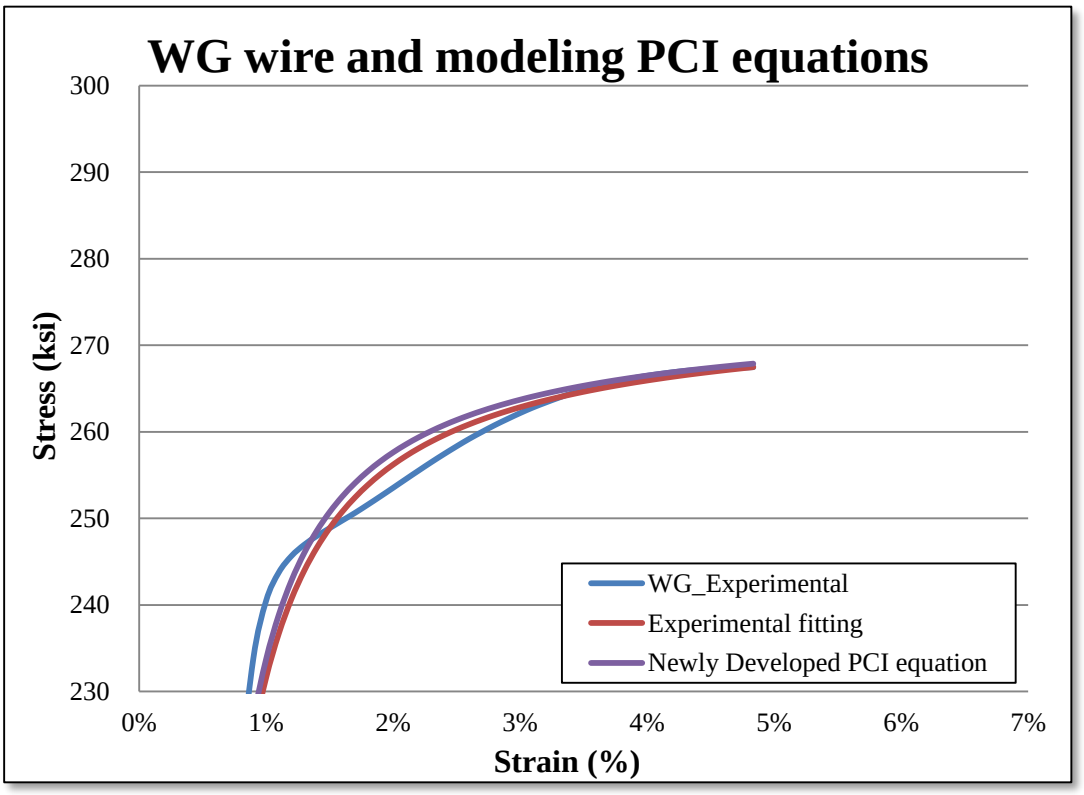

Appendix E. 6. Comparing modeling PCI equation curves to experimental curve for WH wire

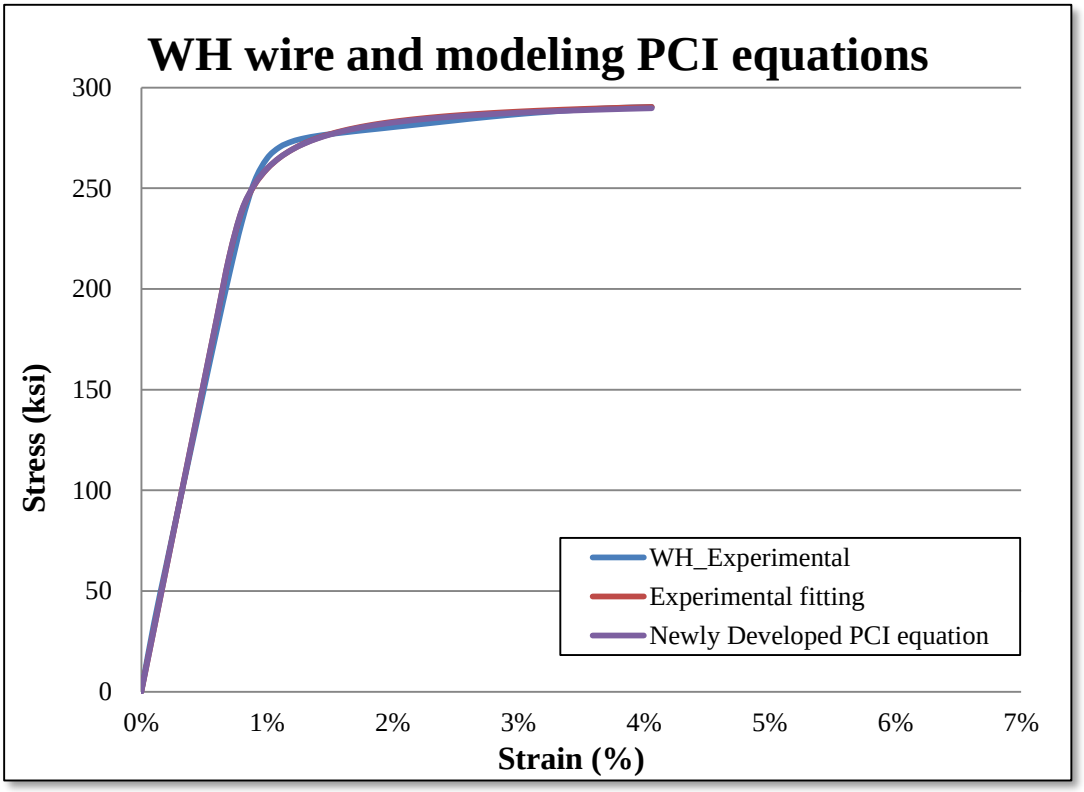


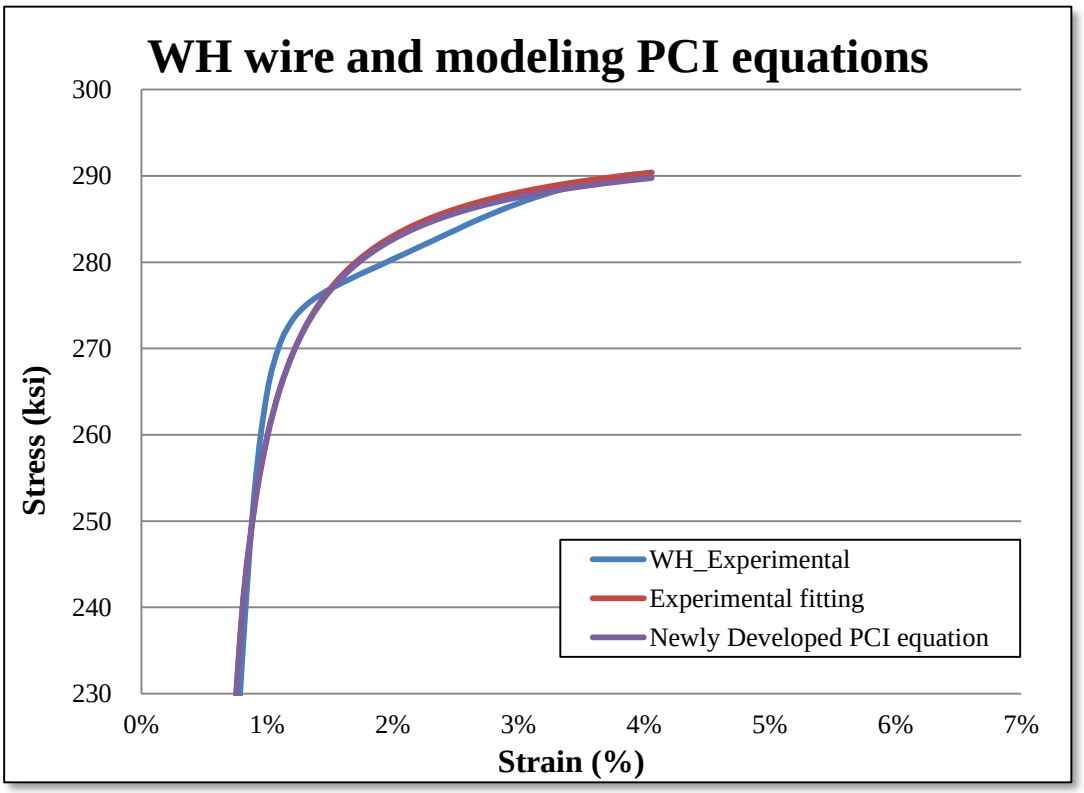

Appendix E. 7. Comparing modeling PCI equation curves to experimental curve for WI wire

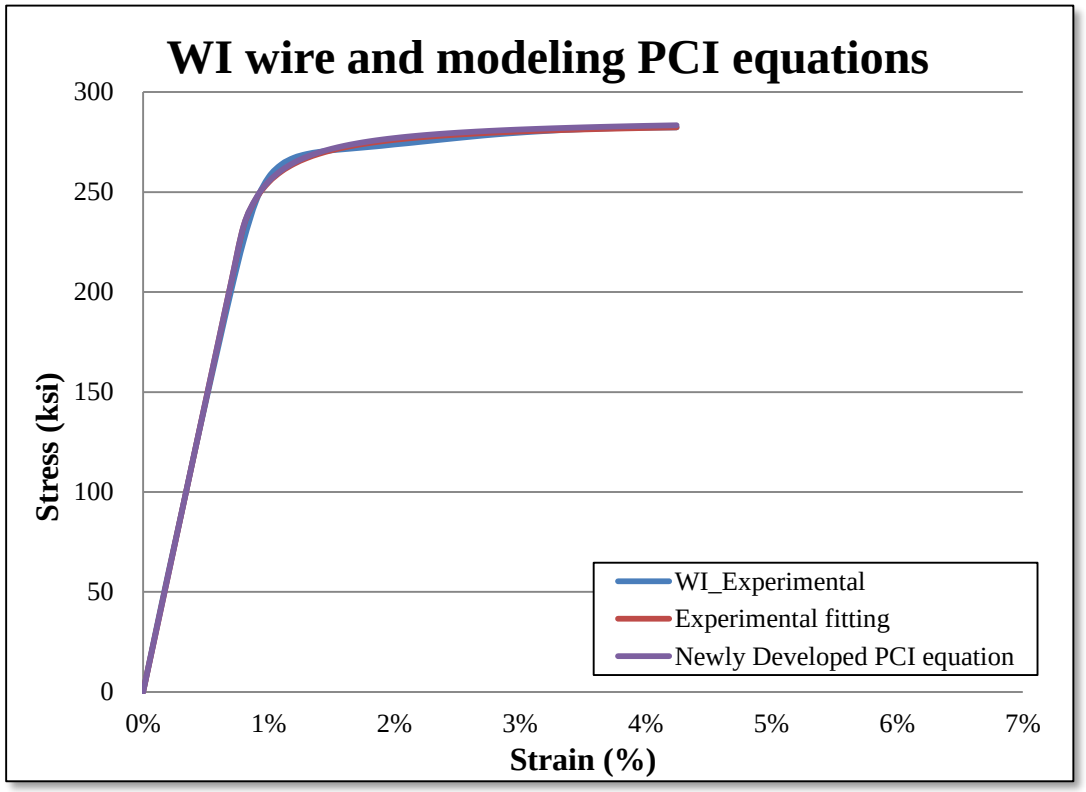


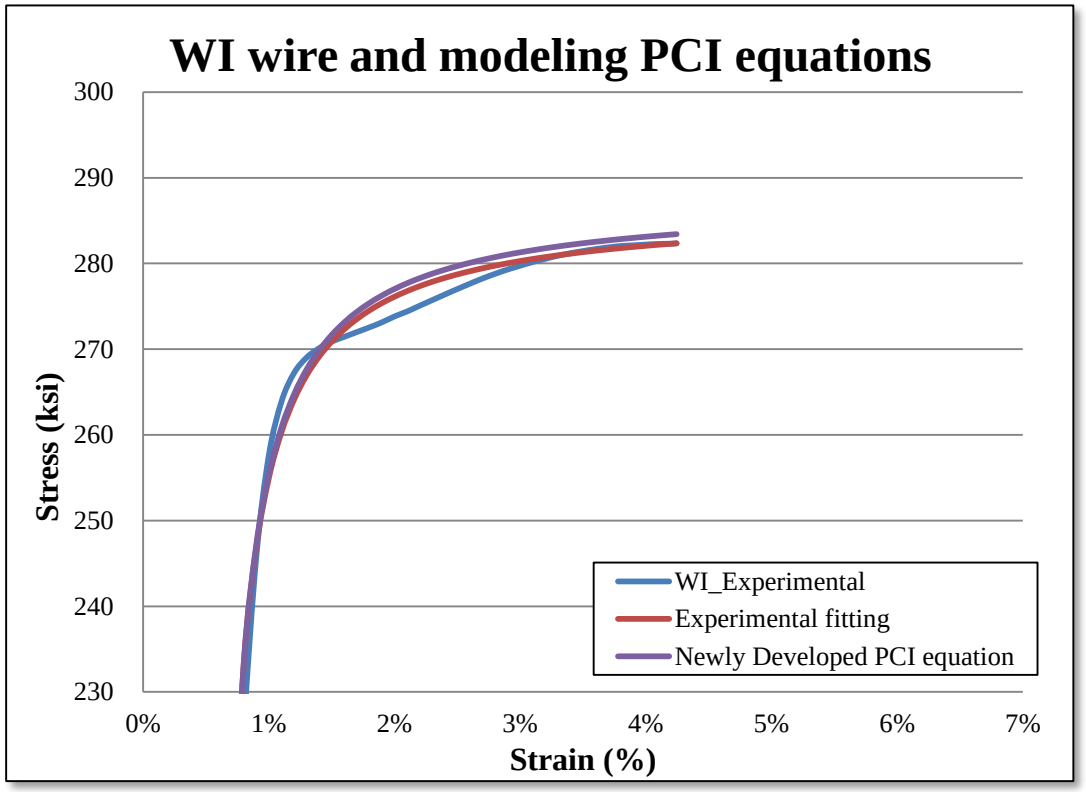

Appendix E. 8. Comparing modeling PCI equation curves to experimental curve for WJ wire

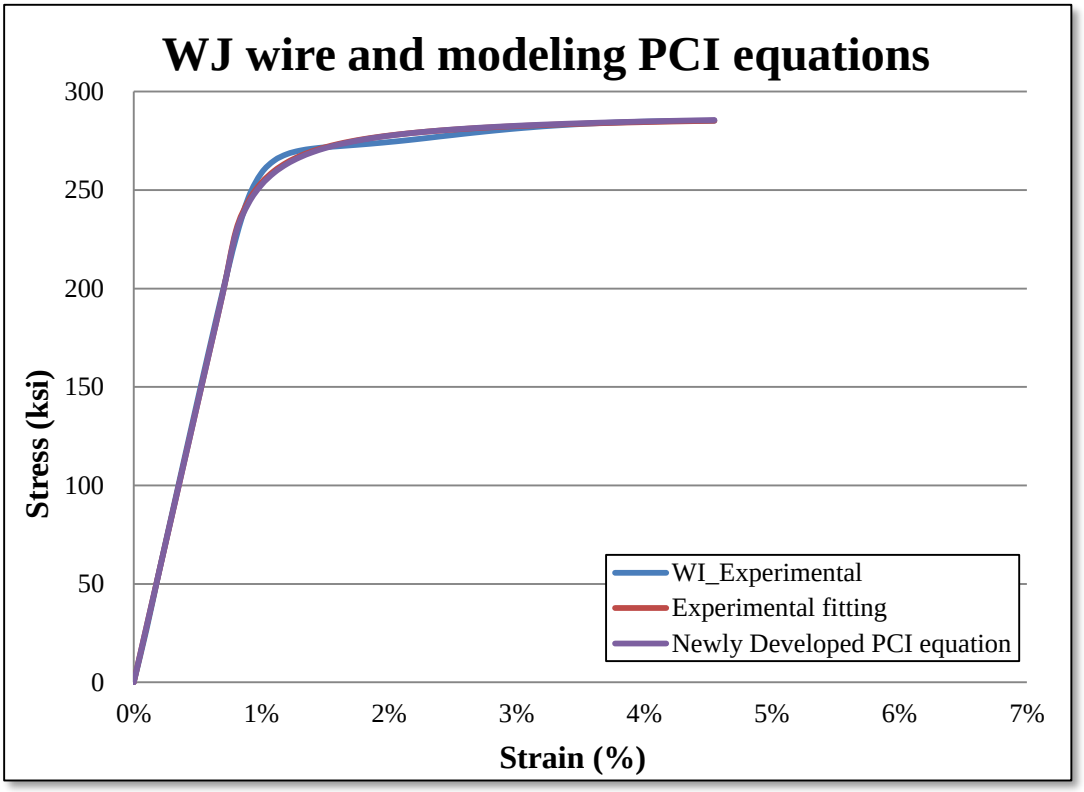


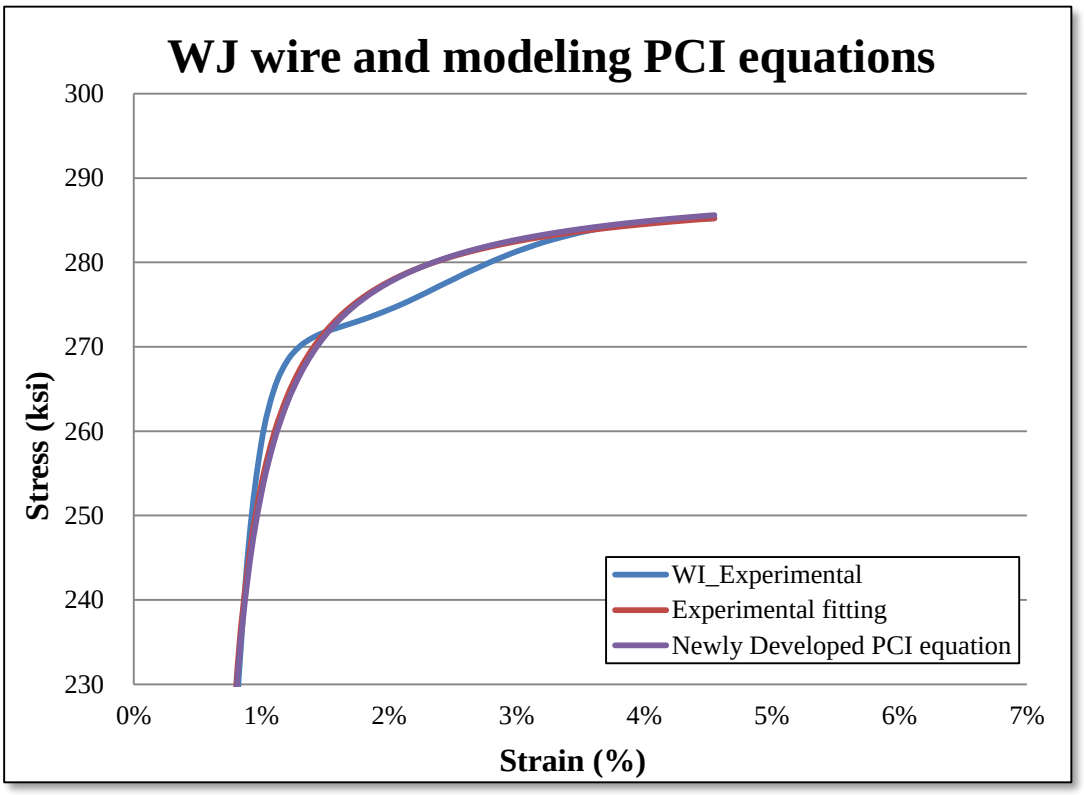

Appendix E. 9. Comparing modeling PCI equation curves to experimental curve for WL wire

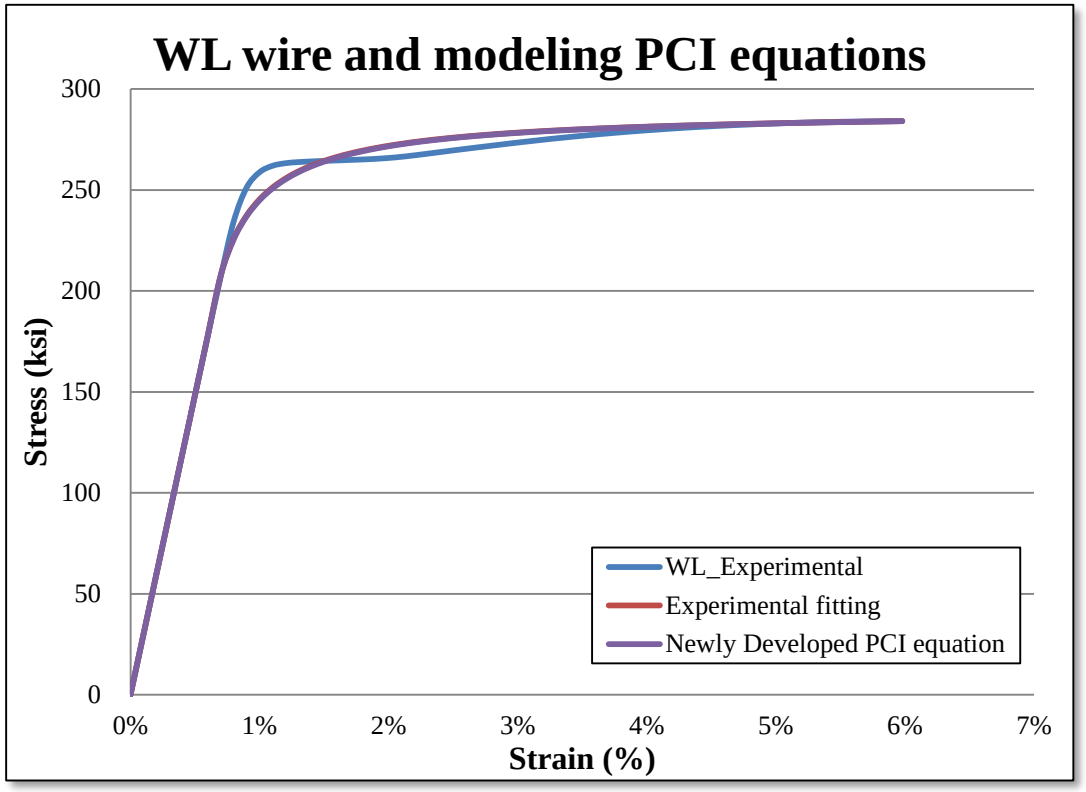


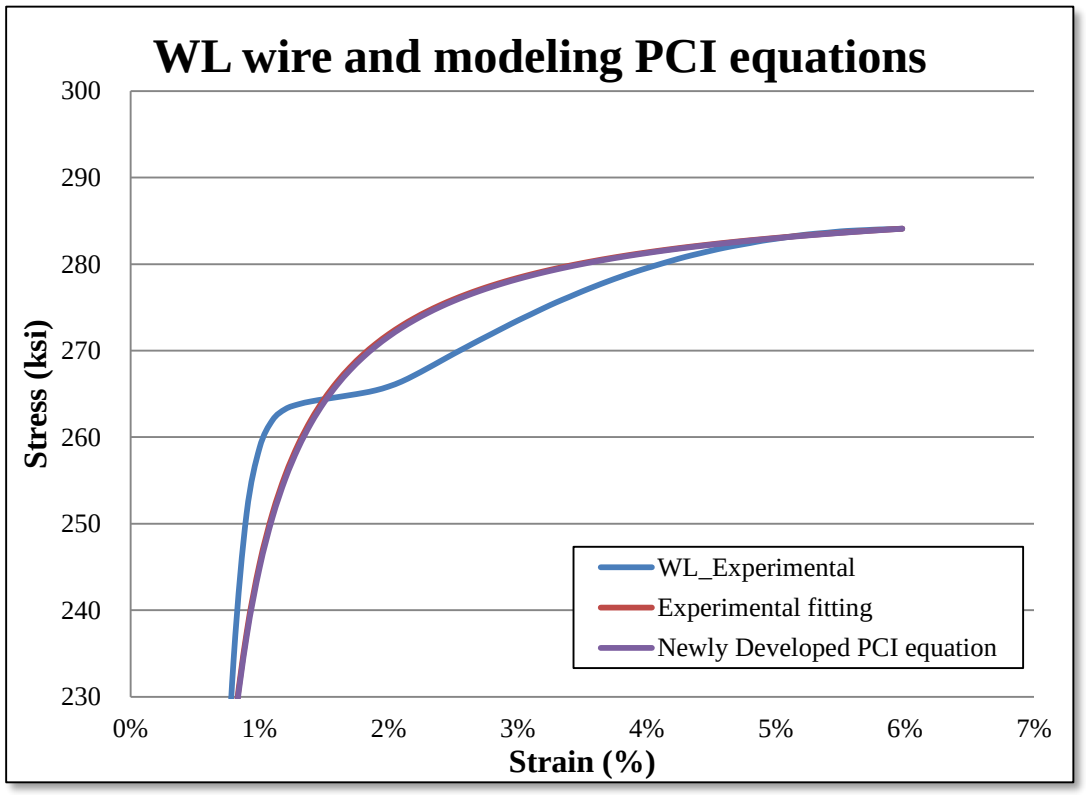

Appendix E. 10. Comparing modeling PCI equation curves to experimental curve for WM wire